Enriched Finite Elements for the Solution of Hyperbolic PDEs

Mayank Drolia

Submitted for the degree of
Doctor of Philosophy

Heriot-Watt University

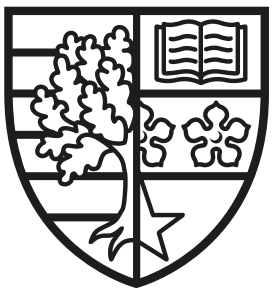

Institute for Infrastructure and Environment,
School of Energy, Geoscience, Infrastructure and Society.

March, 2020

Abstract

This doctoral research endeavors to reduce the computational cost involved in the solution of initial boundary value problems for the hyperbolic partial differential equation, with special functions used to enrich the solution basis for highly oscillatory solutions. The motivation for enrichment functions is derived from the fact that the typical solutions of the hyperbolic partial differential equations are wave-like in nature. To this end, the nodal coefficients of the standard finite element method are decomposed into plane waves of variable amplitudes. These plane waves form the basis for the proposed enrichment method, that are used for interpolating the solution over the elements, and thus allow for a coarse computational mesh without jeopardizing the numerical accuracy.

In this research, the time dependant wave problem is established into a semi-discrete finite element formulation. Both implicit as well as explicit discretization schemes are employed for temporal integration. In either approach, the assembled system matrix needs to be inverted only at the first time step. This inverted matrix is then reused in the subsequent time steps to update the numerical solution with evolution of time. The implicit approach provides unconditional stability, whereas the explicit scheme allows lumping the mass matrix into blocks that are cheaper to invert as opposed to the consistent mass matrix. These methods are validated with several numerical examples. A comparison of the performances of the implicit and the explicit schemes, in conjunction with the enriched finite element basis, is presented. Numerical results are also compared to gauge the performance of the enriched approach against the standard polynomial based finite element approaches. Industrially relevant numerical examples are also studied to illustrate the utility of the numerical methods developed through this research.

Keywords. Wave Equation; Finite Elements; Partition of Unity; Field Enrichment; Time Domain; Lumped Mass; Electromagnetics.

To Shadi and Omar, who made this possible.

Acknowledgements

"The two most powerful warriors are patience and time."

— Leo Tolstoy

I am grateful to my supervisors Dr M Shadi Mohamed, and Prof. Omar Laghrouche, for their constant support and guidance throughout my research. I would like to thank them for their belief in myself, for nurturing my curiosity in the subject, and above all for their patience and time.

During this research, I had numerous discussions with Dr Mohammed Seaid and Prof. Jon Trevelyan, from Durham University, which have proved to be very useful and insightful. I would also like to extend my gratitude to Dr Heiko Gimperlein, from the MACS department at Heriot-Watt University, who provided me with the opportunity to gain some experience as a research assistant under his supervision. I also am grateful for his suggestions and discussions , on various topics with brilliant research potential.

During my research, I had the pleasure of working with my colleagues Muhammad Iqbal and Konstantinos Christodoulou, whom I could not thank enough for their suggestions, guidance and friendship. I would also like to extend my thanks to the Heriot-Watt University for their financial support, and for their fantastic staff and infrastructure. Finally, this acknowledgement would not be complete without the mention of my family and friends, who have shown boundless care and affection and have supported me morally throughout the course of this research.

Research Thesis Submission

Please note this form should be bound into the submitted thesis.

Name:	Mayank Drolia		
School:	EGIS		
Version: *(i.e. First, Resubmission, Final)*	Final	Degree Sought:	PhD

Declaration

In accordance with the appropriate regulations I hereby submit my thesis and I declare that:

1. The thesis embodies the results of my own work and has been composed by myself
2. Where appropriate, I have made acknowledgement of the work of others
3. The thesis is the correct version for submission and is the same version as any electronic versions submitted*.
4. My thesis for the award referred to, deposited in the Heriot-Watt University Library, should be made available for loan or photocopying and be available via the Institutional Repository, subject to such conditions as the Librarian may require
5. I understand that as a student of the University I am required to abide by the Regulations of the University and to conform to its discipline.
6. I confirm that the thesis has been verified against plagiarism via an approved plagiarism detection application e.g. Turnitin.

ONLY for submissions including published works

Please note you are only required to complete the Inclusion of Published Works Form (page 2) if your thesis contains published works)

7. Where the thesis contains published outputs under Regulation 6 (9.1.2) or Regulation 43 (9) these are accompanied by a critical review which accurately describes my contribution to the research and, for multi-author outputs, a signed declaration indicating the contribution of each author (complete)
8. Inclusion of published outputs under Regulation 6 (9.1.2) or Regulation 43 (9) shall not constitute plagiarism.

* *Please note that it is the responsibility of the candidate to ensure that the correct version of the thesis is submitted.*

Signature of Candidate:	Mayank Drolia	Date:	

Submission

Submitted By *(name in capitals):*	
Signature of Individual Submitting:	
Date Submitted:	

For Completion in the Student Service Centre (SSC)

Limited Access	Requested	Yes		No		Approved	Yes		No	
E-thesis Submitted ***(mandatory for final theses)***										
Received in the SSC by *(name in capitals):*						Date:				

Inclusion of Published Works

Please note you are only required to complete the Inclusion of Published Works Form if your thesis contains published works under Regulation 6 (9.1.2)

Declaration

This thesis contains one or more multi-author published works. In accordance with Regulation 6 (9.1.2) I hereby declare that the contributions of each author to these publications is as follows:

Citation details	Explicit time integration with lumped mass matrix for enriched finite elements solution of time domain wave problems, Applied Mathematical Modelling, (2019).
Author 1	M. Drolia (50%) - Computational model, Analysis of data.
Author 2	M. S. Mohamed (25%) - Initial ideas and draft of paper.
Author 3	O. Laghrouche (10%) - Provision of underpinning understanding.
Author 4	M. Seaid (10%) – Provision of underpinning understanding.
Author 5	A. El-Kacimi (5%) - Provision of underpinning understanding.
Signature:	Mayank Drolia
Date:	

Citation details	Enriched finite elements for initial-value problem of transverse electromagnetic waves in time domain, Computers and Structures, 182:354–367 (2017).
Author 1	M. Drolia (50%) - Computational model, Analysis of data.
Author 2	M. S. Mohamed (25%) - Initial ideas and draft of paper.
Author 3	O. Laghrouche (10%) - Provision of underpinning understanding.
Author 4	M. Seaid (10%) – Provision of underpinning understanding, and draft of paper.
Author 5	J. Trevelyan (5%) - Provision of underpinning understanding.
Signature:	Mayank Drolia
Date:	

Please included additional citations as required.

Contents

List of Tables

List of Figures

Nomenclature and Abbreviations

Abbreviations

2D	two dimensions
3D	three dimensions
BEM	Boundary Element Method
CAD	Computer-Aided Design
CBF	Characteristic Basis Function
CBFM	Characteristic Basis Function Method
CFL	Courant–Friedrichs–Lewy
CPU	Central Processing Unit
DEM	Discontinuous Enrichment Methods
FDM	Finite Difference Method
FEM	Finite Element Method
FFT	Fast Fourier Transform
GFEM	Generalised Finite Element Method
IGA	Isogeometric Analysis
LSM	Least-Squares Method
MLSF	Moving Least Square Function
MoM	Method of Moments

PDE	Partial Differential Equation
PML	Perfectly Matched Layers
PUBEM	Partition of Unity Boundary Element Method
PUFEM	Partition of Unity Finite Element Method
PUIGA	Partition of Unity Isogeometric Analysis
PUM	Partition of Unity Method
PWDGM	Plane Wave Discontinuous Galerkin Method
RKM	Runge-Kutta Method
SVD	Singular Value Decomposition
TOTDOF	Total Degrees of Freedom
UWVF	Ultra Weak Variational Formulation
VTCR	Variational Theory of Complex Rays
XFEM	Extended Finite Element Method

Nomenclature

(r, θ)	polar coordinates in a 2D space
(x, y)	Cartesian coordinates in a 2D space
$\bar{a}, \bar{b}$	vectors in abstract vector space
$\Im\{\cdot\}$	imaginary part of a complex number
$\langle \cdot \vert \cdot \rangle$	Bra-Ket notation for inner product of vectors
$\langle \cdot, \cdot \rangle$	inner product operator in an abstract vector space
$\mathcal{E}_q$	functions that enrich the finite element solution space
$\mathcal{N}$	finite element shape functions
ϕ	weighting function in the space of test functions

$\Re\{\cdot\}$	real part of a complex number
C^k	differentiability class of a function, whose first k derivatives exist and are continuous.
H	Hamiltonian operator
∇^2	Laplacian operator
$\mathrm{H}_0^{(1)}(\cdot)$	Hankel function of the first kind and order zero
c	phase velocity in the 2D wave equation
k	wavenumber
T	total simulation time
t	time variable
t_n	n-th discrete time step, *i.e.*, $t_n = 0 + n\Delta t$, for integer values of n
Δt	step-size for discretizing the time variable
λ	wavelength
ω	angular frequency
$\mathbb{R}$	ordered set of real numbers
Ω	open bounded domain in 2D
Γ	Lipschitz continuous boundary in 2D
$\hat{\mathbf{v}}$	outward unit normal on domain boundary Γ
$\mathbf{x}$	Cartesian position vector of a point in 2D
Ω_h	computational domain obtained as the finite element approximation of the problem geometry
$\mathcal{T}_i$	i-th finite element discretization of the computational domain
$\mathbf{x}_i$	Cartesian position vector of the i-th mesh point in the computational domain

N_d	total number of nodes in the finite element mesh
M	total number of nodes in an element
$\mathcal{K}_i$	i-th reference element
(ξ, η)	Cartesian coordinates of a point in the 2D reference element
δ_{ij}	Kronecker delta function
W_h	function space for the finite element test and trial functions
$\mathcal{N}_i$	i-th global shape function
φ_i	i-th local shape function
$Y_i(\mathbf{x})$	invertible injective function that maps a reference element to the i-th global element $\mathcal{T}_i$
Ψ_m	set of all basis functions defined on a reference element
$\widehat{\psi}(\mathbf{x})$	basis function defined on the global element $\mathcal{T}_i$
$\Psi(\mathcal{T}_i)$	set of all basis functions defined on the global element $\mathcal{T}_i$
$\widetilde{W_h}$	enriched function space for the PUFEM test and trial functions
$E(t, \mathbf{x})$	exact solution to the 2D wave equation
$V(t, \mathbf{x})$	first order time derivative of the exact solution to the 2D wave equation
$E^n(\mathbf{x})$	value of $E(t_n, \mathbf{x})$
$V^n(\mathbf{x})$	value of $V(t_n, \mathbf{x})$
$E_h(t, \mathbf{x})$	numerical solution to the 2D wave equation
$V_h(t, \mathbf{x})$	numerical approximation of the first order time derivative of the exact solution to the 2D wave equation
$E_h^n(\mathbf{x})$	value of $E_h(t_n, \mathbf{x})$

α_q	propagation angle for the q-th plane wave enrichment function
$A_i^{q,n}$	amplitude for the q-th plane wave enrichment function at the i-th node and at the n-th time step
B_i^n	scaling coefficient for the constant term used in enrichment at the i-th node and at the n-th time step
$\mathcal{A}_{ij}$	elementary matrix of size $Q \times Q$ that corresponds to a block in the global system matrix at the i-th row and j-th column, for the implicit PUFEM
$\mathbf{A}$	global system matrix for the implicit PUFEM
$\mathbf{b}$	global load vector for the implicit PUFEM
$\mathbf{b}_i$	elementary load vector of size Q corresponding to the i-th node, for the implicit PUFEM
$\mathbf{E}^n$	global solution vector, corresponding to time t_n, for the PUFEM
$\mathbf{E}_i$	column vector of size Q that contains the solution coefficients corresponding to the i-th node, for the implicit PUFEM
M_q	total degrees of freedom per element
N_{dof}	total degrees of freedom
Q	total number of enrichments used at each mesh point
τ	number of degrees of freedom per wavelength
$\mathbf{K}$	global stiffness matrix for the explicit PUFEM
$\mathbf{M}$	consistent global mass matrix for the explicit PUFEM
$\bar{\mathbf{M}}$	approximate global mass matrix for the explicit PUFEM, obtained using mass lumping
$\hat{E}_i^q(t)$	time dependent coefficient for the PUFEM solution, corresponding to the i-th node and q-th enrichment function

$\hat{V}_i^q(t)$	time dependent coefficient of the first order time derivative of the numerical solution, corresponding to the i-th node and q-th enrichment function, for the PUFEM
a_{ij}	elements of the RKM matrix
b_i	weights of the RKM integration scheme
c_i	abscissas of the RKM integration scheme
$\mathbf{k}_i$	intermediate increments computed in the RKM integration scheme
$J_{\mathcal{D}}$	Jacobian matrix for the transformation $\mathcal{D}$

Chapter 1

Thesis introduction

1.1 Introduction

In our endeavours to understand the world we live in, and to engineer tools and products to cater to our needs, we rely heavily on modelling the physical world with mathematical equations. Owing to their complexity, these equations are often non-trivial to solve with analytic approaches. Thus, we develop strategies and procedures to solve these problems numerically.

Of particular interest to this thesis, is the domain of time dependent wave problems. These problems arise in various engineering fields, such as computational electromagnetics, acoustics and fluid dynamics. There has been considerable research on developing numerical methods to solve the wave equation. Amongst the list of numerical techniques suitable for solving the wave equation are methods such as the finite difference schemes [78], and the finite element procedures [160]. The finite difference schemes are easy to implement however their utility is limited to simple computational geometries. Whereas, the finite element techniques are very useful when dealing with complex geometries and heterogeneous material properties. Both these methods are useful for solving the interior problem but suffer with complexities associated with implementing non finite domain boundaries. Nonetheless, there exist techniques, such as the boundary element method [136], that are more suited for obtaining solutions on the domain boundary. However, these strategies suffer from scalability issues when solving for highly oscillatory wave problems. It is thus attempted through this thesis to develop efficient methodologies to solve the

wave problems, particularly suitable for high frequency applications, using the finite element approach.

1.2 Aim and objectives

Through this research it is aimed to develop special finite elements capable of solving the wave equation in the time domain. Currently, standard polynomial based finite element approaches use very fine mesh grids to capture the oscillatory behaviour of the solution. In general, this requires substantial computational effort in terms of memory and processing time. The new approach is envisaged to use very coarse mesh grids with field enrichments based on oscillatory functions. These novel elements would lead to significant reduction in the computational efforts and to better quality results in comparison to the standard finite element approach. To this end, the following research objectives are defined:

- Review the existing literature on various enrichment methodologies developed in the context of the finite element method for the numerical solution of the time dependent wave problems.
- Develop an unconditionally stable implicit approach, with enriched finite element basis using oscillatory functions, to solve the wave equation in the time domain.
- Compare the numerical accuracy of the proposed method against the standard polynomial based finite element approach.
- Formulate an explicit discretization in time and investigate the possibility of lumping the mass matrix, in conjunction with the enriched finite element basis.
- Compare the proposed implicit and explicit approaches and gauge their performance with various numerical examples.

1.3 Thesis outline

The research outlined in this thesis is presented through six chapters. In the following chapter, a brief review of different enrichment methodologies that are developed for solving the wave equation, using the finite element technique is presented. The

discussion highlights the ideas developed by various research groups that have contributed towards improving the finite element procedures in the context of solving high frequency wave problems. The chapter also motivates the use of *a priori* knowledge of physical features of the governing partial differential equation into the solution space of finite element approaches. Chapter 3 proposes a novel finite element technique using plane wave functions to enrich the solution space, for the solution of the time dependent wave equation. A semi-discrete finite element scheme in space coupled with a fully-implicit finite difference discretization in time is presented. The proposed enriched method is compared against standard high order polynomial based finite element methods in chapter 4. Several numerical examples are considered to gauge the performance of the proposed method. Further, in chapter 5, an explicit integration scheme is proposed. This explicit method is also investigated for the possibility of using a lumped mass approach with potential benefits in computational cost reduction. Suitability of the proposed enrichment method is investigated in chapter 6, for the use of various high order temporal integration schemes available in the Runge-Kutta family of methods. The algorithmic aspects of the numerical code developed to implement the proposed enrichment techniques are discussed in chapter 7, along with some real-world example problems solved using the methods developed in this research. Finally, the thesis concludes with a summary of observations made in these chapters along with some remarks on future work as discussed in chapter 8.

1.4 Research outcomes

The work carried out through this research has led to multiple journal publications and several conference papers. An account of these, including research posters presented during the course of this research for the dissemination of this work, is provided here.

1.4.1 Journal publications

- M. Drolia, M.S. Mohamed, O. Laghrouche, M. Seaid, and A.El Kacimi. Explicit time integration with lumped mass matrix for enriched finite elements

solution of time domain wave problems, *Applied Mathematical Modelling*, 2019.

- M. Drolia, M.S. Mohamed, O. Laghrouche, M. Seaid, and J. Trevelyan. Enriched finite elements for initial-value problem of transverse electromagnetic waves in time domain, *Computers and Structures*, 2017.

1.4.2 Conference presentations

- M. Drolia, M.S. Mohamed, O. Laghrouche, and M. Seaid. Numerical solution of the wave equation using the Partition of Unity Finite Element Method with explicit integration in time, *ECCM-ECFD*, UK, 2018.
- M. Drolia, M.S. Mohamed, O. Laghrouche, M. Seaid, and J. Trevelyan. Novel Finite Elements for initial value problems of light waves in the time domain, *Association of Computational Mechanics in Engineering*, UK, 2016.
- M. Drolia, M.S. Mohamed, O. Laghrouche, M. Seaid, and J. Trevelyan. Enriched finite elements for numerical solution of time dependent wave problems, *Association of Computational Mechanics in Engineering*, UK, 2015.

1.4.3 Research posters

Poster title - Numerical solution of Maxwell equations. Presented at:

- *ICE Scotland AGM poster session*, UK, 18th Nov 2014.
- *IIE Graduate School Poster Event*, Heriot-Watt University, UK, 12th Nov 2014.
- *Infrastructure and Environment Scotland PG Conference*, Edinburgh University, UK, 2nd Sept 2014.

Chapter 2

Literature review

2.1 Overview

The theory of the finite element method plays a vital role in the domain of numerical sciences. The full extent of its success and the scope of its applications could be found in various standard textbooks for the subject, see for example [53, 160] amongst others. Through this chapter it is attempted to portray the core ideas behind the enrichment methodologies used to improve the finite element technique itself, from various perspectives, in order to facilitate a broader, and more intuitive, understanding of the literature, and also to preserve the author's vantage point as an engineer. The language herein is kept simple and direct to cater to a wider audience. Section 2.2 introduces some aspects of functional analysis and discusses the foundation of the finite element method and its enrichment. Section 2.3 provides a brief review of advances in a select family of enriched finite element methods, and their application to wave propagation problems, and a summary of the discussion is outlined in the final section.

2.2 The Laplacian, the inner product and the enriched space

The Laplacian operator ∇^2 and the solution of the Laplace equation

$$\nabla^2 u = 0, \tag{2.1}$$

perhaps could be seen as the harbinger of a multitude of revolutionizing ideas in analysis. Coupled with the time derivative as

$$\frac{\partial^k u}{\partial t^k} + \alpha \nabla^2 u = b,$$

it provides a template to study the elliptic ($k = 0$), parabolic ($k = 1$) and hyperbolic ($k = 2$) family of partial differential equations. These equations arrive in a multitude of real-world problems. The elliptic family denotes steady state systems that have somehow forgotten about their history, and only depend on the boundary conditions, *e.g.* the distribution of static potential inside a charged capacitor. The parabolic family could be used to study mixing problems such as the diffusion of heat inside a material, or diffusion of chemical agents that form patterns on animal skins. The hyperbolic family, which has the center stage for this thesis, is well suited to study the oscillatory behavior observed in systems such as mechanical springs and electromagnetic waves. For simplicity, only the two dimensional (2D) problems are studied, although the ideas developed herein could be well extended to three dimensional (3D) problems.

The Laplacian also provides a great way to introduce the ideas behind various numerical techniques, and the context of this thesis in particular. Consider, for example, the solutions to the partial differential equation given by

$$\frac{\partial^2 u(x,y)}{\partial x^2} + \frac{\partial^2 u(x,y)}{\partial y^2} = 0. \tag{2.2}$$

Clearly, the solutions to (2.2) are of the form

$$u(x,y) = 1 + x + y + x^2 - y^2 + 2xy + x^3 - 3xy^2 + \dots. \tag{2.3}$$

For given boundary condition(s) the exact solution could easily be computed by scaling the individual polynomial terms appropriately to satisfy those conditions. The functions in the null space of the Laplace operator are termed as harmonic functions. The polynomials of the form (2.3) are thus often called harmonic polynomials. On a closer inspection, one can notice the fact that using the complex

numbers, the solution in (2.3) could be re-written in closed form as

$$u(x,y) = \Re\{(x+\mathrm{i}y)^n\} + \Im\{(x+\mathrm{i}y)^n\}, \tag{2.4}$$

for non-negative integer values of n. Or, using the polar form of complex numbers and the Euler's identity one could say that the solution could also be represented compactly as

$$\begin{aligned} u(x,y) &= \Re\{re^{\mathrm{i}n\theta}\} + \Im\{re^{\mathrm{i}n\theta}\}, & \text{(2.5a)} \\ &= r\cos(n\theta) + r\sin(n\theta), & \text{(2.5b)} \end{aligned}$$

for some θ and r that linearly transform the coordinates. The solution is thus visualized as a sum of sinusoidal terms of different harmonics. Decomposing a function into constant amplitude sinusoids has been known since Fourier, who used such an analysis to study the linear diffusion equation [16, 144]. Similarly, a Laplace transform reconstructs a function with sinusoids of exponential amplitudes, *i.e.*, amplitudes of the form $r = e^{\sigma}$, for real values of σ.

In order to appreciate the technique, and to develop an intuitive idea about such decomposition methods, one must seek to understand the inner products. In simple vector algebra, the inner product could be thought of as the dot product $\bar{a}\cdot\bar{b}$ that is used to define the component of a vector $\bar{a}$ in the direction of another vector $\bar{b}$. A more abstract extension of this idea is the definition of inner product $\langle\cdot,\cdot\rangle$ as (bi)linear functionals, often termed as (bi)linear forms, that linearly map a vector space to a scalar field. The Fourier and Laplace transforms could thus be thought of such linear functionals of the form

$$\begin{aligned} F(s) &= \int f(t)e^{-st}dt \\ &= \langle f(t), e^{-st}\rangle, & \text{(2.6)} \end{aligned}$$

where the latter expression suggests that the transform $F(s)$ could be seen as the component of $f(t)$ on e^{-st}. In other words, the inner product $\langle f(t), e^{-st}\rangle$ could be thought of as a way to measure just how much of $f(t)$ is contained in e^{-st}. It is rather

quite common in the field of signal processing, wherein such a linear functional is used to measure the correlation between various signals and filter out undesired components present, or to detect the occurrence of a specific event characterized by the presence of a particular signal type. Such expressions are also frequently used in the realm of physics, especially quantum mechanics. For instance, using the Bra-Ket notation, as introduced by Dirac, the inner product expression $\langle\psi|H|\psi\rangle$ is used to denote measurable quantities, such as the expectation value of the total energy of some state represented by Ket $|\psi\rangle$, scaled under the transform given by the Hamiltonian operator H.

The idea behind the Finite Element Method (FEM) is to arrange a set of well defined test functions ϕ that have compact support and belong to a suitable differentiability class C^k. These test functions are then used as the basis functions, to decompose the numerical solution inside the normed space spanned by the basis. When applied to solve a physical problem such as the wave equation

$$\frac{\partial^2 u}{\partial t^2} + \alpha\nabla^2 u = b,$$

the FEM uses the inner products to essentially construct a system of linear equations given as

$$\langle\phi, \mathcal{D}\tilde{u}\rangle = \langle\phi, b\rangle. \tag{2.7}$$

Here $\mathcal{D}$ represents the second order partial derivative operators in time and space, (*i.e.*, $\mathcal{D}\tilde{u} = \frac{\partial^2\tilde{u}}{\partial t^2} + \alpha\nabla^2\tilde{u}$) and $\tilde{u}$ denotes the best approximation of the solution to the wave equation in the vector space of the trial functions. The system of linear equations in (2.7), often termed as the weak form, is satisfied for all the functions in the test space.

Transforms, such as the one shown in equation (2.6), are used to decompose a function into an infinite series of sinusoids of continuosly varying frequencies, (*i.e.*, $s \in \{-\infty, \infty\}$). Similarly, a function can also be decomposed in terms of an infinite sum of polynomials such as

$$f(x) = \sum_{n=0}^{\infty} a_n x^n.$$

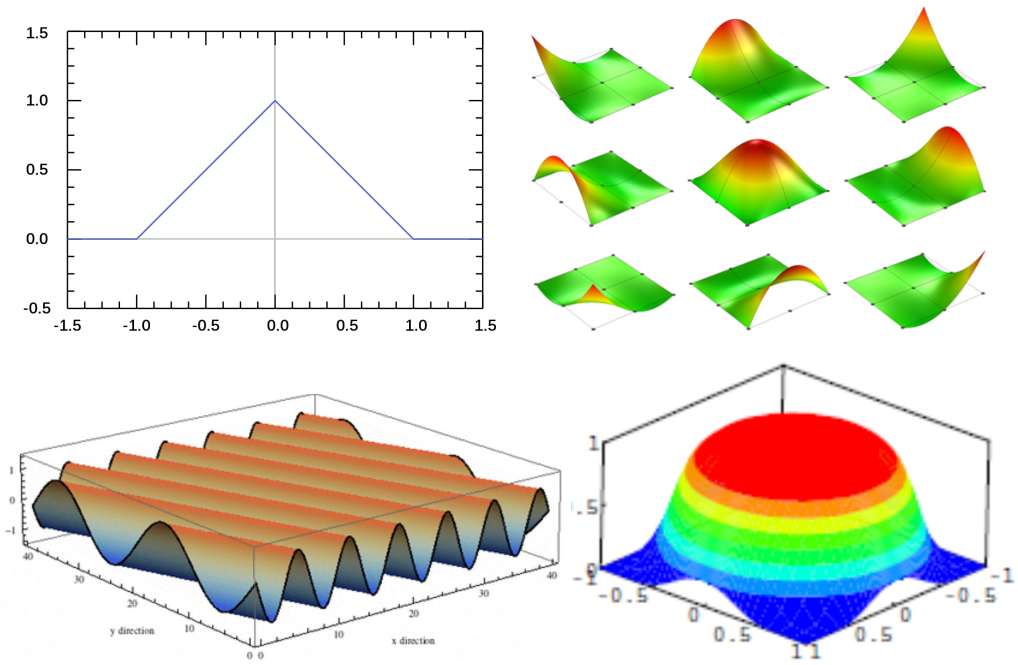

Figure 2.1: Examples of finite element hat functions $\mathcal{N}$ in 1-dimension (top-left) and 2-dimensions (top-right). Examples of enrichment functions $\mathcal{E}_q$ in 2-dimensions, a plane wave function (bottom-left) and a Gaussian function (bottom-left), are also shown in the figure.

Although such analyses are robust and useful, the computational resources are often finite and limited. Moreover, there is a range of physical problems, such as in telecommunications and high energy laser applications, in which the dominant frequencies are generally band-limited or discrete. Such problems could benefit from a reduced space of trial functions, that resemble the predicted solutions, to be used as a basis for numerical solutions. The core ideas explored in this thesis revolve around constructing trial functions of the form

$$\phi = \mathcal{N}\mathcal{E}_q,$$

where $\mathcal{N}$ represents the distributions (for example the bump function) that provide the locality and global regularity for the numerical solution, and $\mathcal{E}_q$ represents the functions that provide *a priori* knowledge to enrich the solution space and reduce the net computational cost. Some examples of these functions are shown in the Figure 2.1.

2.3 Enrichement methods and their application to wave propagation problems

The standard low-order techniques using the finite element approach face challenges when solving wave problems, pertaining to the linear dependence of the total degrees of freedom per direction on the solution wavenumber. Thus, for problems with high wavenumber, the standard FEM requires very fine meshes for analysis. Owing to this dense spatial discretization requirement, the numerical analysis of wave problems for high frequencies is computationally demanding [161].

This section discusses some promising improvements suggested by various groups and individuals to improve the efficiency of the finite element techniques, for the regime of problems wherein the solutions have large wavenumber. The common theme for the below mentioned approaches is to incorporate some *a priori* knowledge of the physical features of the solution into the approximation space of the finite element techniques. The core ideas and the application of these methodologies to various wave problems are also discussed.

2.3.1 Generalized Finite Element Method

In the standard FEM, the trial functions are composed of simple low order polynomials, often obtained using interpolation polynomials in the Lagrange form. The method converges to a desired numerical accuracy as one increases the number of nodes in an element (p-version of FEM), reduces the element size (h-version of FEM), or applies a combination of both (hp-FEM). In [4], these techniques are shown to provide exponential convergence for a suitable combination of h and p refinements. However, the computational complexity of algorithms developed with these techniques, when applied to problems with highly oscillatory solutions (*e.g.* the wave equation), is inversely proportional to the solution wavelength. Also, the singularities induced in solutions, such as due to abrupt changes in boundary conditions, are poorly resolved with standard FEM unless one uses properly refined meshes. These issues provide the motivation to search for faster and better algorithms.

Babuška *et al.* [3] propose an alternative, referred to as special finite element methods as they are of finite element type but consist of special shape functions. This

method is used to model the numerical solutions pertaining to elliptic Partial Differential Equations (PDE) for boundary value problems with highly oscillatory coefficients. They also establish the existence of solutions in the proposed trial space and also discuss convergence properties of the method when solving problems of the form

$$a_1 \frac{\partial^2 u}{\partial x^2} + a_2 \frac{\partial^2 u}{\partial x \partial y} + a_3 \frac{\partial^2 u}{\partial y^2} = f,$$

for sharply varying coefficients. This work is also discussed in [138, 140], where the authors completely generalize the special finite element method by constructing the test space as a sum of a family of special functions mixed with the polynomial shape functions. Fittingly, they term the approach as the Generalized Finite Element Method (GFEM).

2.3.2 Partition of Unity Methods

Melenk [108] in his thesis details the structure of the GFEM, introducing features such as the ability to include information about the structure of the underlying PDE to construct the finite element space. In particular, the work analyses solutions to the Laplace and the Helmholtz equations with the proposed method that exhibit approximation properties similar to those of harmonic polynomials. The work derives its motivation from reducing computational costs incurred in prohibitively expensive flavors of the h-version and the p-version of the FEM, especially for problems with sudden changes in boundary conditions or steep variations in the source term [3]. The method is shown to satisfy good local approximation properties of the trial space owing to the resemblance of the enrichment functions to the structure of the considered PDE. Melenk also presents the contrast between using a partition of unity to enforce conformity (or inter-element continuity) as compared to other methods such as using the Lagrange multipliers or using specially constructed polynomials that vanish on the element boundaries. Melenk's ideas are also summarised and published in [107], where the authors refer to it as the Partition of Unity Finite Element Method (PUFEM). The approach is also discussed in [5], where it is termed as the Partition of Unity Method (PUM). The work also outlines *a posteriori* error estimation for the PUM. Laghrouche *et al.* [92] investigate the utility of the

PUFEM in the context of time-harmonic wave problems. They suggest the usage of only a handful of plane waves clustered around the main directions of propagation, to efficiently capture the numerical solution. Moreover, owing to the continuous nature of the approximations, the number of plane wave enrichment functions used per node could vary along the finite element mesh. The method is proposed as a first step towards self-adaptive approaches for short wave problems. Their work, along with the enrichment methods proposed by Mohamed *et al.* [110] form the basis for inspiration behind the research presented in this thesis.

Rokhlin [134] presents an algorithm to provide fast solutions of the Helmholtz equation for scattering problems in two dimensions, based on decomposing the solution into Hankel functions. Beylkin *et al.* [17] propose wavelet based transforms to reduce the computational costs, whereas Canning [23] performs post-processing on the system matrix to get rid of undesired coefficients and significantly reduce the solution cost using Fast Fourier Transforms (FFT). However, he also points out that a FFT cannot be easily applied to three dimensional structures and is also restricted to uniform meshes. Canning's ideas are explored and extended by Bourdonnaye [36] to solve scattering problems in homogeneous media, using plane wave enrichments, similar to what was proposed by Melenk. Mayer *et al.* [106] also propose very similar ideas to enrich the solution space with plane waves in a predetermined set of directions close to the dominant wave propagation directions, coupled with low order finite element basis functions.

Kergrene *et al.* [84] numerically investigate the stability of GFEMs for various choices of enrichment functions. Their work also discusses the performance of iterative solvers to arrive at a converged solution for second order elliptic PDEs with piecewise smooth coefficients, using these methods. In order to account for stability of a method, they investigate the conditioning of the associated system matrix, along with the order of convergence. They account linear dependency of various test functions as a contributor to deteriorate the conditioning. Hence, to measure the degree of linear dependency between two given vector spaces, they introduce the concept of an "angle" between two vector spaces, in the sense of a predetermined inner product of the form

$$\langle u, v \rangle = \int_{\Omega} \nabla u \cdot \nabla v d\mathbf{x}.$$

Such an integral is very commonly seen in the finite element formulations of PDEs involving the Laplace operator, and form the elements of what is generally termed as the stiffness matrix. In [138], the authors suggest the usage of high performance solvers with partial pivoting to circumvent the issue of linear dependency of the finite element space and the enrichment space. Barros *et al.* [7] provide error estimates for the GFEM using local approximation of the error at the element level. To this end, they define a local error with measures such as an average value of approximation error (*i.e.*, the difference between the exact and the numerical solutions) estimated on boundaries and interior of the elements.

2.3.3 Other enriched variants of the GFEM

The popular theme amongst the above mentioned methods is of using the product of an enrichment (user defined) function with a partition of unity of space that is contained compactly within the support of an element. However, there exist meshless methods as well, such as the one proposed by Duarte [44] in his thesis. In this method, Moving Least Square Functions (MLSF) serve the purpose of a partition of unity. The MLSF are continuous functions that are constructed from a given set of unorganized sample points. To this end, a least square measure is evaluated to minimize a weighted norm. This norm is biased to limit the spread of the interpolating function around the sample points. These functions are then multiplied with polynomials or other suitable class of functions to give the so called *h*-*p* clouds [45]. Just like the trial/test functions of the *p*-FEM, these functions posses high regularity and compactness, but do not require meshes for discretizing the domain [46]. However, unlike the FEM, meshless methods do require additional care to implement the boundary conditions correctly, such as the use of Lagrange multipliers or penalty methods to impose the boundary conditions [152]. These methods also need to address the errors incurred due to the integral quadrature that in turn affects the accuracy of the resulting approximation. Some of these issues are discussed by Strouboulis *et al.* [138], where the authors propose to use the GFEM with exact boundary conditions, and use adaptive integration techniques to limit the errors incurred due to numerical integration. Liszka *et al.* [99] test the convergence of adaptive strategies with *h*-*p* clouds. The work of Oden *et al.* [118] also extends the

idea of *h-p* clouds by using finite element shape functions as the cloud-type basis functions instead of using moving least squares interpolation.

In order to facilitate the transition from Computer-Aided Design (CAD) of complex geometry to the analysis of physical problems defined on such geometry, the Isogeometric Analysis (IGA) approach [34] was introduced. In this approach, the same smooth spline shape functions are used to approximate the field variables as those used to describe the geometry. This is beneficial especially for capturing spurious waves in scattering problems owing to rough boundaries [72]. In [85] the IGA is shown to be less prone to the shift in the phase of the numerical solution, or otherwise known as the pollution error, when solving the time-harmonic wave equation. Therein, the IGA approach is used to solve for one and two dimensional scattering problems with high wavenumber in the solution. IGA has also been developed in the context of the partition of unity [117]. Dinachandra *et al.* [38] propose the Partition of Unity Isogeometric Analysis (PUIGA) approach, combining the benefits of better geometry description of the IGA and the smooth solution basis of the PUFEM. Their work compares the performances of the PUFEM, PUIGA and high order IGA methods for the solution of time-harmonic scattering problems in the two dimensions. It is observed that the PUIGA offers better convergence as compared to the PUFEM when geometry errors are present due to meshing in the PUFEM. However, the PUIGA is reported to result in poorly conditioned system matrices as compared to the higher order IGA scheme.

Similar to the GFEM, the eXtended Finite Element Method (XFEM) is introduced by Belytschko *et al.* [10, 109]. Their work derives its motivation from the limitation of the FEM for crack growth simulations that required remeshing of the domain. The idea proposed in their work is to add enrichment functions to the approximation space that contain a discontinuous displacement field, combined with the finite element shape functions to correctly represent the crack. The addition of a discontinuous field allows for the entire crack geometry to be modelled independently of the mesh. A review of the GFEM and the XFEM could be found in [11], that summarises the utility of these methods as a dynamic tool for the analysis of problems involving challenges such as modelling discontinuities, singularities, and localized deformations, predominantly common in fracture mechanics.

2.3.4 Enriched Boundary Element Methods

Enrichment methods, relevant for solving the time-harmonic wave equation for high frequency problems, have also been investigated in the context of the Boundary Element Method (BEM). In the BEM, often also termed as the Method of Moments (MoM) in electromagnetics [55], one solves the variational problem obtained through the governing partial differential equations, formulated using boundary integrals. The BEM is effective especially for geometries with low surface to volume ratios [30]. It relies on solving the Green's function, which is essentially the impulse response of the governing equations and initial/boundary conditions for the given problem [2]. The BEM can accurately model wave problems in an unbounded region but is suitable only for homogeneous media. Perrey-Debain *et al.* [122] develop the BEM to include plane wave enrichment functions for wave problems. They term this method as plane wave basis BEM. In their work, they also use extra constraints to form overdetermined system of equations to remedy the non-uniqueness of solution at certain eigenfrequencies. This overdetermined system is then solved using Singular Value Decomposition (SVD) for matrix factorization. For numerical test cases, they study the diffraction of a plane wave by a rigid circular cylinder. Their work provides comparisons of this enriched BEM with the conventional quadratic BEM. The work reports much better convergence in error against increasing solution wavenumber, at the cost of deteriorated conditioning of the system matrix. However, they also point out that, for a given degrees of freedom, the condition number of the system matrix does reduce for higher wavenumber in the solution, suggesting that the method is more suitable typically for high frequency wave problems. Diwan [39] in his thesis, investigates this method, therein addressing it as the Partition of Unity Boundary Element Method (PUBEM). His research also investigates coupling between two methods, the PUBEM and the PUFEM, to solve heterogeneous harmonic wave problems in unbounded media. The methodology is shown to result in significant savings in the total degrees of freedom required to achieve similar accuracy as compared to conventional methods. Perrey-Debain *et al.* [123] use the PUBEM to solve elastic wave scattering problems, modelled with vector based time-harmonic wave equation, with multiple wavenumbers present in the solution. The plane wave basis method, using a combination of compression

and shear waves for enrichment, is reported to provide improved efficiency over conventional BEM for solving plane elastodynamic problems. This work is later extended to assess the efficiency of using plane wave basis as enrichment in both the FEM as well as the BEM in the context of three dimensional time-harmonic wave problems [121]. The work also investigates the utility of using the plane wave basis enrichment method in pushing the limits for computational efficiency, in the regime of high frequency wave problems, as compared to the conventional FEM and BEM. Chandler-Wilde and Langdon [28, 96] review various methods for reducing the computational costs incurred in solving the time-harmonic wave equation. In their work, they also investigate the issue of numerical evaluation of oscillatory integrals, stemming from both the usage of plane waves for enrichment as well as the high frequency kernel of the governing partial differential equation. Their research also provides wavenumber dependent error estimates for their plane wave based enrichment method, applied to solve acoustic scattering problems. Similar approaches used for solving the time-harmonic Helmholtz problems, and their convergence estimates can be found in [14, 69, 119, 120]. More recently, Gimperlein *et al.* [59, 60] propose novel time discretization for the space-time systems derived from Galerkin time-domain boundary element methods for the wave equation. Independent of the aforementioned progress on using enrichment methodologies with the BEM, Prakash *et al.* [131] propose a similar formulation for solving the scattering problems. In their work, the authors divide the geometry into patches, quite similar to the domain discritization methods used for the BEM and the FEM. These patches then provide as a local support for the basis functions. They term these basis functions as the Characteristic Basis Functions (CBF). Further, they use local excitation vectors and compute the enrichment basis as the solution to the local system of linear equations. These basis functions are then ortho-normalized using a version of the Gram-Schmidt process. They fittingly term this method as the Characteristic Basis Function Method (CBFM). The method is used to model antenna arrays [102]. Mutonkole *et al.* [115, 116] extend the CBFM to incorporate multiple frequencies of interest in modelling radiation patterns in antennas over a wide bandwidth.

2.3.5 Ultra Weak Variational Formulation

Another enrichment methodology used for solving the time-harmonic wave equation is proposed by Després and Cessenat [24, 26]. Their method, termed as the Ultra Weak Variational Formulation (UWVF), derives its motivation from eliminating the dependency of numerical accuracy and stability on the mesh size, for solving elliptic linear partial differential equations. To this end, they solve a dual homogeneous Helmholtz problem, to obtain the plane wave solutions that are in turn used to construct the basis functions. Their discretization methodology is discontinuous, providing conformity enforced with extra flux and impedance conditions at element boundaries. Their work shows that the order of convergence of the UWVF method is lower bounded by a linear function of number of basis functions used per element. The UWVF method applied to solve the time-harmonic Maxwell's equations [25] provides computational cost reduction, akin to other enrichment methodologies discussed in this chapter. Huttunen *et al.* [75] validate the UWVF method with numerical examples to solve three dimensional Helmholtz problems using Perfectly Matched Layers (PML) for absorbing boundary conditions. The PML are reported to show superior performance as opposed to a low-order absorbing boundary condition for the considered problem. They also provide a condition number based measure to define the wavenumber of plane waves used as basis for each element [74]. The method is also used to solve acoustic scattering of sound from elastic surfaces, for fluid-solid vibration problems, on relatively coarse meshes. In [101] the UWVF method is extended for evanescent wave basis functions and the use of different element shapes is investigated to lower the condition number and number of degrees of freedom. The work of Buffa *et al.* [22] provides convergence analysis for the UWVF method used in cases where there is no absorbing medium present and also provide some other estimates in the case when absorption is present. In parallel to the UWVF method, Monk *et al.* [114] provide a similar nonconforming enrichment technique for solving Helmholtz problems, albeit not based on variational methods instead using the method of least-squares. They formulate the governing equations with given boundary conditions as a quadratic functional, which is symmetric and positive definite. They solve the linear system of equations, as a minimization problem, using the conjugate gradient scheme. They propose using both plane waves

as well as the Bessel functions for the basis, and provide proof of convergence. The authors address this method as the Least-Squares Method (LSM). Gamallo *et al.* provide a comparison between the LSM, the PUM and the UWVF method in [54, 73]. Their work assess the relative efficiency of each method for solving high frequency wave problems in acoustics and investigates their stability. Similarly, Hu *et al.* [70] propose a variational problem on the space spanned by the plane-wave basis functions for the discretization of time-harmonic Maxwell's equation in three dimensions. They also propose a simple preconditioner based on domain decomposition for the system generated by the proposed variational formula. In their paper, they also compare their method with the UWVF.

2.3.6 Enriched Discontinuous Galerkin Methods

The various discontinuous methods available for solving the wave equation could be seen as a member in the family of the Trefftz methods [86]. In these methods, generally the solution field is composed of two different components. One of the components provides the intra-element solution field such that it forms the kernel of the governing differential equation and minimizes the variation of the solution within the element. Whereas, the other component provides conformity by satisfying the inter-element continuity condition defined on the element boundary [66]. To solve for the wave propagation problems, the natural choice for Trefftz functions are plane waves. These plane waves when used to enrich the basis in a discontinuous Galerkin setting give rise to the Plane Wave Discontinuous Galerkin Methods (PWDGM) [67]. The PWDGM is often considered as a generalization of the UWVF of Cessenat and Després. Kapita *et al.* [83] provide a brief review of the PWDGM for scattering problems in acoustics and propose novel methods for implementing boundary conditions to reduce the errors incurred due to reflections from artificial domain boundaries. In [156–158] Yuan *et al.* investigate the usage of PWDGM for solving the anisotropic time-harmonic Maxwell's equations in the three dimensions. They also derive error estimates for the proposed discretization method for homogeneous problems, that are dependent on the condition number of the coefficient matrix. Their work also present numerical test examples for validation and show that the resulting approximate solutions generated by the PWDG possess high accuracies.

Similarly, Congreve *et al.* [32] propose an *hp*-adaptive refinement methodology for discontinuous Galerkin methods of the Trefftz family, for solving the homogeneous Helmholtz problem. In conjunction with mesh refinement and local basis enrichment, their work also incorporates adaptivity for local directions, depending on the dominant scattering direction. Their work also provides various numerical test examples to outline the efficiency of their approach. Similarly, Ladevèze *et al.* [88–90] suggest Trefftz type enrichment of the solution space when solving unbounded scattering problems. They propose the usage of Herglotz waves to enrich the solution space for the bounded region with Henkel functions to approximate the Sommerfeld radiation condition over the unbounded outer region. Their method, termed as the Variational Theory of Complex Rays (VTCR), is shown to have better convergence rates for unbounded scattering examples in two and three dimensions, against the standard BEM.

2.3.7 Discontinuous Enrichment Method

Partly motivated by the PUM, Farhat *et al.* [47] propose the Discontinuous Enrichment Method (DEM). In this method, the authors enrich the finite element polynomial field within each element using solutions to the governing homogeneous, constant-coefficient, partial differential equation. Albeit, in contrast to the PUM, the DEM harbours these enrichment functions as a sum rather than a product, i.e. the approximate solutions for the DEM are of the form

$$u^h = u^P + u^E,$$

where u^P are the standard piecewise polynomial finite element functions, and u^E are the enrichments. These enrichments do not necessarily require to be continuous along element boundaries. The conformity for the global solution in the DEM is provided in a weak sense, using extra constraints such as the Lagrange multipliers. However, for the DEM, Farhat *et al.* propose to use static condensation to eliminate the need to evaluate coefficients for the u^E. This in turn reduces the global system matrix, and the eliminated field values are computed as a post processing routine for each element. The static condensation is also reported to improve the conditioning

of the system matrix, which is a significant problem with the PUM [91]. The DEM has also been used to investigate its utility for the Helmholtz equation [48, 50], addressing domain decomposition methods with potential for scalability depending on mesh size, and solution wavenumber. Tezaur *et al.* [145] also used the DEM to solve for various scattering problems in three dimensions as well as in two dimensions [52], using plane wave basis as enrichment. Their work also compared the results obtained with the DEM against conventional FEM, and established the advantage of the former especially for short wave problems. The convergence analysis for the DEM in the context of Helmholtz equation is presented in [1], along with an *a posteriori* error estimate based on the errors in the approximation of the interior and exterior boundary conditions as well as on the discontinuities across the elements of the considered partition. Farhat *et al.* [51] further extend the DEM for higher order elements and investigate the utility of this extension for two dimensional Helmholtz problems with scatterers of length about three to thirty times the wavelength. In [159] the DEM is enriched with discontinuous pressure and shear wave functions to solve the time-harmonic elastic wave propagation problem in the frequency domain. Grosu *et al.* [61] evaluate the dispersion and numerical performance of the quadrilateral and triangular DEM elements, and investigate the conditioning of the local enrichment and the global coefficient matrices, when used in conjunction with different trigonometric and exponential enrichment functions. In [62], the authors study the numerical aspects of the hexahedral and tetrahedral DEM elements, for solving Helmholtz problems in three dimensions, showing little pollution error just as in the case of two dimensional elements. To accommodate the solutions for non-homogeneous Helmholtz problems, Tezaur *et al.* [146] investigate the usage of Taylor series expansion of spatially varying wavenumber to enrich the solution space using the DEM. In particular, they consider free-space solutions of approximations of various orders of accuracy of the homogeneous form of the governing equation, albeit with a spatially varying wavenumber within each element. Kalashnikova *et al.* [82] formulate the DEM to solve for the variable-coefficient advection-diffusion problem. To this end, they enrich the solution space with constant-coefficient, homogeneous counterpart of the governing partial differential equation. Further in [147] the DEM is formulated for a non homogeneous domain with two separate media whereby the

solution for the Helmholtz problem included evanescent waves. This work is extended to solve for three dimensional evanescent wave problems in the frequency domain by Massimi *et al.* [104], and also applied to elastodynamic analysis of harmonic vibrations of plates in two dimensions [105]. Petersen *et al.* [127] propose a space-time formulation, allowing for discontinuities in both spatial and temporal discretizations, to solve the wave equation. They use the method for numerical examples of homogeneous initial/boundary value wave propagation problems in one dimension in space. Gillman *et al.* [57] use oscillated polynomials, which are essentially the product of plane wave functions in association with Lagrange polynomials corresponding to the vertices of the spatial elements. In their method, the conformity is weekly enforced with Lagrange multipliers along the element edges. This discontinuity of the approximation enables static condensation, and thus reduces the computational complexity of the method to the total number of Lagrange multiplier degrees of freedom introduced at the edges of the spatial mesh. In [56, 58] they also develop fast solvers for time-harmonic homogeneous scattering problems. An overview and comparison of the DEM with other enrichment methods is provided in [149] for benchmark acoustic scattering problems.

2.4 Summary

A review of various enrichment methodologies developed for the finite element method in the context of numerical solution of wave problems is presented. The discussion outlines promising improvements suggested by various groups, with a common theme of incorporating *a priori* knowledge of physical features of the governing partial differential equation into the solution space of finite element approaches. Amongst the wide spectrum of these enrichment techniques, we find conformal methodologies such as the PUFEM, the GFEM and the PUBEM as well as discontinuous strategies such as the DEM, the UWVF method and the LSM. These methods are applied to a plethora of applications ranging from the solution of the time-harmonic Maxwell's equations in electromagnetics to the analysis of scattering in acoustics. In general, the various methods were developed over two decades for problems in the frequency domain whereas in the time domain based methods with

field enrichment the developments are recent. There are many other applications of these techniques such as in the problems of heat transfer and diffusion, fracture mechanics and fluid dynamics. The usage of discrete plane waves multiplied with the polynomial basis of the FEM, as proposed for the PUFEM, serves as the building block for the research traced in this thesis. The following chapters investigate the usage of the PUFEM in conjunction with different time integration schemes in the context of the hyperbolic wave equation, and provide numerical tests to validate the approach.

Chapter 3

Enriched FEM with implicit time integration

3.1 Overview

This chapter proposes a partition of unity enrichment scheme for the solution of the scalar electromagnetic wave equation in the time domain. A discretization scheme in time is implemented to render implicit solutions of systems of equations possible. The scheme allows for calculation of the field values at different time steps in an iterative fashion. The spatial grid is partitioned into a finite number of elements with intrinsic shape functions to form the bases of solution. Furthermore, each finite element degree of freedom is expanded into a sum of a slowly varying term and a combination of highly oscillatory functions. The combination consists of plane waves propagating in multiple directions, with a fixed frequency. This significantly reduces the number of degrees of freedom required to discretize the unknown field, without compromising on the accuracy or allowed tolerance in the errors, as compared to that of other enriched finite element approaches. Also, this considerably reduces the computational costs in terms of memory and processing time. Parametric studies, presented herein, confirm the robustness and efficiency of the proposed method and the advantages compared to another enrichment method. The contents of this chapter are taken from the published work in [43].

3.2 Introduction

We live in an age in which we have harnessed electromagnetic waves to engineer a wide variety of products and systems on which modern societies have come to rely. Medical imaging devices, mobile communications and electrical power generation are just a few examples of technologies that are entirely reliant on electromagnetic phenomena. While the underlying differential equations that govern these phenomena were developed in the 19th century, their application to realistic engineering problems requires numerical approximations, and engineers continue to develop more advanced computational methodologies capable of delivering these approximations with higher fidelity and with efficient use of computational resources. In this chapter we specifically address short wave problems, which are of increasing importance with the prospect of moving to millimetre wave technologies for 5G wireless systems.

We confine ourselves in this discussion to the deterministic methods, i.e. those giving a unique solution given a well-posed problem subject to prescribed boundary and initial conditions. Common numerical methods include the Finite Difference Method (FDM) [142, 143, 155] the Finite Element Method [35, 80, 129] and the Boundary Element Method [19–21]. Among these methods, the FEM is well established for dealing with complicated geometries or inhomogeneous media, and the other methods also offer certain advantages, but they all remain constrained in terms of the problem size. This is mainly due to the fact that the computational domain may be very large (electromagnetic waves often propagate in free space), so that the size of the analysis domain and of scattering objects can greatly exceed the wavelength, typically by multiple orders of magnitude [41, 150]. Since a certain number of degrees of freedom are required to capture the solution over each wavelength, such problems can result in a very large system of equations. This can render them completely intractable using conventional FEM, FDM and BEM methodologies. Different authors vary in their recommendations, but a typical rule of thumb suggests the use of ten degrees of freedom in each wavelength for linear elements. To illustrate the problem, engineers may seek to analyse the scattering of a radar wave by an aircraft. Even if the analysis domain is confined to a 100 m cube surrounding the aircraft, a finite element model would require at least 10^{12} degrees of freedom to model the scattering of a radar wave of 100 mm wavelength

to engineering accuracy.

To overcome this limitation without compromising the accuracy, the Partition of Unity enrichment method was proposed in [107] for harmonic wave problems governed by the Helmholtz equation. The method consists of enriching the approximation space with oscillatory functions that have better approximation properties compared to the standard low order polynomials usually used in the FEM. The enrichment idea spawned a large body of literature including the work on the Partition of Unity Finite Element Method (PUFEM) [40, 93, 94, 110] and also similar enrichment techniques such as the Generalised Finite Element Method [139, 141] the Ultra-Weak Variational Formulation [76, 100] and the Discontinuous Enrichment Method [49, 82, 146]. The enrichment approach is also used in other methods such as the BEM [124–126]. A recent survey on various enrichment approaches could be found in [67].

The enrichment functions used in the case of harmonic wave problems, as presented above, are in the form of plane waves or radial waves and are solutions of the partial differential equations governing the problems. This latter aspect, while useful, is not necessary for incorporating *a priori* knowledge of the solution behaviour in the approximating field. This inspired the use of intuitive field enrichment functions capable of capturing the solution behaviour while not necessarily being solutions of the problem PDE. Such enrichment was proposed for solving heat transfer problems in the time domain [111–113]. The temperature field was enriched with Gaussian functions capable of modelling the high temperature gradients and led to the use of coarse mesh grids, instead of the very fine meshes employed in standard FEM, and hence to considerable savings in the computational effort. In spite of the problem being time dependent, the enrichment functions are independent of time, which permits the re-use of a single system matrix for all time steps, resulting in even further computational saving. The success of this approach has motivated the current work in developing the field-enrichment technique to solve time-dependent wave problems. It is worth noting that an enriched model for wave propagation in one dimensional problems was presented in [87]. Recently this was extended into two-dimensional transient wave problems [63] where the solution field within each finite element is discretized with the usual Lagrangian functions and enriched with harmonic func-

tions, each with a prescribed frequency. In the current work, the PUFEM is used for the first time to solve the wave equation in the time domain. In previous work on the PUFEM only time harmonic problems were considered when solving the equation in the frequency domain. Instead here it is shown that the method could also be used for solving non-time-harmonic problems in the time domain. The wave field solution is presented as a sum of a slowly varying term and a highly oscillatory part, which is expanded into a sum of plane waves propagating in multiple directions. However, unlike other enrichment technique [63] here the plane waves have a fixed frequency. The performance of this approach is assessed for different test wave models where exact solutions are available. The results are compared to those obtained by a polynomial based FEM and also to another enrichment approach where the proposed scheme provides better accuracy at a reduced computational cost.

The chapter is organised as follows. In section 3.3 the considered problem is introduced. Then in section 3.4 the proposed PUFEM model is presented, while in sections 3.5, 3.6 and 3.7 the model is validated on several numerical test cases with analytical solutions. The chapter finishes with some concluding remarks and recommendations for future work in section 3.8.

3.3 Transverse electric mode of propagation

To describe the techniques used for enriched finite elements, consider a linear wave equation in a two-dimensional domain. Hence, let $\Omega \subset \mathbb{R}^2$ be an open bounded domain with Lipschitz continuous boundary Γ and let $[0, T]$ be the time interval for the wave propagation. The boundary-value problem considered in the current study is defined as

$$\frac{\partial^2 E}{\partial t^2} - c^2 \nabla^2 E = f(t, \mathbf{x}), \qquad (t, \mathbf{x}) \in [0, T[\times \Omega, \tag{3.1a}$$

$$\frac{\partial E}{\partial \hat{\mathbf{v}}} + hE = g(t, \mathbf{x}), \qquad (t, \mathbf{x}) \in [0, T[\times \Gamma, \tag{3.1b}$$

$$E(0, \mathbf{x}) = E^0(\mathbf{x}), \qquad \mathbf{x} \in \Omega, \tag{3.1c}$$

$$\frac{\partial E}{\partial t}(0, \mathbf{x}) = V^0(\mathbf{x}), \qquad \mathbf{x} \in \Omega, \tag{3.1d}$$

where $\mathbf{x} = (x, y)^\top$ are the Cartesian coordinates, t is the time variable, $\hat{\mathbf{v}}$ the outward unit normal on Γ, c and h are constants, and $E(t, \mathbf{x})$ the magnitude of the transverse electric field in the direction perpendicular to the domain plane. In (3.1), $f(t, \mathbf{x})$ and $g(t, \mathbf{x})$ are respectively, prescribed source and boundary functions, $E^0(\mathbf{x})$ and $V^0(\mathbf{x})$ are given initial conditions. Note that the model (3.1) represents the basis of many linear electromagnetic and acoustic wave propagation problems. For instance, applied to separate components of the linear electromagnetic field, it can represent an accurate and efficient solution for a short pulse propagating over long distances. The time integration of the system (3.1) can be carried out using any implicit scheme including Newmark methods to avoid the very small time steps that may be required in simulations for explicit time integration schemes. However, the proposed spatial enrichment is time independent and hence independent of the choice of the integration scheme. The spatial discretization is introduced after the temporal one to enable changing the temporal discretization independently on the enrichment approach presented here. Alternative integration schemes can also be found in [9, 64]. For simplicity consider the backward Euler method. The latter is well known and details could be found in standard text books [8]. Thus, to integrate the equations (3.1) in time, divide the time interval into N subintervals $[t_n, t_{n+1}]$ with length $\Delta t = t_{n+1} - t_n$ for $n = 0, 1, \ldots$. Let us use the notation W^n to denote the value of a generic function W at time t_n. Thus, given the solutions E^{n-1} and E^n at times t_{n-1} and t_n the solution at the next time step t_{n+1} is updated according to the semi-discrete equation

$$\begin{aligned} \frac{E^{n+1} - 2E^n + E^{n-1}}{\Delta t^2} - c^2 \nabla^2 E^{n+1} &= f(t_{n+1}, \mathbf{x}), \qquad n = 0, 1, 2, \ldots, \\ E^0(\mathbf{x}) &= E^0(\mathbf{x}), \\ E^{-1}(\mathbf{x}) &= E^0(\mathbf{x}) - \Delta t V^0(\mathbf{x}). \end{aligned} \tag{3.2}$$

Note that to update the solution E^{n+1} in the semi-discrete formulation (3.2) one has to solve a linear system at each time step. The structure of this linear system is mainly dependent on the mesh used in the spatial discretization and the time step

used in the time integration.

For the spatial discretization, let us multiply the equation in (3.2) by a weighting function $\phi(\mathbf{x})$, and then integrate over Ω. Using the divergence theorem and using the boundary condition (3.1b) one obtains the following weak formulation of the problem (3.1)

$$\int_\Omega E^{n+1}\phi \, d\Omega + (c^2\Delta t^2)\int_\Omega \nabla E^{n+1}\cdot\nabla\phi \, d\Omega + (c^2\Delta t^2)\oint_\Gamma (hE^{n+1})\phi \, d\Gamma = \int_\Omega \Big(2E^n - E^{n-1} + (\Delta t^2) f(t_{n+1},\mathbf{x})\Big)\phi \, d\Omega + (c^2\Delta t^2)\oint_\Gamma g(t_{n+1},\mathbf{x})\phi \, d\Gamma. \quad (3.3)$$

To solve the weak formulation (3.3) with the finite element method let us discretize the spatial domain Ω into a set of finite elements $\mathcal{T}_i$ with the index i referring to the i-th element. The combination of all these elements forms the computational domain $\Omega_h = \cup_i \mathcal{T}_i$, with $\Omega_h \subseteq \Omega$. If $\mathcal{T}_i$ and $\mathcal{T}_j$ are two different elements of Ω_h, then $\mathcal{T}_i \cap \mathcal{T}_j$ is either a mesh point, or a common side, or the empty set. The conforming finite element space for the solution that is used is defined as

$$W_h = \left\{ E_h^{n+1}(\mathbf{x}) \in C^0(\Omega) : \quad E_h^{n+1}(\mathbf{x})\Big|_{\mathcal{T}_i} \in \Psi(\mathcal{T}_i), \quad \forall\ \mathcal{T}_i \in \Omega_h \right\}, \quad (3.4)$$

with

$$\Psi(\mathcal{T}_i) = \left\{ \psi(\mathbf{x}) : \quad \psi(\mathbf{x}) = \widehat{\psi}\circ Y_j^{-1}(\mathbf{x}), \quad \widehat{\psi} \in \Psi_m(\widehat{\mathcal{K}}_e) \right\},$$

where $\widehat{\psi}(\mathbf{x})$ is a basis function defined on the element $\mathcal{T}_i$ and $\Psi_m(\widehat{\mathcal{K}}_e)$ is the set of all basis functions defined on the reference element $\widehat{\mathcal{K}}_e$. Here, $Y_i(\mathbf{x}) : \widehat{\mathcal{K}}_e \longrightarrow \mathcal{T}_i$ is an invertible one-to-one mapping.

Next, the finite element solution to $E^{n+1}(\mathbf{x})$ can be formulated as

$$E_h^{n+1}(\mathbf{x}) = \sum_{j=1}^{N_d} E_j^{n+1}\mathcal{N}_j(\mathbf{x}), \quad (3.5)$$

where N_d is the number of solution mesh points in the partition Ω_h. The coefficients E_j^{n+1} are the corresponding nodal values of the functions $E_h^{n+1}(\mathbf{x})$. They are defined as $E_j^{n+1} = E_h^{n+1}(\mathbf{x}_j)$ where $\{\mathbf{x}_j\}_{j=1}^{N_d}$ are the set of solution mesh points in the partition

Ω_h. In (3.5), $\{\mathcal{N}_j\}_{j=1}^{N_d}$ are the set of global nodal basis functions of W_h characterized by the property $\mathcal{N}_i(\mathbf{x}_j) = \delta_{ij}$ with δ_{ij} denoting the Kronecker symbol. Let us introduce $\{\mathbf{x}_1, \mathbf{x}_2, \ldots, \mathbf{x}_M\}$ as the set of M nodal points in the element $\mathcal{K}_j$. Also define $\{\varphi_j\}_{j=1}^{M}$ as the set of element basis coefficients for $\mathcal{K}_j$ in W_h characterized by the property $\varphi_i(\mathbf{x}_j) = \delta_{ij}$. Hereafter in this chapter, unless otherwise stated, the subscripts h and j are used to refer to coefficients associated with the whole mesh Ω_h and a mesh element $\mathcal{K}_j$, respectively. Note that the set $\{\varphi_j\}_{j=1}^{M}$ is a local restriction on the element $\mathcal{K}_j$ of the set of the global basis functions $\{\mathcal{N}_j\}_{j=1}^{M}$. The approximation space is then defined as

$$\widetilde{W}_h = \text{span}\left\{\mathcal{N}_h, \quad E_h^{n+1} = \sum_{j=0}^{N_d} E_j^{n+1}\mathcal{N}_j\right\}.$$

It should be stressed that most existing finite element methods applied to the model problem (3.1) employ in their formulation Lagrangian polynomials for the basis functions $\mathcal{N}_j(\mathbf{x})$. Linear and quadratic shape functions have been widely used in the literature for the finite element solution of equations (3.1), see for example [35, 129].

3.4 Partition of unity enrichment

In many applications in electromagnetic waves modelled using the equations (3.1) the solution is expected to be highly oscillatory and is often recovered over vast domains. In these situations, the numerical solution obtained by a conventional finite element method either develops spurious oscillations or it is affected by a large numerical diffusion. Spurious oscillations and excessive numerical diffusion often deteriorate the accuracy of the finite element solution, so the numerical solution may become physically unacceptable. For this reason, in most finite element methods, very fine meshes have to be used to resolve wave propagation in transient wave problems. In order to avoid the principal drawback of the conventional finite element methods (3.5), that is the requirement of very fine meshes, this research incorporates enrichment functions into the finite element space. Indeed, using the partition of unity method [107] it is possible to enrich the solution space with basis functions that have better approximation properties than the conventional polynomial basis

functions. In the current study, let us introduce a further approximation by stating that the nodal values E_i^{n+1} consist of two terms; a slowly varying term and a highly oscillatory term. The former term captures slow variations in the solution, possibly a constant, and the latter term captures the highly oscillatory variations of the solution. This yields the following enriched finite element solution

$$E_h^{n+1}(\mathbf{x}) = \sum_{i=1}^{M} \mathcal{N}_i \left(B_i^{n+1} + \sum_{q=1}^{Q-1} A_i^{q,n+1} \; e^{\mathrm{i}k(x\cos\alpha_q + y\sin\alpha_q)} \right), \tag{3.6}$$

where k is a constant wavenumber and i the imaginary number ($\mathrm{i} = \sqrt{-1}$). The approximation space enriched with plane waves, is thus now given as

$$\widetilde{W}_h = \text{span}\left\{ \mathcal{N}_h, \quad \mathcal{N}_h \; e^{\mathrm{i}k(x\cos\alpha_q + y\sin\alpha_q)}, \quad E_h^{n+1} \right\}.$$

Given the aim of this work, which is to validate the proposed enrichment model for time-dependent wave problems, the wavenumber of the enrichment functions is chosen to coincide with that of the exact solution. However, in practical applications usually involving wave scattering from physical bodies, the wavenumber of the enrichment functions should coincide with that of the impinging wave field [68]. The exponential term represents a plane wave propagating in the direction $(\cos\alpha_q, \sin\alpha_q)^\top$ with $\alpha_q = 2\pi \; q/(Q-1)$. The unknown variables are not the nodal values of the electric field any more but the amplitudes B_i^{n+1} and $A_i^{q,n+1}$ both given at the time step $n+1$ and node i. The amplitudes of $A_i^{q,n+1}$ are also given with respect to each direction α_q. For a standard FEM approach to the solution of expression (3.5) the elementary matrices are of dimension $M \times M$, whereas for the proposed model of expression (3.6) the size of the elementary matrices increases to $M_q \times M_q$ with $M_q = M \times Q$. However, the use of enrichment usually leads to coarse meshes, and hence smaller linear systems of equations to be solved.

Gauss–Legendre quadrature scheme is adopted for the evaluation of the integrals given by the weak form (3.3). Notice that in the case of the PUFEM the enrichment functions are integrated over multi-wavelength sized elements using a high number of integration points. This is important to accurately capture the oscillations within such elements. However, the computational costs remain moderate despite the large

number of integration points within each element due to the relatively small total number of elements compared to the standard FEM. It is also worth remarking that the enrichment functions in (3.6) are written using the global coordinates $\mathbf{x}$, but they are multiplied by the nodal shape functions $\mathcal{N}_j$ which are expressed in the local coordinates. For a given element $\mathcal{T}_i$, the elementary matrix is reconstructed by blocks $\mathcal{A}_{ij}$ as

$$\begin{pmatrix} \mathcal{A}_{11} & \mathcal{A}_{12} & \dots & \mathcal{A}_{1M} \\ \mathcal{A}_{21} & \mathcal{A}_{22} & \dots & \mathcal{A}_{2M} \\ \vdots & \vdots & \ddots & \vdots \\ \mathcal{A}_{M1} & \mathcal{A}_{M2} & \dots & \mathcal{A}_{MM} \end{pmatrix} \begin{Bmatrix} \mathbf{E}_1 \\ \mathbf{E}_2 \\ \vdots \\ \mathbf{E}_M \end{Bmatrix} = \begin{Bmatrix} \mathbf{b}_1 \\ \mathbf{b}_2 \\ \vdots \\ \mathbf{b}_M \end{Bmatrix}, \tag{3.7}$$

where the unknown solution $\mathbf{E}_j$, the right-hand side $\mathbf{b}_j$ and the sub-matrices $\mathcal{A}_{ij}$ are blocks that are defined below. It should be pointed out that in the proposed finite element method, the enrichment functions are associated with nodal points in each element. Hence, each block matrix $\mathcal{A}_{ij}$ in the system (3.7) is associated with the nodes i and j whereas, the corresponding block vectors $\mathbf{E}_j$ and $\mathbf{b}_j$ are associated with the node j. It is also evident that the size of the elementary matrix and the associated vectors (3.7) vary depending on the number of the element nodes as well as the number of enrichment functions Q. The higher the number of element nodes or the higher Q is the larger the size of the elementary matrix (3.7). The individual

blocks $\mathcal{A}_{ij}$, $\mathbf{E}_j$ and $\mathbf{b}_j$ can be reformulated as

$$\mathcal{A}_{ij} = \begin{pmatrix} a_{ij}^{11} & a_{ij}^{12} & \dots & a_{ij}^{1Q} \\ a_{ij}^{21} & a_{ij}^{22} & \dots & a_{ij}^{2Q} \\ \vdots & \vdots & \ddots & \vdots \\ a_{ij}^{Q1} & a_{ij}^{Q2} & \dots & a_{ij}^{QQ} \end{pmatrix}, \qquad \mathbf{E}_j = \begin{Bmatrix} B_j^{n+1} \\ A_j^{2,n+1} \\ \vdots \\ A_j^{Q,n+1} \end{Bmatrix}, \mathbf{b}_j = \begin{Bmatrix} b_j^1 \\ b_j^2 \\ \vdots \\ b_j^Q \end{Bmatrix},$$

Assuming that the nodes i and j are not on the domain boundary then entries of the above blocks can be written as

$$b_j^1 = \int_\Omega \Big(2E_j^n - E_j^{n-1} + \Delta t^2 f(t_{n+1}, \mathbf{x})\Big)\mathcal{N}_j \, d\Omega,$$

and

$$b_j^s = \int_\Omega \Big(2E_j^{s,n} - E_j^{s,n-1} + \Delta t^2 f(t_{n+1}, \mathbf{x})\Big)\mathcal{N}_j e^{\mathrm{i}k(x\cos\alpha_s + y\sin\alpha_s)} \, d\Omega$$

where $s = 2, 3, \dots, Q$. Also,

$$a_{ij}^{11} = c^2\Delta t^2 \int_\Omega \Big(\nabla\mathcal{N}_i \cdot \nabla\mathcal{N}_j + \mathcal{N}_i\mathcal{N}_j\Big) \, d\Omega,$$

and

$$a_{ij}^{sq} = c^2\Delta t^2 \int_\Omega \Big(\nabla\left(\mathcal{N}_i e^{\mathrm{i}k(x\cos\alpha_s + y\sin\alpha_s)}\right) \cdot \nabla\left(\mathcal{N}_j e^{\mathrm{i}k(x\cos\alpha_q + y\sin\alpha_q)}\right)$$

$$+ \left(\mathcal{N}_i e^{\mathrm{i}k(x\cos\alpha_s + y\sin\alpha_s)}\right)\left(\mathcal{N}_j e^{\mathrm{i}k(x\cos\alpha_q + y\sin\alpha_q)}\right)\Big) \, d\Omega$$

where $s = 2, 3, \ldots, Q$ and $q = 2, 3, \ldots, Q$. Assembling the elementary matrices, the numerical solution of the problem (3.1) is obtained by solving at each time step a linear system of the form

$$\mathbf{A}\mathbf{E}^{n+1} = \mathbf{b}, \tag{3.8}$$

where the system matrix $\mathbf{A}$ is symmetric and composed of the block matrices $\mathcal{A}_{ij}$ which are zero block matrices unless the nodes i and j belong to the same element. Note that similar to the standard finite element methods, the assembly process needs to consider the nodes shared between the elements. However, in the proposed enriched finite element method the overlapping part of the matrix includes an entire block matrix $\mathcal{A}_{ij}$ rather than a single entry.

It is worth remarking that at each time step, the solution procedure automatically provides the amplitudes of the different enrichment functions used. In the current study, the system matrix is factorized using an LU decomposition at the first time step; thus, the solution is reduced into backward/forward substitutions. This can significantly increase the efficiency when a large number of time steps is needed, compared to updating the matrix and fully solving the system at every time step. Note that the conventional finite element method also offers time independence, but the considerably greater system size may preclude us from computing, storing and re-using an LU decomposition.

Next, to evaluate the performance of the proposed partition of unity finite element method (PUFEM) let us solve several numerical tests for transverse electromagnetic waves. To this end, let us use models with known analytical solutions of the boundary-value problem (3.1) such that the error can be quantified. Here, the analytical solutions involved in the first test cases include a plane wave, waves with a varying wavenumber and a Hankel source then in the second case it is a progressive cylindrical wave while in the last case it is a wave front progressing inside a stationary domain. Let us calculate the relative error in $L^p(\Omega)$ as

$$\text{Error} = \frac{\|E_h - E\|_{\mathrm{L}^p(\Omega)}}{\|E\|_{\mathrm{L}^p(\Omega)}},$$

where E_h is the numerical solution and E the analytical solution of the problem under study. The first test examples are taken from reference [63]. The performance

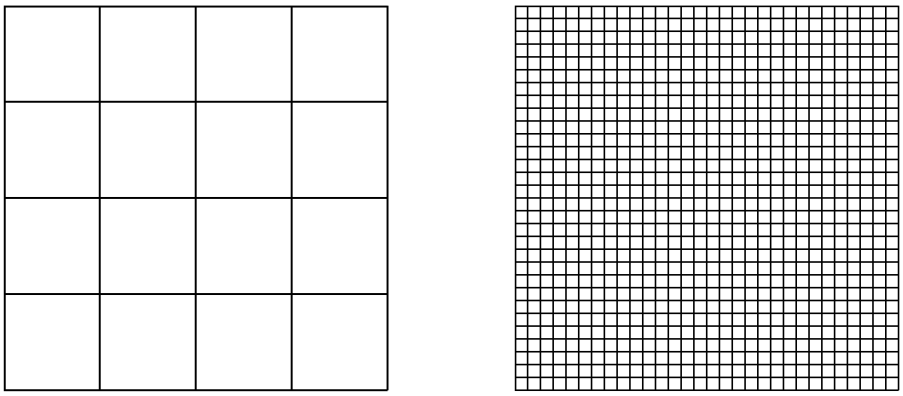

Figure 3.1: Mesh with 25 nodes used in the PUFEM mesh (left) and mesh with 961 nodes used in the FEM (right).

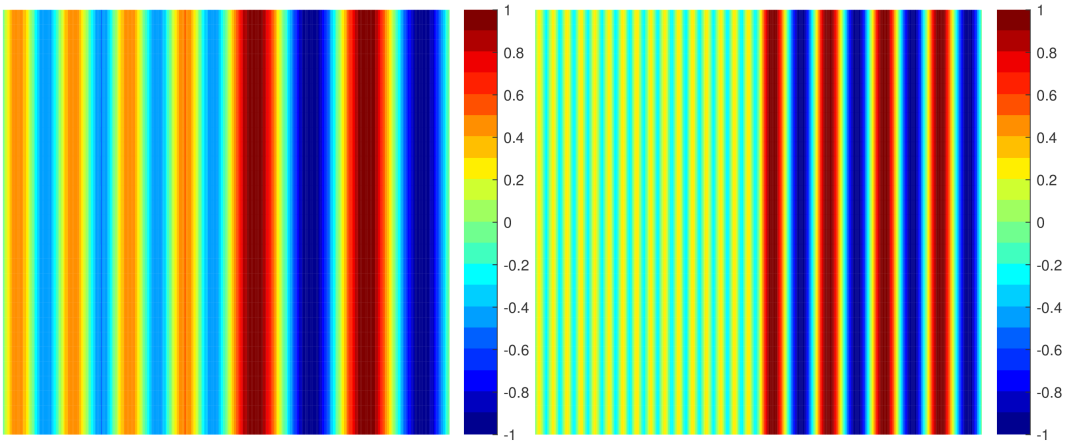

Figure 3.2: Comparison with previous work: PUFEM solution of the discontinuous k case 1 (left) and case 2 (right).

of the approach presented here is compared to the approach used in [63]. For the last two test examples the numerical results obtained using the PUFEM are compared to those obtained using the conventional finite element method results. The Central Processing Unit (CPU) time is measured in seconds on a machine running Ubuntu 14.04 LTS (64 bit) with an Intel® Core™2 Quad CPU Q8300 @ 2.50GHz × 4 and 4GB of RAM.

3.5 Comparison with previous work

In this section the aim is to compare the performance of the PUFEM to a previous approach [63]. It should be noted that all the following problems are initialized at $t = 0.0$ and solved for a single iteration in time with the step size $\Delta t = 10^{-4}$.

First, let us choose the progressive plane wave example proposed in [63] where the

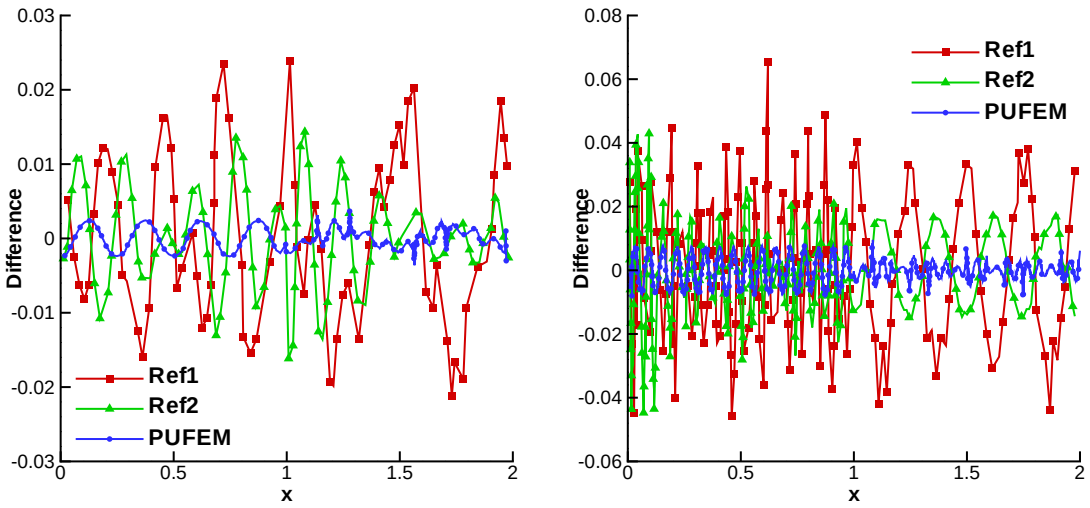

Figure 3.3: Comparison with previous work: absolute difference between the exact and the numerical solutions of the discontinuous k at $y = 0$ case 1 (left) and case 2 (right).

exact solution is given by $E = A\sin(kx - \omega t)$. Here A is the wave amplitude and ω is the angular frequency. A constant wavenumber $k = 4\pi$ and a constant phase velocity $c = \frac{\omega}{k} = 1$ are also considered. The problem is solved over the spatial domain $[0, 1] \times [0, 1]$ which is discretized into a 4×4 uniform mesh of 4-noded linear elements, with a total of $M = 25$ nodes in the mesh, as shown in Figure 3.1. Two plane waves with the same k as that of the problem and at the angles 0 and π, are used for enrichment together with the slowly varying term, *i.e.*, $Q = 3$ here. Hence, the total number of degrees of freedom is $25 \times 3 = 75$. The solution L_2-norm error is $7.9 \times 10^{-5}\%$. The same problem is solved in [63] on a 10×10 uniform mesh of 4-noded elements and with the cutoff numbers $(2, 2)$ leading to 3025 degrees of freedom and an L_2-norm error of the order 1.0%. When comparing these parameters, *i.e.*, total degrees of freedom and numerical error, with those for the PUFEM, the reduction of overall degrees of freedom and the improvement of the numerical approximation confirms the efficiency of the PUFEM in solving this type of problems.

To compare the two approaches further let us consider another test example that is also published in [63]. Again let us consider the same exact solution as before but now A, k and ω may vary in space in a piecewise-constant fashion. The spatial domain is $[0, 2] \times [0, 2]$. In the reference the problem is solved for two cases. Each case involves different wavenumbers which are also considered here. In the first half of the domain $[0, 1] \times [0, 2]$ we have $A = 0.5, k = 8\pi$ and $\omega = 8\pi$ (case 1) and

$A = 0.25, k = 32\pi$ and $\omega = 32\pi$ (case 2) while in the second half $[1, 2] \times [0, 2]$ we have $A = 1, k = 4\pi$ and $\omega = 4\pi$ (case 1) and $A = 1, k = 8\pi$ and $\omega = 8\pi$ (case 2). Compared to the previous test this is a more challenging problem due to the discontinuous parameters. The computational domain is discretized using 14 uniform 4-noded linear elements and a total of 30 nodes in case 1 and 24 uniform 4-noded linear elements and a total of 50 nodes in case 2. The same enrichment as before is also used where the enrichment wavenumbers at each node are chosen to match those of the problem at the same node. The total number of degrees of freedom is now 90 in case 1 and 150 in case 2. Figure 3.2 shows the numerical solution obtained with the PUFEM for both cases. Figure 3.3 shows at the cross section ($y = 0$) the difference between the exact solution and the numerical solution using the PUFEM, compared to that of the solution in [63]. Note that in the figure, the errors on the boundary are not zero. This is simply because we do not solve a Dirichlet problem on the boundary, as is evident from equation (3.1). The results in [63] are obtained with enrichment and using linear elements and quadratic elements which are referred to as Ref1 and Ref2, respectively, in the figure. The results show that using similar numbers of degrees of freedom or even fewer, the PUFEM leads to about one order of magnitude smaller differences compared to the results in [63]. Obviously, the two previous test examples can be reduced into one-dimensional problems. To confirm that the PUFEM approach can also work for two-dimensional problems let us again consider the second test example but with the exact solution now given as $E = A\sin(kr - \omega t)$ where r is the distance from the point $(0.5, 0)$. The wave is now cylindrical while it was plane before. The amplitude A, wavenumber k and the angular frequency ω are now dependent on r such that for $0 \leq r < 1.5$ we have $A = 0.5$, $k = \omega = 8\pi$ and otherwise $A = 1$, $k = \omega = 4\pi$. The computational domain is bounded on the outside by the square $[-2.0, 2.0] \times [-2.0, 2.0]$ and on the inside by a unit circle centred at the origin. To solve the problem with the PUFEM the domain is meshed into eight 9-noded quadratic elements shown in Figure 3.4 with the total number of nodes being 48. The solution space is enriched with 27 functions including 26 evenly spaced plane waves. Again here the wavenumber of the enrichment functions at any node, is chosen to match the problem wave number at the same node. The total number of degrees of freedom in this case is 1296.

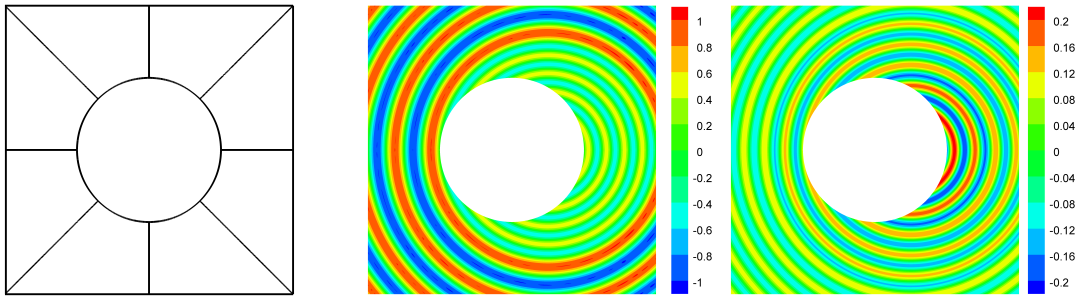

Figure 3.4: Comparison with previous work: Mesh (left) and the real part of the numerical solution for the cylindrical wave (middle) and the Hankel source (right).

Figure 3.4 shows the PUFEM solution of the problem where the achieved L_2-norm error in this case is 0.5%.

Finally, let us consider the Hankel source test example that is also published in the same reference [63]. The exact solution of the problem is given by $E = \mathrm{H}_0^{(1)}(kr)e^{-\mathrm{i}\omega t}$ where $r = \sqrt{(x-x_0)^2 + (y-y_0)^2}$ and $\mathrm{H}_0^{(1)}$ is the Hankel function of the first kind and order zero while $x_0 = 0.5$, $y_0 = 0$ and $k = \omega = 22$. The same computational domain and mesh as in the previous case are also considered here, however, now use $Q = 25$. The PUFEM solution is shown in Figure 3.4 where the L_2-norm error is 0.2% and is achieved with $M \times Q = 48 \times 25 = 1200$ degrees of freedom. The error achieved in the reference is about 4% using 9-noded elements with the total number of nodes being 576. In the reference, the used cut-off number is $(2, 2)$ which leads to the total number of degrees of freedom 14400. Again the efficiency of the proposed approach can be clearly seen from the reduction in overall degrees of freedom and improvement of numerical accuracy.

3.6 Cylindrical progressive wave problem

In the section let us consider the problem of recovering a progressive cylindrical wave in a unit squared domain. Here let us solve the boundary-value problem (3.1) in $\Omega = [0.1, 1.1] \times [0.1, 1.1]$ subject to the initial conditions

$$E_0 = e^{\mathrm{i}kr},$$

$$V_0 = e^{\mathrm{i}kr}\big(-\mathrm{i}\omega\big),$$

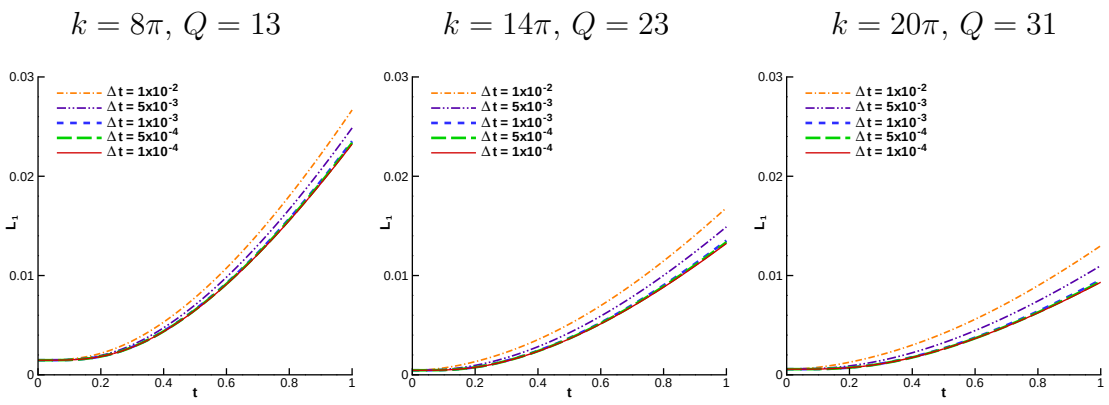

Figure 3.5: Cylindrical wave problem: the relative errors for different wavenumbers and different time step sizes.

where $r = \sqrt{x^2 + y^2}$ is the length of the position vector. The source term $f(t, x, y)$ and the boundary $g(t, x, y)$ function in (3.1) are defined such that the analytical solution of this test problem is a progressive cylindrical wave given by

$$E(t, x, y) = e^{\mathrm{i}(kr - \omega t)}. \tag{3.9}$$

Note that the function $g(t, x, y)$ is defined on each domain edge according to the relevant normal direction and the constant $c = \omega/k$ in equation (3.1a) becomes the phase velocity.

3.6.1 Sensitivity of the results on time steps

The first aim in this test example is to study the convergence of the proposed approach with respect to the time step size. Three wavenumbers are considered, namely $k = 8\pi$, 14π, and 20π with only one angular frequency $\omega = 1$. Therefore, the phase velocity c decreases with increasing wavenumber. The number of wavelengths contained in the domain will increase from 4 with the smallest wavenumber to 10 with the highest wavenumber considered in the simulations. The problem is solved using the PUFEM on the coarse mesh of 16 uniform 4-noded linear elements shown in Figure 3.1. The solution space for the wavenumber $k = 8\pi$ is enriched with $Q = 13$. For the higher wavenumbers considered, the number of enrichment functions is increased to $Q = 23$ for $k = 14\pi$ and to $Q = 31$ for $k = 20\pi$. The wavenumber of the enrichment functions is chosen to be the same as the wavenumber of the exact solution. Consider five time steps in the simulation, $\Delta t = 1.0 \times 10^{-2}$,

5.0×10^{-3}, 1.0×10^{-3}, 5.0×10^{-4}, and 1.0×10^{-4}. The results for the cylindrical wave are presented in the time interval $[0, 1.0]$. It should be mentioned that using the same mesh and only changing the number of enrichment functions for different wavenumbers is a particularly useful feature of the proposed PUFEM. Otherwise using the standard FEM, increasing the values of wavenumbers requires refining the mesh.

The evolution of the relative error in time is plotted in Figure 3.5 for all the considered wavenumbers and time step sizes. Note that the numerical error at time $t = 0$ is not zero, which is counter-intuitive because the initial conditions provide the exact values of the solution at time $t = 0$. However, in the plots, the time essentially starts at $t = \Delta t$ and not at $t = 0$. Thus, the first numerical error is essentially the error at time $t = \Delta t$.

For each wavenumber the figure shows that decreasing the time step Δt always reduces the relative error. At very small time steps this reduction in the error becomes insignificant. This can be seen with the relative errors for $\Delta t = 1.0 \times 10^{-3}$ and 5.0×10^{-4}, which are very close to each other, while those for $\Delta t = 5.0 \times 10^{-4}$ and 1.0×10^{-4} are almost identical. This is attributed to the fact that for small time steps the errors in the simulated solutions are dominated by the spatial discretization rather than the time integration procedure. Once the error in the numerical solution becomes dominated by the spatial error, refining Δt cannot further reduce the relative errors. The same behaviour is consistently observed for the three wavenumbers considered in the simulations. It also can be added that the proposed approach is similar to the standard FEM in that the convergence in time needs to be checked by considering a finer time step and rerunning the analysis. Once the error cannot be further reduced by refining the time step one may conclude that the solution has converged in time.

The results show that the proposed enrichment approach is stable as refining Δt reduces the relative errors in the obtained results. Another observation about this set of results is that for a given time step Δt, the accuracy of the numerical solution increases with a higher wavenumber. For example the maximum relative error with $k = 8\pi$ and for $\Delta t = 1.0 \times 10^{-2}$ is about 0.028 at time $t = 1$, while for the same Δt and at the same time $t = 1$ the error is about 0.012 for $k = 20\pi$. This is expected

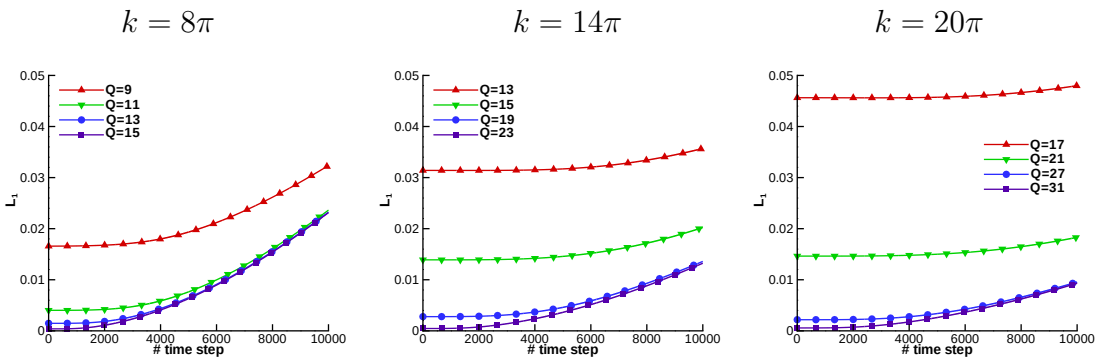

Figure 3.6: Cylindrical wave problem: relative errors obtained for the three considered wavenumbers and for different Q where $\Delta t = 1.0 \times 10^{-04}$.

because for a higher wavenumber, the phase velocity $c = \frac{\omega}{k}$ becomes smaller. Hence, for a given time step Δt it is more accurate to capture a slower variation than a quicker one.

3.6.2 Sensitivity of the results on number of enrichments

The next aim in this test example is to study the convergence of the proposed approach for an increased number of enriching plane waves. As mentioned earlier the use of at least ten degrees of freedom per wavelength is a requirement for the FEM to achieve engineering accuracy of about 1%. This number is reduced to about 2.5 degrees of freedom per wavelength or even less when using the PUFEM [93].

Here, the same wavenumbers and angular frequency are retained from the previous set of results. The problem is solved using the PUFEM on the previous mesh and using the time step size $\Delta t = 1.0 \times 10^{-4}$ as this leads to the lowest error in the previous set of results. The numbers of enrichment functions considered for $k = 8\pi$ are $Q = 9$, 11, 13 and 15. The numbers of enrichments for $k = 14\pi$ are $Q = 13$, 15, 19 and 23 while for $k = 20\pi$ use $Q = 17, 21, 27$ and 31. The simulation is carried out for 10000 time steps.

As in the previous situation, Figure 3.6 presents the evolution in time of the relative errors computed for each wavenumber. It is evident that adding more plane waves in the enriched finite element space improves the solution accuracy for all considered cases. This can be clearly seen in Figure 3.6 at the early time steps. As the simulation progresses in time the error accumulates faster with a higher Q and the difference between the errors obtained with different numbers of enrichment

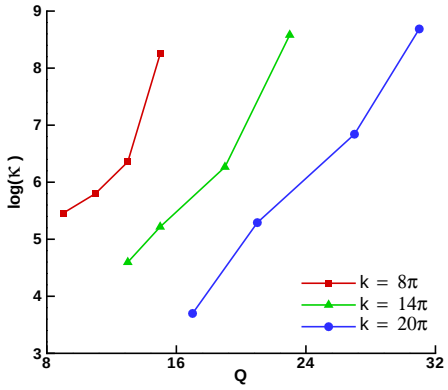

Figure 3.7: Cylindrical wave problem: conditioning of the linear system of equations resulting from the PUFEM for the cases shown in Figure 3.6 plotted against Q.

functions becomes smaller. For example for $k = 8\pi$ after 4000 time steps the errors with $Q = 13$ and 15 become similar and then after 7000 time steps the errors with $Q = 11$, 13 and 15 become similar. For the considered wave conditions, as a higher wavenumber is considered in the simulations the accumulation of errors in time seems to become slower. However, for a given fixed wavenumber, a higher number of enrichment functions always accumulates errors faster.

It is also worth remarking in Figure 3.6 that for the same number of enrichment functions Q the relative error in the numerical solution accumulates faster for a lower wavenumber. For example, using $Q = 15$ with $k = 8\pi$ the relative error increases from less than 4×10^{-4} at the first time step to about 0.025 at the final time $t = 1$. However, for the same number of enrichment functions $Q = 15$ but with $k = 14\pi$ the relative error is 0.014 at the first time step and 0.020 at the end time $t = 1$. The relatively faster increase in the relative error at a lower wavenumber compared to a higher wavenumber may be attributed to the conditioning in the associated linear system that is well-known to affect the PUFEM; see for example [93, 110]. To further demonstrate this issue, let us display in Figure 3.7 the condition numbers κ of the system matrix of equation (3.8), for the cases considered in Figure 3.6. These results show that for the same enrichment number Q a higher wavenumber always leads to a better conditioned linear system. The plots also reveal that for $k = 8\pi$, a condition number of order 10^8 is the outcome for the case with $Q = 15$ while the number of enrichment functions which produce a comparable condition number is $Q = 23$ for $k = 14\pi$ and $Q = 31$ for $k = 20\pi$. Hence, for a fixed mesh and a

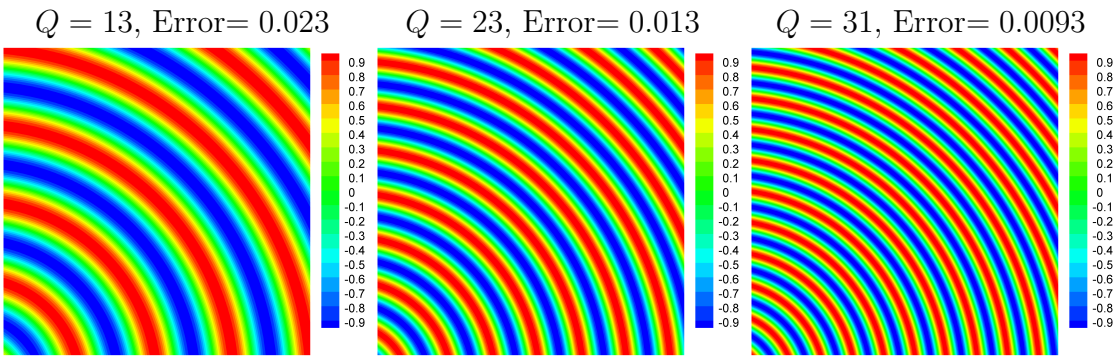

Figure 3.8: Cylindrical wave problem: imaginary part of the PUFEM solution at $t = 1.0$ for the wavenumbers $k = 8\pi, 14\pi$ and $k = 20\pi$ from left to right.

fixed condition number the number of enrichment functions can be increased when a higher k is considered. In fact the ratio between the element size and the wavelength determines the maximum number of enrichment functions that will lead to the ill-conditioning being controlled such that an accurate solution can be obtained. Having larger elements that span more wavelengths leads to better conditioned systems even with higher numbers of enrichment functions. For a better insight we also display in Figure 3.8 the imaginary parts of the numerical solutions obtained sing the PUFEM.

3.6.3 Comparison to the standard finite element method

The final aim in this test problem is to compare the performance of the proposed approach to the standard FEM. The aspects compared include the number of degrees of freedom and the CPU time required to achieve a fixed relative error and the accumulation of relative errors in time. For this study let us consider the test case with wavenumber $k = 6\pi$ and angular frequency $\omega = 1$ while keeping the time step fixed to $\Delta t = 1.0 \times 10^{-4}$ over the time interval $[0, 1]$. It should be noted that the selected wavenumber is relatively small because of the excessive computational cost required for the FEM to resolve this test problem, since a large number of time steps is considered to measure the accumulation of errors in time.

The problem is first solved using the FEM on the fine mesh shown in Figure 3.1. The relative error achieved using the FEM at the first time step is about 0.0026 where the total number of degrees of freedom is $N_{dof} = 961$. Then the problem is solved using the PUFEM on the coarse mesh shown in Figure 3.1. Two different

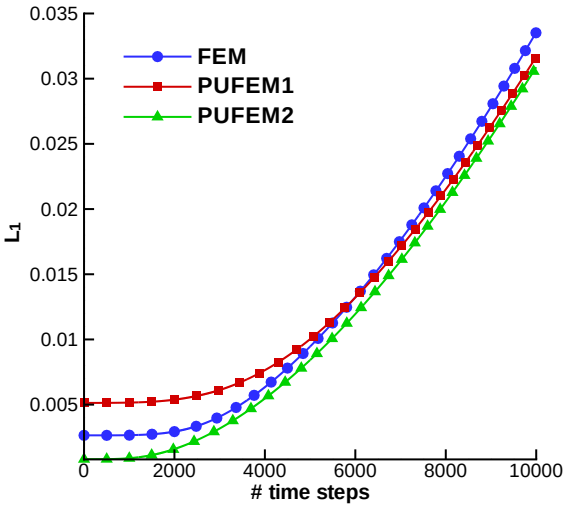

Figure 3.9: Cylindrical wave problem: relative error norms observed with the PUFEM and the FEM.

numbers of enrichment functions are considered, namely $Q = 9$ and $Q = 11$. The solution with the first enrichment number is referred to as PUFEM1 while the second as PUFEM2. The errors obtained at the first time step with PUFEM1 is 0.005 while with PUFEM2 it is 0.0008. The total numbers of degrees of freedom with the PUFEM1 and PUFEM2 are $N_{dof} = 225$ and $N_{dof} = 275$, respectively. In comparison to the FEM this is a reduction of about $77\% \sim 71\%$ in the required number of degrees of freedom to achieve a similar or even better relative error in this test problem. When using the FEM the CPU time needed to build the linear system of equations is 48.4s at the first time step. However, this time is reduced to 6.1s with PUFEM1 and 6.3s with PUFEM2. Starting from the second time step the FEM needs 37.7s to update the right hand side of the linear system while both PUFEM1 and PUFEM2 require less than 0.1s. To solve the linear system the CPU needs less than 0.1s in all the cases due to the relatively small system matrix.

Figure 3.9 illustrates the error accumulation in time for the FEM compared to the PUFEM1 and the PUFEM2. The plot shows that the accumulation of the relative error is faster using the FEM compared to the PUFEM1. Note that the PUFEM1 starts from a higher error than the FEM, however at about 6000 time steps the relative error using the FEM and the PUFEM1 becomes equal to 0.0132. Thereafter the relative error using the PUFEM1 becomes better than that obtained using the FEM. The relative errors obtained using the PUFEM2 remain consistently lower than those with the FEM and the PUFEM1. At the end of the simulation after

10000 time steps, the relative errors obtained using the FEM, the PUFEM1 and the PUFEM2 are 0.034, 0.032 and 0.031, respectively.

To compare the number of degrees of freedom let us calculate the number of degrees of freedom per wavelength $\tau = \lambda\sqrt{N_{dof}}$. For an acceptable engineering accuracy, a rule of thumb is to use at least ten degrees of freedom per wavelength when solving similar wave problems with the FEM. The number used here is $\tau \approx 10.33$. On the other hand for the PUFEM and in order to achieve a similar or a better accuracy $\tau \approx 5$ is enough in this set of results. In fact in the previous set of results where wavenumbers higher than $k = 6\pi$ are considered, $\tau = 2.5$ is sufficient to obtain reasonable engineering accuracy in this test example. For instance, in the first set of results for $k = 20\pi$ and $Q = 31$ an accuracy better than 1% is achieved with $\tau \approx 2.7$. This shows the potential of the proposed approach for solving transient wave problems.

As a final comment it is worthy to mention that the effect of eliminating the slowly varying part of the enrichment (3.6) referred to by B_i^{n+1}, has an insignificant effect on the accuracy of the results in this test example. All the simulations presented in the current study are also repeated with the term B_i^{n+1} having been eliminated from the equation (3.6). This elimination has not changed the results, and this is expected because the solution varies quickly throughout the computational domain. The slowly varying term does not contribute to the numerical solution of this wave problem. However, the second test example provides an alternative platform to study the effect of including the slowly varying terms in the enrichment (3.6). It should be stressed that when B_i^{n+1} is eliminated the directions of the plane waves vary according to $\alpha_q = 2\pi q/Q$ and not $\alpha_q = 2\pi q/(Q-1)$ as before, such that the nodal degrees of freedom are expanded into plane waves only.

3.7 Moving envelope problem

In this section let us consider the problem of a moving envelope governed by the transient wave problem (3.1). The source and boundary functions in (3.1) are defined such that the exact solution of this problem is given by

$$E(t,x,y) = Ae^{\mathrm{i}wf_L(t,x,y)}, \tag{3.10}$$

where $f_L(t, x, y)$ is the propagator function which provides a means to control the initial condition of the problem and can be used to manipulate the envelope of the moving wave such that the solution is a wave expanding symmetrically about the origin with evolution in time. In this example let us examine the performance of the proposed PUFEM for this test example using two types of propagators F_1 and F_2 described in detail in Appendix A.1 and Appendix A.2, respectively. Here, the propagator function F_1 behaves like a signum function and hence exhibits a sudden peak at the start of the envelope due to its discontinuous derivative as shown in Appendix A.1, whereas the other function F_2 has a continuous derivative and provides a smoother transition slope, which can be seen in Appendix A.2.
The computational domain in this test case is also considered to be a unit square and two wavenumbers $k = 4\pi$ and 8π are considered in the simulations. The time step and the angular frequency are $\Delta t = 1.0 \times 10^{-2}$ and $\omega = 1$, respectively. The domain is placed such that the wave will only enter after a time period equivalent to 100 time steps. The wave is initiated at the centre of the coordinate system, hence, the domain is defined by $\Omega = [c \times 100\Delta t, c \times 100\Delta t + 1] \times [c \times 100\Delta t, c \times 100\Delta t + 1]$. The considered time span starts from the wave entrance into the domain until the oscillations cover the entire computational domain. The problem is initialized with E^0 and V^0 which are obtained from the analytical solution (3.10) and its derivative at time $t = 0$. As in the previous test example, let us use the weak form (3.3) and solve for the amplitudes.

3.7.1 Discontinuity in time

The first aim in this example is to compare the proposed PUFEM to the standard FEM when recovering the solution with and without a discontinuity in time. The analytical solution with the F_1 propagator is used to measure the relative errors for the discontinuous case while the F_2 propagator is used for the continuous case. Let us solve the problem for $k = 4\pi$ using the PUFEM with $Q = 11$ on the coarse uniform mesh shown in Figure 3.1. In this situation, the total number of degrees of freedom is $N_{dof} = 275$. The wavenumber of the exact solution is also considered for the enrichment. The problem is then solved again using the FEM on two meshes. The first mesh, referred to as FEMc, is relatively coarse and composed of 361 uniform

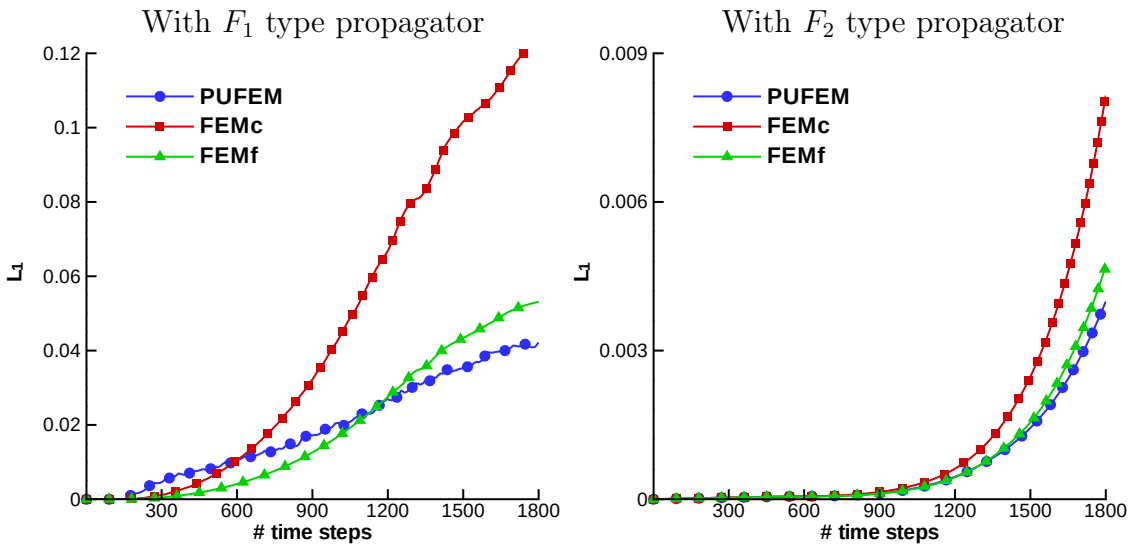

Figure 3.10: Moving envelope problem: comparison of the PUFEM with $Q = 11$ and the FEM on different meshes for the two types of propagators and for $k = 4\pi$

linear elements and 400 nodes. The second mesh is referred to as FEMf and is a fine mesh composed of 1521 elements and 1600 nodes. The obtained results are depicted in the time interval $[0, 18]$.

Figure 3.10 shows the evolution of the relative errors for both propagators F_1 and F_2 using the FEM on the two meshes as well as the PUFEM. The results using the F_1 propagator illustrate a relatively rapid increase in the relative error for both the FEM and the PUFEM. At earlier time steps the relative error increases faster in time for the PUFEM than for the FEM, hence, at $t = 4.0$ the results obtained using the PUFEM exhibit an error of about 0.006 while errors in the results obtained using the FEMc and the FEMf are 0.003 and 0.001, respectively. Thereafter the accumulation of the relative error in time becomes faster with the FEM such that at about $t = 6.0$ the error with the PUFEM (0.010) becomes slightly smaller than with the FEMc (0.011). Later at about $t = 11.5$ the PUFEM error (0.024) also becomes smaller than the FEMf error (0.025). At the end of the considered time span the errors with the PUFEM, the FEMc and the FEMf become $0.042, 0.124$ and 0.053, respectively.

On the other hand the results using the F_2 propagator show a gradual increase in the relative error compared to the discontinuous case. The final error with both methods remains below 1% at $t = 18$. Therefore one may conclude that the high values of relative errors in the previous case are mainly due to the discontinuous

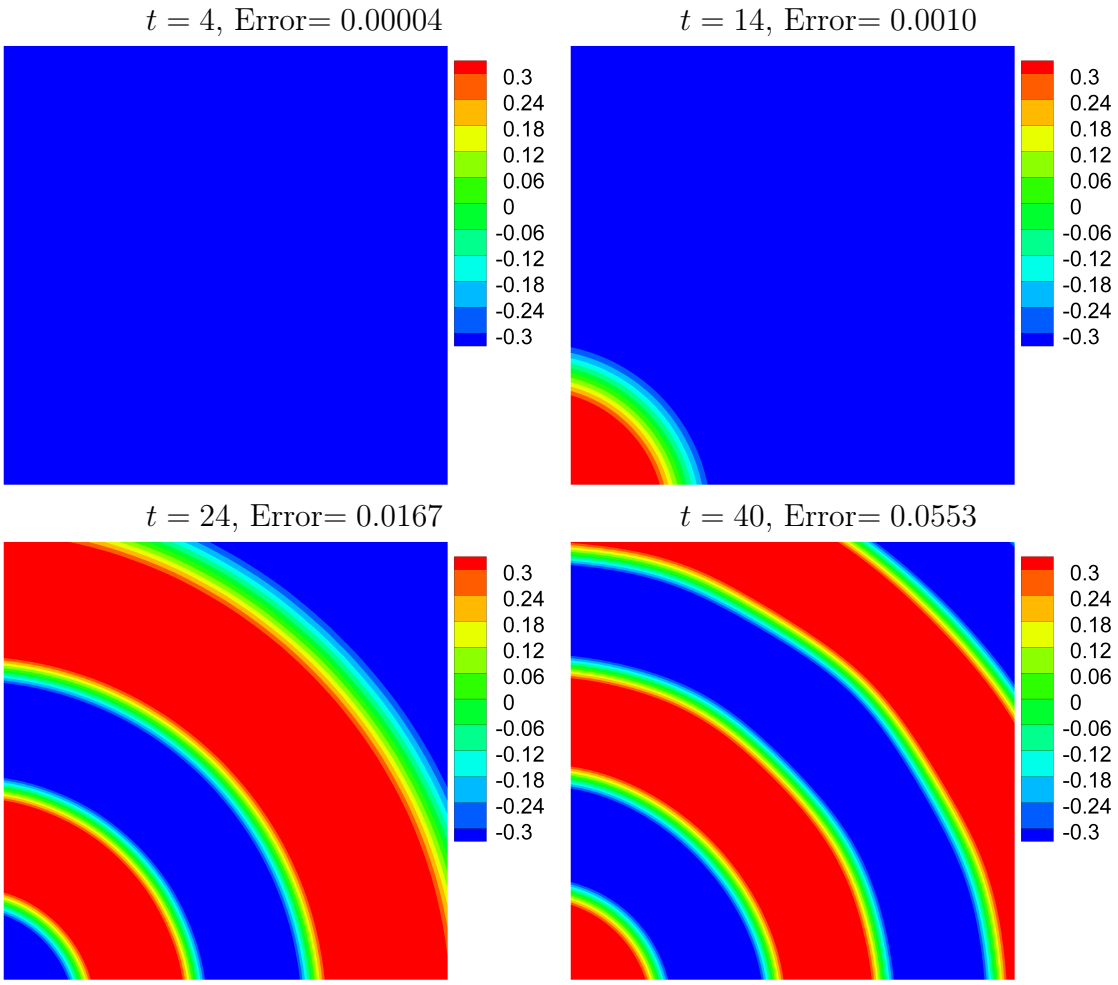

Figure 3.11: Moving Envelope problem: imaginary part of the PUFEM solution at different time instances for $k = 4\pi$, $Q = 11$, F_2 propagator and $\Delta t = 10^{-2}$

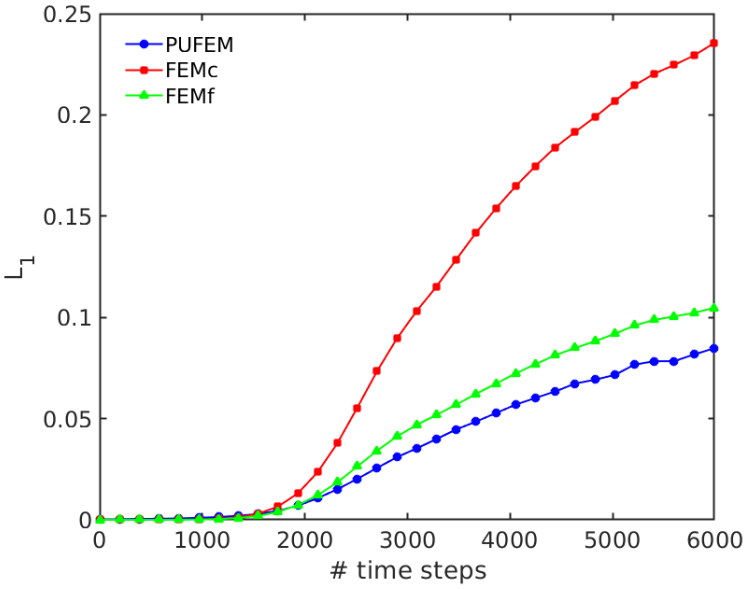

Figure 3.12: Extended time evolution (upto 6000 time steps) of the errors incurred in the PUFEM and the FEM for the Moving envelope problem using F_2 type propagator, with $k = 4\pi$

gradient, hence, having the second type propagator F_2 significantly improved the numerical results. Using the F_2 propagator and up to $t = 8$ the relative error seems to be unchanged using the FEM on either mesh or using the PUFEM. Thereafter the relative error starts to increase more rapidly using the FEMc compared to the FEMf and the PUFEM. Then at about $t = 15$ the relative error increases more rapidly using the FEMf than the PUFEM such that at the end of the simulation the values of the relative error obtained using the PUFEM, the FEMc and the FEMf become 0.0041, 0.0082 and 0.0047, respectively. To see the trend in the growth of the errors incurred in the PUFEM an the FEM for the F_2 type propagator, another extended simulation is run. The evolution of error is then plotted in Figure 3.12. Clearly, the PUFEM provides stable results even after 6000 time steps when the error reaches 0.0847 for the PUFEM, 0.1049 for the FEMf and 0.2359 for the FEMc.

The results in Figure 3.10 reveal a consistent behaviour of the relative error which, up to a certain point in time, remains similar to the errors obtained using the FEM and the PUFEM with some advantage for the FEM as can be seen from the results obtained using the F_1 in Figure 3.10. Then the relative error starts to build up quickly using the FEM but becomes smaller with the PUFEM. This behaviour is mainly attributed to the propagation structure of the wave into the

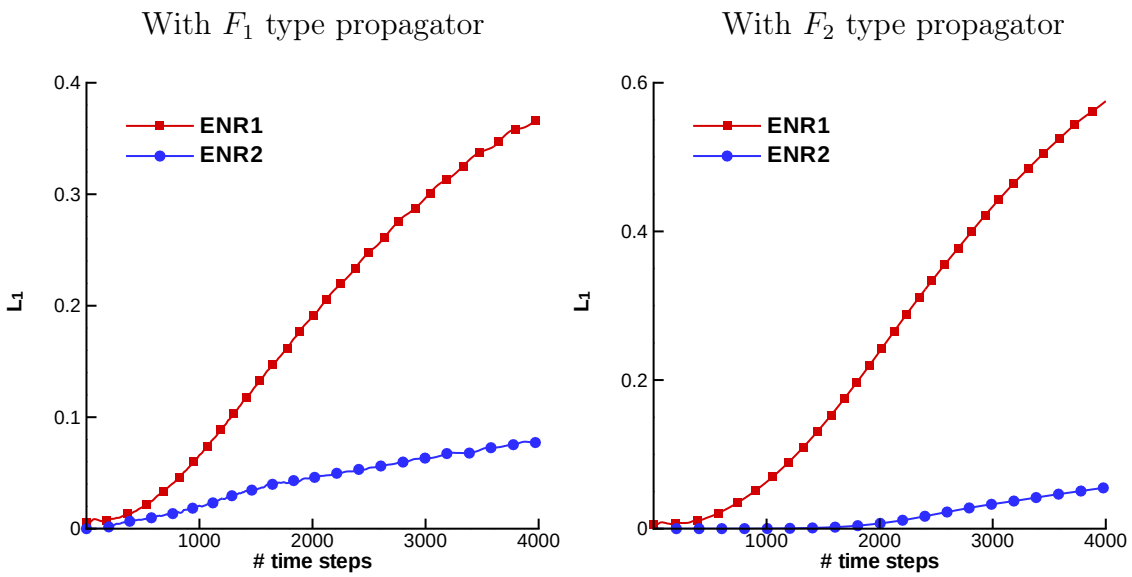

Figure 3.13: Moving Envelope problem: comparison of the PUFEM solution with $Q = 12$ (ENR1) and $Q = 11$ (ENR2) for $k = 4\pi$

computational domain. Figure 3.11 presents snapshots of the numerical solutions obtained using the PUFEM at three different instants corresponding to the initial time, the phase when the wave progresses into the domain and until the domain is fully covered with oscillations. At the first few time steps the domain is mainly stationary and the solution is merely constant. The linear finite element can be very efficient in recovering such a constant solution. However, as the time passes, the oscillations start to cover a wider area of the computational domain while a smaller area remains stationary. As the time evolves, the numerical error starts to build up at a high rate with the FEM. Eventually, the relative errors obtained using the FEM tend to become larger than those obtained using the PUFEM. It is clear that the PUFEM outperforms the FEM in terms of total degrees of freedom required for similar or better numerical accuracy, and thus is much more efficient than the FEM in recovering such oscillations.

3.7.2 Slowly varying enrichment term

Next let us investigate the effect of the constant solution on the accuracy of the PUFEM. To achieve this let us study the outcome of eliminating the slowly varying term B_i^{n+1} in the enrichment function from equation (3.6). The problem is solved again for $k = 4\pi$ using the PUFEM with 12 plane waves but without including

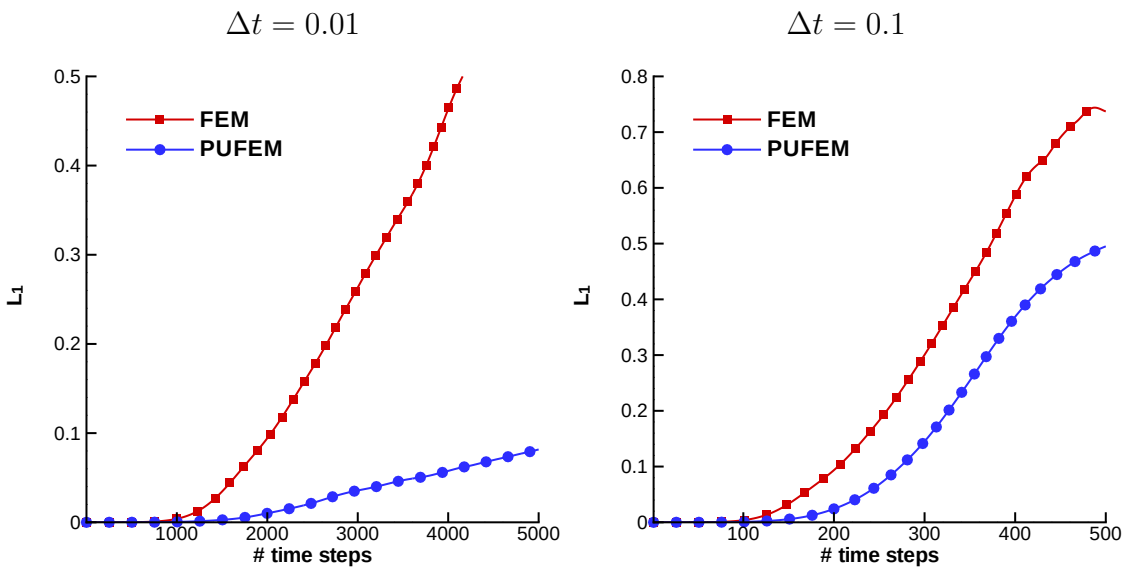

Figure 3.14: Moving Envelope problem: comparison of the results from PUFEM and FEM for $k = 8\pi$ with F_2 type propagator and $Q = 13$. The step size in time Δt is depicted over the plots.

the terms B_i^{n+1} in the enrichment. The computed solution is then compared to the solution obtained using the previous PUFEM where $Q = 11$, *i.e.*, ten plane waves with the term B_i^{n+1} are included in the enrichment. All the problem parameters are retained but a longer time interval $[0, 40]$ is considered in this study. Figure 3.13 presents a comparison of the relative errors between the results obtained using the PUFEM without B_i^{n+1} (referred to as ENR1 in the plots) and those obtained using the terms B_i^{n+1} (referred to as ENR2 in the plots). Although a larger number of enrichment functions is used for ENR1, the relative error for ENR2 is much smaller than for ENR1. Clearly the PUFEM does not produce useful results when B_i^{n+1} is eliminated and the relative error quickly increases to more than 10 %. Obviously removing the slowly varying terms B_i^{n+1} from the enrichment makes the PUFEM less efficient in capturing the stationary part of the numerical solution in this test example. The significant increase in the relative errors deteriorates the overall accuracy of the PUFEM applied to such waves problem in time domain.

3.7.3 Error accumulation in time

Finally, let us evaluate the accumulation in time of the relative error for the enriched finite elements compared to non-enriched finite elements. To this end let us solve the problem using the PUFEM and the FEM for $k = 8\pi$ and with the F_2 type

propagator. For the PUFEM solution, the same mesh is retained from previous simulations but with $Q = 13$ such that $N_{dof} = 325$. For the FEM a mesh refinement is considered where the new mesh consists of 3481 uniform 4-noded linear elements and 3600 nodes. Note that such a fine mesh is necessary for the FEM in order to fulfil the ten degrees of freedom requirement for the high wavenumber considered in this case. The accumulation of the relative errors in time is summarized in Figure 3.14 using both methods and for two different time steps, namely $\Delta t = 0.1$ and 0.01. The time interval considered is $[0, 50]$.

Despite the much lower number of degrees of freedom with the PUFEM, it is clear that the error accumulates much more slow in time compared to the FEM. For $\Delta t = 0.01$ the FEM error reaches 0.1 at about $t = 20$ and it becomes 0.5 at about $t = 40$. On the other hand the PUFEM error does not exceed 0.08 for the entire time domain. Similar observations can also be made for the FEM and the PUFEM performance with $\Delta t = 0.1$. Figure 3.14 shows how the FEM error increases quickly with $\Delta t = 0.1$, and reaches Error = 0.1 at $t = 20.1$ and Error = 0.5 at about $t = 37.0$ while the PUFEM error reaches Error = 0.1 at $t = 27.0$ and 0.5 at the end of the simulation. When comparing the CPU time at the first time step the FEM requires 164.1s to solve the problem while the PUFEM requires 8.5s. At subsequent time steps this number is reduced to 147.7s with the FEM while it is only 1.3s with the PUFEM. Figure 3.15 shows snapshots of the PUFEM solution at several stages of the considered time span. The results and concluding remarks are consistent with those of the previous example.

3.8 Conclusions

In this chapter, a class of enriched finite elements has been presented for solving the scalar electromagnetic wave equation in the time domain. An implicit time integration procedure has been used to advance the numerical solution in the time domain. Using ideas from the partition of unity the finite element solution is enriched using plane wave functions. These techniques significantly reduce the number of degrees of freedom required for a fixed accuracy in the obtained solution compared to those needed for another enriched finite element method.

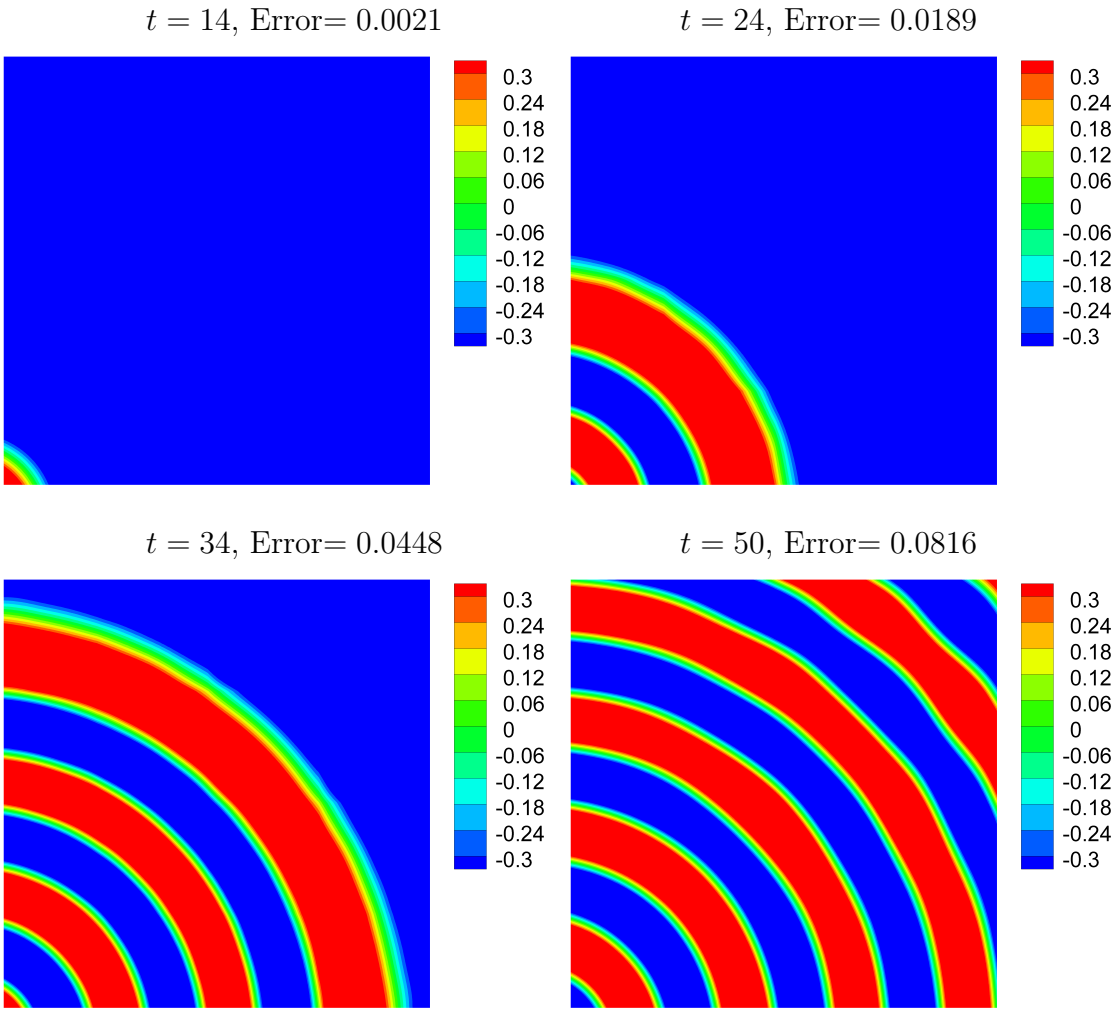

Figure 3.15: Moving Envelope problem: imaginary part of the recovered wave ($k = 8\pi$) with the propagator F_2, obtained using the proposed PUFEM with $Q = 13$, and $\Delta t = 10^{-2}$.

The performance of the proposed enriched finite element method is assessed for several test examples. First, the method is assessed by comparing its results to another enrichment technique where a number of published test cases are considered. Next the performance of the method is assessed in two cases, namely a progressive cylindrical wave and a moving envelope, where the exact solutions are known. The accuracy of the proposed approach has been verified using the relative errors at different time steps and different numbers of enrichment functions. Comparison to the standard finite element method has also been presented. The numerical results confirm the accuracy of the proposed enriched finite element method and its performance for transient wave problems.

The results discussed in this chapter show that the partition of unity finite element method has the advantage of requiring less computational resources for the time-dependent wave problems compared to another enriched finite element method. We see that the degrees of freedom per wavelength $\tau \approx 5$ is sufficient for very good numerical accuracy when considering low wavenumbers. The total number of mesh points in the computational domain, along with τ could be used to determine the number of enrichment functions required per node. Also, it is seen that the requirement on τ gets further relaxed for higher wavenumbers. This fact, as well as its favourable stability properties, make it an attractive alternative for solvers based on finite element techniques for the electromagnetic wave equation in the time domain where the considered problem involves few dominant frequencies. However, it is surely of interest to solve for problems with perhaps a bandwidth of frequencies present in the solution. This could form a basis for future work on developing other enrichment functions to deal with a wide spectrum of frequencies. It is also worthwhile to remark that the time integration scheme can be easily changed according to the transient wave problem under consideration. The advantages achieved with the enrichment approach can be further enhanced by considering a more efficient time integration scheme. Extension of the proposed enriched finite element method to three space dimensions is of particular interest as well, as it will result in an extensive reduction in the computational resources compared to the classical methods. Furthermore, developing highly efficient solvers for the associated linear systems in order to resolve issues related to the conditioning and also developing efficient

analytical integration procedures can further enhance the method.

Chapter 4

PUFEM vs *p*-FEM

4.1 Introduction and overview

In solving partial differential equations, the technique of finite elements provides various useful features such as the ability to model complex geometry and heterogeneous material properties. Moreover, the FEM provides ease of implementation to solve different physical problems, especially when using low order elements. However, for solving wave problems, usually the accuracy of the low order FEM scales directly with the product of the element size and the dominant wavenumber of the governing equation [77]. The quality of numerical results therein deteriorates with the increasing wavenumber [37]. To remedy this, various high order polynomial based finite elements are proposed and developed for example by Bériot *et al.* [13, 15] to measure the dispersion and amplitude errors of the *p*-FEM. Optimised design parameters such as the choice of the integration quadrature in conjunction with the distribution of nodes inside an element are also studied and analysed [53]. A detailed description of such high order polynomial based methods could be found in various standard textbooks [130]. Similarly, field enrichment based methods are also proposed for wave problems, as discussed in chapter 2. Recently, Christodoulou *et al.* [29] compared the plane wave based PUFEM against high-order Lagrangian-polynomial based finite element models for solving the Helmholtz equation. A review of several high-order finite element techniques developed in the context of the wave problems is presented in their work, and the references therein. This chapter derives its motivation from the study presented in their work, and aims at extending the

investigation into the time-dependent wave equation.

4.2 High-order *p*-FEM with implicit time integration

In the previous chapter, the plane wave based PUFEM is proposed for the wave equation, and its performance is compared against the linear FEM. In this chapter, a comparison against Lagrangian-polynomial based high-order FEM is presented. Referring to the model wave problem as discussed in section 3.3 of chapter 3, the p-FEM approximation is formulated as

$$E_h^{n+1}(\mathbf{x}) = \sum_{j=1}^{N_d} E_j^{n+1} \mathcal{N}_j(\mathbf{x}), \tag{4.1}$$

where $N_d = (p+1)^2$ is the number of solution mesh points in an element for a p^{th} order polynomial basis. For the purposes of this research, Lagrange basis polynomial functions are used to construct the solution space. The mesh points are evenly distributed inside an element. The Gauss-Legendre quadrature scheme is used for numerical integration required for computing the elementary matrices. Also, the weak form for the wave model of equation (3.3) remains unchanged for the p-FEM approximations. It is well known that for a given number of integration points, say n, the Gauss-Legendre quadrature scheme can accurately compute integrals for polynomials upto the order $2n-1$. However, in case of plane wave based PUFEM, the solution basis contains oscillatory sine and cosine functions. Thus, to obtain a good accuracy in numerical integration required for the elementary matrices in the PUFEM, the number of integration points to be used per element depends on the wavenumber of the enrichment functions. A higher wavenumber would require large number of integration points per element. However, the computational costs remain moderate despite the large number of integration points within each element due to the relatively small total number of elements required in case of the PUFEM as compared to the polynomial based FEM. For the purposes of this research, 10 integration points per wavelength are used. Moreover, exact integration schemes could also be developed for the PUFEM to bypass the need for numerical integration

when computing the elementary matrices. In the following section, a numerical test case is considered to gauge the performance of the proposed PUFEM against high-order p-FEM solutions.

4.3 Numerical tests

In this section, the progressive cylindrical wave problem of section 3.6 is considered, for which the exact solution is given by

$$E = e^{\mathrm{i}(kr-\omega t)}.$$

The problem domain is $\Omega = [0.1, 1.1]\times[0.1, 1.1]$. The frequency in time is kept constant at $\omega = 1$. The total simulation time is $T = 1$, using step-size $\Delta t = 0.001$. Three different wavenumbers are considered *i.e.*, $k = \{9\pi, 12\pi, 15\pi\}$, and the wave speed is $c = \omega/k$. Uniform, rectangular elements are used for meshing the domain, for both p-FEM as well as PUFEM solutions. For the p-FEM solutions, upto fourth order polynomials are considered. Three different meshes m1, m2, and m3 with a total of 16, 81 and 196 elements respectively are used as shown in Figure 4.1. The solutions obtained with the p-FEM are termed as Pimj, corresponding to the i^{th} order and using mesh mj. For the linear p-FEM solutions three extra meshes m4, m5, and m6 are used. These meshes correspond to a total of 361, 576 and 900 elements, respectively. The solutions obtained with these meshes are termed as P1m4, P1m5 and P1m6, respectively. For all the PUFEM solutions shown in this section, the mesh m1 of Figure 4.1 is used. A set of five different number of enrichment functions $Q = \{3, 9, 15, 21, 27\}$ are used in conjunction with the PUFEM for q-refinement. These PUFEM solutions are termed as $Q$$i$m1 corresponding to the i^{th} number of nodal enrichment functions used with mesh m1.

4.3.1 Comparing PUFEM and p-FEM

Table 4.1 lists the L_1-norm errors, as per the error definition used in the numerical examples of chapter 3, associated with the PUFEM and the p-FEM solutions for the progressive cylindrical wave problem for the three different wavenumbers considered.

Figure 4.1: The uniform meshes m1, m2, and m3 with a total of 16, 81 and 196 elements respectively, from left to right.

Method	$k = 9\pi$, Error (%)		$k = 12\pi$, Error (%)		$k = 15\pi$, Error (%)		TOTDOF
	$(t = \Delta t)$	$(t = T)$	$(t = \Delta t)$	$(t = T)$	$(t = \Delta t)$	$(t = T)$	
Q1m1	80.31	80.52	88.14	88.24	91.63	91.68	75
Q2m1	2.49	3.84	10.84	11.54	27.63	27.92	225
Q3m1	0.08	2.08	0.52	1.67	2.02	2.53	375
Q4m1	0.02	-	0.02	1.71	0.21	1.28	525
Q5m1	-	-	0.73	-	0.01	-	675
P1m1	90.22	90.38	88.9	89.57	81.73	83.75	25
P1m2	37	40.36	69.76	70.66	87.89	87.88	100
P1m3	9.68	14.30	24.35	28.58	46.56	49.16	225
P1m4	3.69	7.39	9.23	13.59	19.03	23.42	400
P1m5	1.78	4.80	4.39	8.01	8.98	13.18	625
P1m6	0.90	3.45	2.18	5.07	4.41	7.88	961
P2m1	58.14	61.37	92.22	92.98	97.9	98.02	81
P2m2	6.14	8.17	12.23	15.33	23.98	28.49	361
P2m3	2.13	4.02	4.29	6.09	7.22	9.10	841
P3m1	20.29	24.36	47.55	53.16	80.14	83.21	169
P3m2	1.47	2.72	4.40	5.34	9.12	10.77	784
P3m3	0.23	2.10	0.79	1.82	1.95	2.58	1849
P4m1	7.55	10.71	22.45	26.98	42.91	51.21	289
P4m2	0.14	2.10	0.53	2.12	1.67	3.84	1369
P4m3	0.01	2.08	0.06	1.57	0.19	1.34	3249

Table 4.1: The accuracy of numerical solutions for the progressive cylindrical wave problem, obtained with the PUFEM and the p-FEM. For each solution, the error percentage at the first time step ($t = \Delta t$) and at the final time step ($t = T$) are listed. The degrees of freedom (TOTDOF) associated with each solution are also shown.

	Condition number (κ)		
Method	$k = 9\pi$	$k = 12\pi$	$k = 15\pi$
Q1m1	9.61E+01	2.87E+01	2.31E+01
Q2m1	9.12E+04	6.00E+02	4.19E+01
Q3m1	3.07E+08	5.60E+04	3.56E+04
Q4m1	1.99E+09	8.35E+07	1.27E+06
Q5m1	9.63E+07	1.21E+08	6.60E+07

Table 4.2: The condition number κ of the system matrices associated with the PUFEM solutions, for the numerical solution of the progressive cylindrical wave problem corresponding to the three different wavenumber considered.

The error percentage for the first time step ($t = \Delta t$) and for the final time step ($t = T$) are given. The TOTDOF in this table refers to the TOTal Degrees Of Freedom associated with the respective solutions. For instance, for the Q1m1 solution, $Q = 3$ and the total number of nodes in the mesh m1 is 25 which results in TOTDOF = 75. Similarly, for the P2m1 solution, the mesh used is m1 which has 16 elements with 9 nodes each (for second order polynomial basis functions), thus resulting in TOTDOF = 81. The condition number of the system matrix associated with these solutions is also listed in the table. The "-" in the table entries corresponds to the cases where the PUFEM solutions become unstable.

It is clear that both, PUFEM and p-FEM solutions provide better accuracy with increasing TOTDOF, using q-refinement and mesh refinement respectively. At time $t = T$ the error associated with Q2m1 solution is 3.84%, which is comparable to 3.45% obtained with P1m6. However, the TOTDOF associated with the PUFEM solution is roughly 75% less than that of the first order p-FEM. This is expected as discussed and observed in subsection 3.6.3 of chapter 3. Similarly, for the second order p-FEM solution obtained with P2m3 is approximately as accurate as the PUFEM solution obtained with Q2m1. The reduction in the TOTDOF when using the PUFEM is again about 75% as compared to the second order p-FEM. Whereas, compared to the best solutions obtained with the third and the fourth order p-FEM, the reduction in the TOTDOF when using the PUFEM is about 80% and 88% respectively, for the same numerical accuracy, as seen from Table 4.1. Similar trends are observed for the cases $k = 12\pi$ and $k = 15\pi$ as can be seen in the table. These trends are summarized in the error vs TOTDOF plots of figures 4.2, 4.3 and 4.4 for the three different wavenumbers considered. In this figure, four different time

Method	Condition number (κ)
P1m1	1.49E+01
P1m2	1.54E+01
P1m3	1.57E+01
P1m4	1.58E+01
P1m5	1.59E+01
P1m6	1.59E+01
P2m1	2.96E+01
P2m2	2.91E+01
P2m3	2.92E+01
P3m1	6.08E+01
P3m2	6.08E+01
P3m3	6.11E+01
P4m1	1.47E+02
P4m2	1.49E+02
P4m3	1.48E+02

Table 4.3: The condition number κ of the system matrices associated with the p-FEM solutions, for the numerical solution of the progressive cylindrical wave problem for wavenumber $k = 9\pi$. The change in κ with the change in the problem wavenumber is negligible for the p-FEM matrices. This is explained in subsection 4.3.2.

instances are shown. The top row corresponds to time $t = \Delta t$. For this row, it can be seen that the rate of convergence of the error against the TOTDOF is the maximum for the fourth order p-FEM solutions amongst the four non-enriched approaches considered, as expected. However, this advantage in the rate of convergence when using higher order polynomials gets diminished as the solutions evolve in time, as depicted by the second row in the figure which corresponds to time $t = T/4$. At the final time step, *i.e.*, $t = T$ corresponding to the final row in the figure, the rate of convergence for all the p-FEM solutions are very similar. However, as can be seen, one gains a consistent advantage in the rate of convergence when using the enriched version of the FEM, as compared to the polynomial based p-FEM, for all the wavenumbers considered.

4.3.2 Conditioning comparisons

Further, a comparison of the condition number κ of the system matrices associated with the PUFEM and the p-FEM solutions is presented in tables 4.2 and 4.3. It is clear that the condition number associated with the p-FEM solutions is negligible

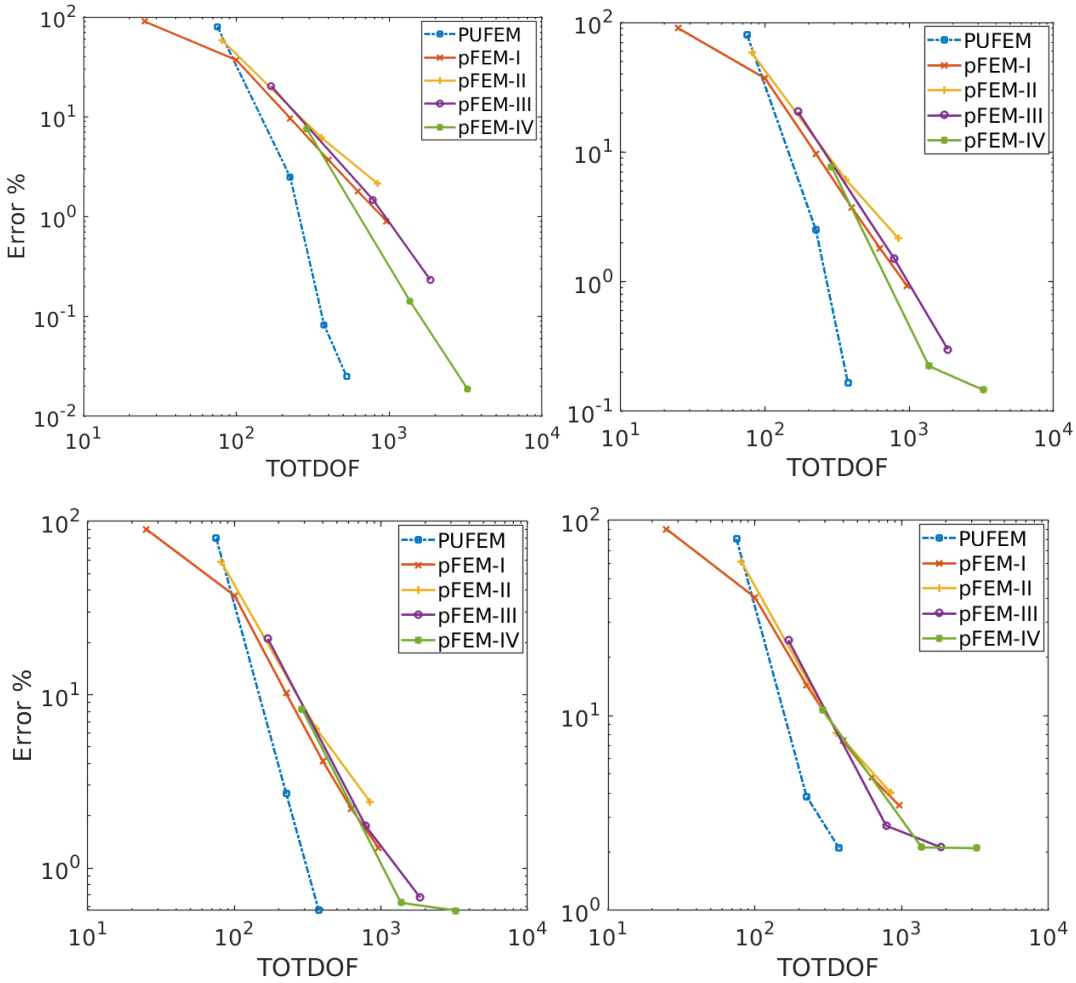

Figure 4.2: The error vs TOTDOF plots for the numerical solutions obtained using the PUFEM and the p-FEM for the progressive cylindrical wave problem, with problem wavenumber $k = 9\pi$. The plots correspond to time $t = \Delta t$ (top left), $t = T/4$ (top right), $t = T/2$ (bottom left) and $t = T$ (bottom right) from top to bottom, respectively.

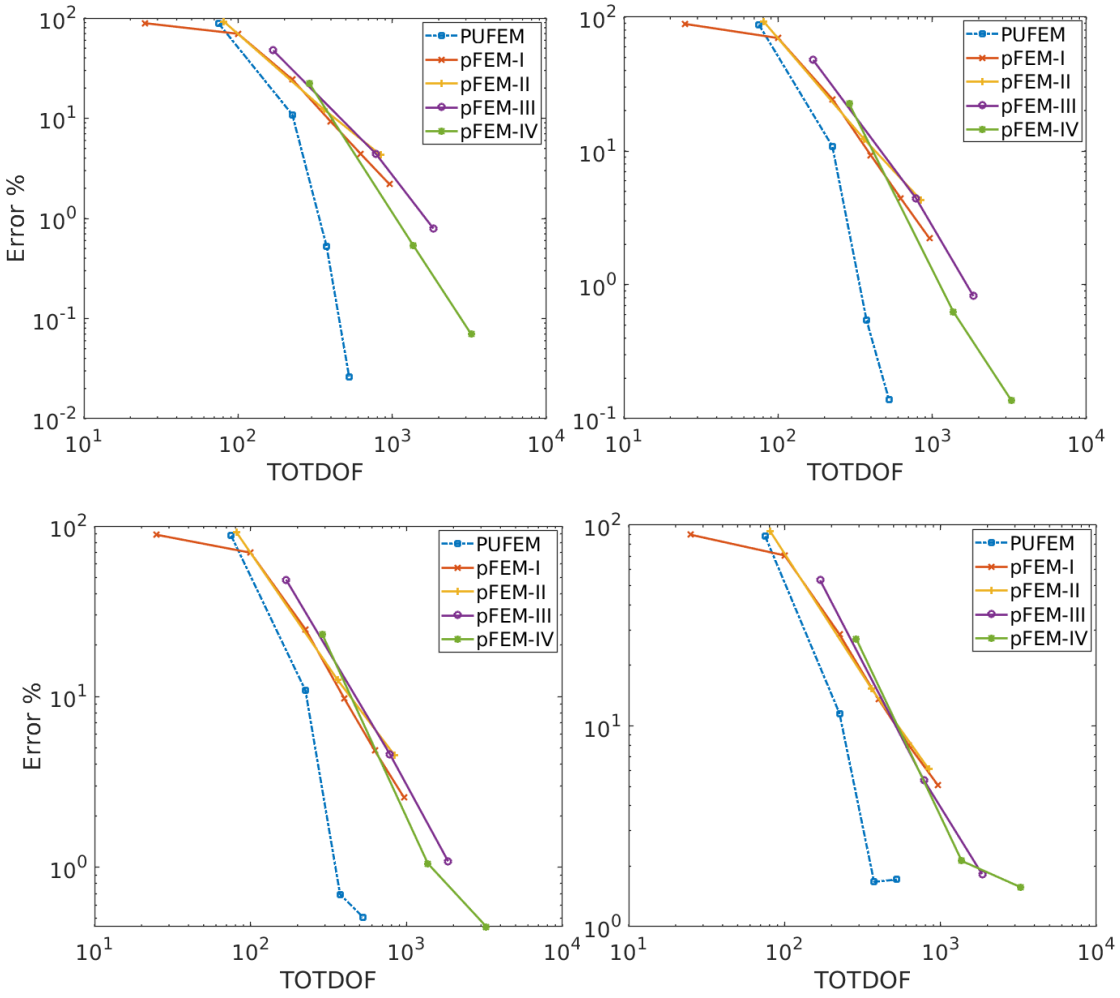

Figure 4.3: The error vs TOTDOF plots for the numerical solutions obtained using the PUFEM and the p-FEM for the progressive cylindrical wave problem, with problem wavenumber $k = 12\pi$. The plots correspond to time $t = \Delta t$ (top left), $t = T/4$ (top right), $t = T/2$ (bottom left) and $t = T$ (bottom right) from top to bottom, respectively.

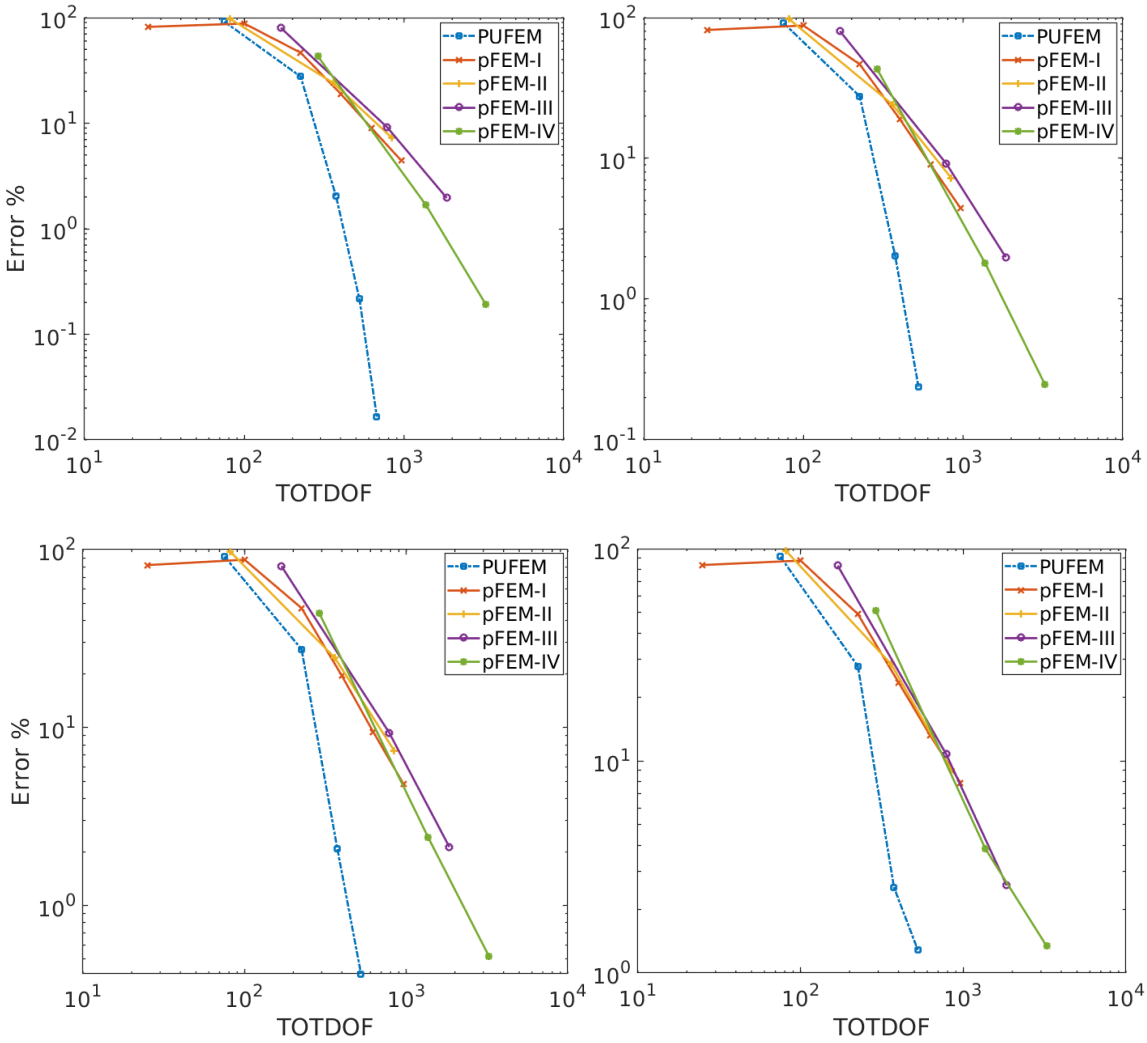

Figure 4.4: The error vs TOTDOF plots for the numerical solutions obtained using the PUFEM and the p-FEM for the progressive cylindrical wave problem, with problem wavenumber $k = 15\pi$. The plots correspond to time $t = \Delta t$ (top left), $t = T/4$ (top right), $t = T/2$ (bottom left) and $t = T$ (bottom right) from top to bottom, respectively.

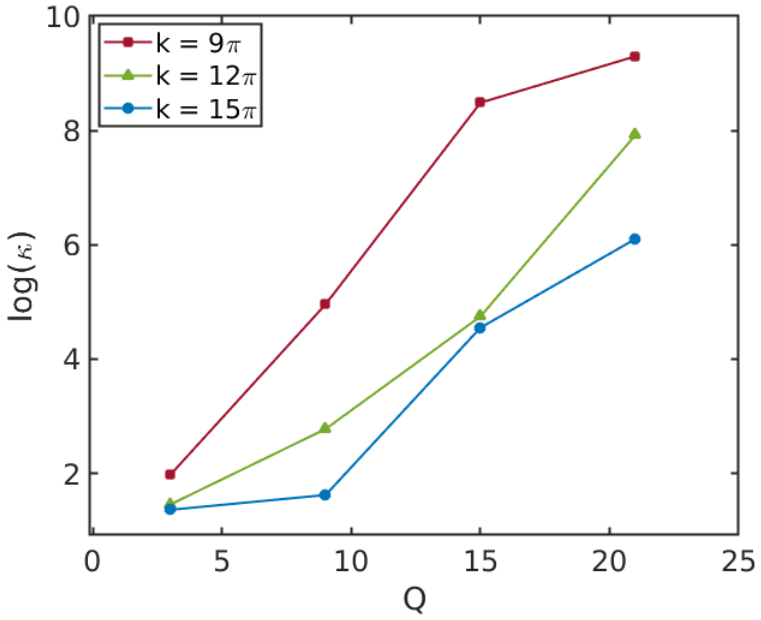

Figure 4.5: Condition numbers vs number of enrichment functions Q associated with the PUFEM for the three different wavenumbers considered for the progressive cylindrical wave problem.

as compared to that of the PUFEM. Also note that the system matrices for both PUFEM and p-FEM are dominated by the elements from the mass matrix since the stiffness matrix is scaled by a factor of $c^2\Delta t^2$, as seen in the weak form of equation (3.3). This scaling factor can also be written as $\frac{\omega^2\Delta t^2}{k^2}$. The frequency $\omega = 1$ and $\Delta t = 0.001$ for all the cases considered in this section. For $k = 9\pi$ the scaling factor is of the order of 10^{-9} and decreases further to 10^{-10} for $k = 15\pi$. This dominance of the mass matrix is clearly visible as the condition numbers for the p-FEM remain unchanged for the three different wavenumbers considered. This is because the mass matrix does not change with a change in the problem wavenumber for the p-FEM. However, this is not the case for the system matrix associated with the PUFEM. This is because the PUFEM basis functions contain the information of the wavenumber used for enrichment. From Table 4.2 it is clear that the conditioning of the system matrix for the PUFEM deteriorates with increasing number of enrichment functions used. Poor conditioning leads to unstable solutions. Note that for the case $k = 9\pi$, the PUFEM fails for $Q > 20$, as seen in Table 4.1. Similarly, for the cases $k = 12\pi$ and $k = 15\pi$, the value of $Q = 27$ leads to too high a condition number that results in unstable PUFEM solutions. However, for the same TOTDOF, the conditioning of the system matrix improves for increasing wavenumber of the enrichment functions.

This is seen more clearly, in the condition number vs number of enrichment functions plot of Figure 4.5. This is similar to what is observed in subsection 3.6.2 of Chapter 3. Thus, the choice of using plane wave functions for enrichment becomes more viable for highly oscillatory wave problems.

4.4 Conclusions

In this chapter, a comparison between the performances of the plane wave based PUFEM and the high order polynomial based FEM, in conjunction with the implicit integration scheme in time is presented for the time dependent wave equation. Upto fourth order polynomials are considered. The numerical trends investigated in this chapter are in coherence with the results and conclusions derived in a similar work [29] for the case of the Helmholtz equation. The plane wave based PUFEM is reported to show significant reduction in the total degrees of freedom required to solve the wave equation, when comparing with higher order polynomial based FEM solutions of similar numerical accuracy. The conditioning of the system matrix associated with the polynomial based FEM is much better than that for the PUFEM. However, for a given total degrees of freedom, the conditioning for the PUFEM improves with increasing wavenumber of the enrichment plane waves, which makes the method more suitable for short wavelength problems.

Chapter 5

Enriched FEM with explicit time integration

5.1 Overview

In this chapter a partition of unity finite element method for wave propagation problems in the time domain using an explicit time integration scheme is presented. Like previous chapters, plane wave enrichment functions are introduced at the finite elements nodes, within the semi-discrete formulation, which allows us to use a coarse mesh at low order polynomial shape functions even for high wavenumbers. The initial condition is formulated as a Galerkin approximation in the enriched function space. Also shown is the possibility of lumping the mass matrix which is approximated as a block diagonal system. The proposed method, with and without lumping, is validated using various test cases and compared to the implicit time integration approach, as developed in previous chapters. The stability of the proposed approach against different factors such as the choice of wavenumber for the enrichment functions, the spatial discretization, the distortions in mesh elements or the timestep size, is tested in the numerical studies. The method performance is measured for the solution accuracy and for the CPU processing times. The results show significant advantages for the proposed lumping approach which outperforms other considered approaches in terms of stability. Furthermore, the resulting block diagonal system only requires a fraction of the CPU time needed to solve the full system associated with the non-lumped approaches. The work presented in this

chapter forms the basis for the journal publication [42].

5.2 Introduction

In this chapter let us look into the solution of the wave equation using an enriched finite element method and an explicit time integration scheme with a lumped mass matrix. The problem is relevant to a vast range of applications such as acoustic scattering, mobile phones and MRI-scanners and arises frequently in designing novel devices [12, 148]. For example the design of waveguides and antennas are carried out routinely in the laboratories to aid in the design of transceiver circuits used in mobile phones [35, 97]. The problem also arises in the design of concert halls to provide best acoustic experience. Solving such applications with deterministic approaches, requires discretization of the governing partial differential equations and a solution of the resulting system of algebraic equations. It is known that a deterministic approach provides a unique solution to a well-posed problem associated with given boundary and initial conditions. However, such an approach can be computationally demanding, in cases that require the solution of a very large number of unknown variables.

The idea is to enrich the approximation space with oscillatory functions. As an example, the partition of unity finite element method (PUFEM) is developed for solving the Helmholtz problems at high frequencies [29], wherein it is showed that the method outperforms the FEM with the standard polynomials basis functions. The partition of unity enrichment technique led to a vast amount of literature comprising different approaches. The PUFEM is also adapted for solving forward problems for elastic waves [81, 103] and more recently for inverse problem [79].

The wave propagation can be recovered by solving the partial differential equations using either the frequency- or the time-domain analysis. However wave equations in the time domain can deal with a much wider range of applications than its frequency-domain counterpart. For example pulse sources cannot be modelled by the frequency domain which require harmonic sources. The frequency domain approach also fails in cases which require a large range of frequencies such as in radar applications. To deal with time-domain wave problems, an enriched model for wave propagation

is developed for two-dimensional transient wave problems in [63]. A PUFEM approach for time-domain electromagnetic waves is also developed in [43] using an implicit time stepping method, as discussed in chapter 3. In [154], the authors present the usage of numerical manifold method to construct finite element patches that cover the numerical domain and produce diagonalised lumped mass matrices that satisfy mass conservation of the elements for elastodynamic problems. In [153], an explicit scheme for discontinuous deformation analysis is presented for elasticity problems. Similarly, in [27] a multi-patch approach is used with discontinuous Galerkin isogeometric analysis to form block diagonalised lumped mass matrices for wave propagation. The presented numerical analysis for transient hyperbolic problems shows that the step-size in time scales as $O(h/p)$ for stability where h is the mesh size and p is the order of approximation. An explicit time stepping scheme with lumped mass matrix can be highly beneficial for enrichment methods when solving wave problems. However, this was still not achieved. In general high order numerical schemes for time domain integration are limited by the fact that they have more restrictive Courant–Friedrichs–Lewy (CFL) conditions and suffer from challenging memory requirements. They are derived from the Taylor series expansion of the derivatives and assuming coefficients from multiple previous time steps [31]. In these methods, the mass matrix could pose a problem for computation as it would be required to be inverted in every time step. One way to reduce computational cost could be diagonalizing this matrix using the so called lumped mass approach. There are essentially a handful of ways to achieve a lumped mass matrix [71]. For instance one can use the nodal quadrature technique. In essence it requires usage of numerical integration points located at the nodes of each element. In the p-FEM, the banded mass matrix could be reduced to a diagonal matrix by the usage of Gauss-Lobatto scheme for both interpolation and numerical integration. This is effective especially for third or higher order polynomials used in the finite element approximation. The only two criteria are that the order of accuracy must be maintained, and that the same points must be used for interpolation as for numerical integration i.e. including the end points [160]. However, due to the contribution of the enrichment functions it is not possible to diagonalise the mass matrix using similar quadrature techniques.

In [137], a variational approach is develolped to approximate the consistent mass matrix for partition of unity methods, which is in line with the classical row-summation technique for linear FEM. In this chapter a similar approach is presented using plane wave enrichments, and the benefits of mass lumping are investigated in terms of improved conditioning, and also in terms of performance over both structured and unstructured meshes. The contribution in this work is also derived from projecting arbitrary non-zero initial conditions over local approximation spaces for the enriched PUFEM. The formulation of block diagonal lumped mass matrix approach significantly simplifies the solution of the linear systems arising from the spatio-temporal discretizations of the time-domain wave problems. The mass matrix lumping also allows to improve the conditioning of such systems which are known to be ill conditioned. The focus is on the difficulties related to capturing the oscillatory nature of solutions to wave phenomenon, such as the Maxwell's equations with a source term (*i.e.*, a non-zero right-hand side). The results obtained herein can be applied to other fields such as acoustics with the same basic principles, superimposed in a linear manner. Although developed for the PUFEM method, this lumping approach can be also used in other enrichment techniques without significant changes. The rest of this chapter is organised as follows. First, the problem and the considered finite element method are defined. These definitions are consistent with those used in previous chapters, and are included herein for the reader's convenience and to properly setup the background for analysis. Details about the time integration schemes and the lumping of the mass matrix are provided in section 5.3. Next, several numerical experiments are presented in sections 5.4, 5.5 and 5.6. Finally, section 5.7 contains some concluding remarks and recommendations for future work.

5.3 Wave problem and FEM approximations

First, let us present a linear wave equation in two dimensions which would be the basis of all analysis presented in this chapter. Let us define an initial boundary value problem on $\Omega \subset \mathbb{R}^2$ being an open bounded domain with Lipschitz continuous boundary Γ evolving in $[0, T]$ which is the time interval for the wave propagation.

The problem is defined as

$$\frac{1}{c^2}\frac{\partial^2 E}{\partial t^2} - \nabla^2 E = f(t,\mathbf{x}), \qquad (t,\mathbf{x}) \in [0,T[\times\Omega, \tag{5.1a}$$

$$\frac{\partial E}{\partial \hat{\mathbf{v}}} + hE = g(t,\mathbf{x}), \qquad (t,\mathbf{x}) \in [0,T[\times\Gamma, \tag{5.1b}$$

$$E(0,\mathbf{x}) = E^0(\mathbf{x}), \qquad \mathbf{x} \in \Omega, \tag{5.1c}$$

$$\frac{\partial E}{\partial t}(0,\mathbf{x}) = V^0(\mathbf{x}), \qquad \mathbf{x} \in \Omega, \tag{5.1d}$$

where $\mathbf{x} = (x,y)^\top$ are the Cartesian coordinates, t is the time variable, $\hat{\mathbf{v}}$ the outward unit normal on Γ and E the magnitude of the transverse electric field in the direction perpendicular to the plane of numerical domain while c and h are constants. The functions $f(t,\mathbf{x})$ and $g(t,\mathbf{x})$ in (5.1) are the prescribed source and boundary functions, respectively. The functions $E^0(\mathbf{x})$ and $V^0(\mathbf{x})$ denote the given initial conditions. This model can be used to represent various linear electromagnetic and acoustic wave propagation problems, just as discussed in earlier chapters.
Let us reduce the second order differential equation of (5.1a) to a system of first order derivatives as follows

$$\frac{\partial E}{\partial t} = V, \tag{5.2a}$$

$$\frac{1}{c^2}\frac{\partial V}{\partial t} = f(t,\mathbf{x}) + \nabla^2 E. \tag{5.2b}$$

For discretization in space, approximate the solution space as a linear sum of traditional, class $C^0(\Omega)$, hat functions denoted by $\mathcal{N}(\mathbf{x}) = (\mathcal{N}_1, \cdots, \mathcal{N}_{N_d})^\top$ characterized by the property $\mathcal{N}_i(\mathbf{x}_j) = \delta_{ij}$ with δ_{ij} denoting the Kronecker symbol. These hat functions are, as usual, defined over the finite elements $\mathcal{T}_i$ used to discretize the spatial domain Ω. Hence, the field E and its first derivative V are defined in the partition Ω_h as

$$E_h(t,\mathbf{x}) = \sum_{j=1}^{N_d} E_j(t)\mathcal{N}_j(\mathbf{x}), \quad V_h(t,\mathbf{x}) = \sum_{j=1}^{N_d} V_j(t)\mathcal{N}_j(\mathbf{x}), \tag{5.3}$$

where N_d is the total number of nodal points in the partition and h is the discretization parameter of the mesh. Thus, $E_j(t)$ and $V_j(t)$ are the nodal values of the global functions $E_h(t, \mathbf{x})$ and $V_h(t, \mathbf{x})$, respectively. Note that only the nodal values of the field (or its derivative) are functions of time t at a given time. This is just to signify that the coefficients of the hat functions depend on time, and that the hat functions themselves have no dependency on time whatsoever.

Hence a weak form is obtained by multiplying both sides of (5.2) with a weighting function $\phi(\mathbf{x})$ and integrating on both sides over Ω. Using the divergence theorem and using the boundary condition (5.1b) obtain the following weak formulation of the problem (5.1)

$$\int_\Omega \frac{\partial E}{\partial t}\phi \, d\Omega = \int_\Omega V\phi \, d\Omega, \tag{5.4a}$$

$$\begin{aligned}\frac{1}{c^2}\int_\Omega \frac{\partial V}{\partial t}\phi \, d\Omega &= -\int_\Omega \nabla E \cdot \nabla\phi \, d\Omega - \oint_\Gamma (hE)\phi \, d\Gamma \\ &+ \oint_\Gamma g(t,\mathbf{x})\phi \, d\Gamma + \int_\Omega f(t,\mathbf{x})\phi \, d\Omega.\end{aligned} \tag{5.4b}$$

Following a partition of unity approximation, each mesh node is enriched with plane waves, thus allowing for a much coarser mesh, and overall a significantly lower total number of degrees of freedom. Thus, the discretization equations in (5.3) are re-written as

$$E_h(t,\mathbf{x}) = \sum_{j=1}^{N_d}\sum_{q=1}^{Q} \hat{E}_j^q(t) e^{\mathrm{i}kz_q}\mathcal{N}_j(\mathbf{x}), \tag{5.5a}$$

$$V_h(t,\mathbf{x}) = \sum_{j=1}^{N_d}\sum_{q=1}^{Q} \hat{V}_j^q(t) e^{\mathrm{i}kz_q}\mathcal{N}_j(\mathbf{x}), \tag{5.5b}$$

where $z_q = x\cos\alpha_q + y\sin\alpha_q$ for $q = 1, \ldots, Q-1$ and $z_Q = 0$. Notice that the solution E is split into two components where $\hat{E}_j^Q$ represents a scaling factor for the nodal shape functions while $\hat{E}_j^q|_{q\neq Q}$ represents the amplitude of different plane waves used as nodal enrichments. Similar argument follows for its first derivative V. Thus, each node has exactly Q degrees of freedom, of which $Q-1$ are the

amplitudes of plane wave enrichments, and the domain Ω_h has a total of $N_d Q$ degrees of freedom. For the numerical integration of these plane wave enrichment functions over the spatial domain, use about 10 integration points per wavelength in each direction. In [81], an explicit closed-form solution for two-dimensional wave-based integrals are developed, for the PUFEM using pressure and shear plane waves for local enrichment. Similar approach could be developed for the work presented in this chapter, that could significantly reduce the computational cost associated with the assembly process. The constant k is problem dependent, albeit it is possible to run a parametric sweep in a selected (discrete) bandwidth to obtain a modal response, however this is beyond the scope of the current work. The angles α_q for the plane wave enrichment functions are selected by uniformly dividing 2π based on $Q-1$. For example, $Q-1=4$ leads to $\alpha_q = 0$, $\pi/2$, π and $3\pi/2$ as the four distinct angles for the plane wave enrichments.

For the time integration let us set two unknown vectors $\mathbf{y}_1(t)$ and $\mathbf{y}_2(t)$ that store the time dependent coefficients, i.e.

$$\mathbf{y}_1(t)|_j = \{\hat{E}_j^1(t), \hat{E}_j^2(t), \ldots, \hat{E}_j^Q(t)\}^\top, \quad \mathbf{y}_2(t)|_j = \{\hat{V}_j^1(t), \hat{V}_j^2(t), \ldots, \hat{V}_j^Q(t)\}^\top, \tag{5.6}$$

where the subscript j denotes reference to a node in the partition Ω_h. Note that both $\mathbf{y}_1(t)$ and $\mathbf{y}_2(t)$ are each of total size $N_d Q$. Using, the definitions given in (5.5) and substituting them in (5.4) obtain the following algebraic system of ordinary differential equations

$$\mathbf{M}\frac{d\mathbf{y}_1}{dt} = \mathbf{M}\mathbf{y}_2, \tag{5.7a}$$

$$\frac{1}{c^2}\mathbf{M}\frac{d\mathbf{y}_2}{dt} = (-\mathbf{K} - \mathbf{M}_\Gamma)\,\mathbf{y}_1 + \mathbf{f}_\Gamma + \mathbf{f}_\Omega. \tag{5.7b}$$

Here, the vectors and matrices in (5.7) are defined as follows:

$$\mathbf{M}_{(i,n)(j,m)} = \int_{\Omega} \mathcal{N}_i e^{\mathrm{i}kz_n} \mathcal{N}_j e^{\mathrm{i}kz_m} d\Omega, \tag{5.8a}$$

$$\mathbf{K}_{(i,n)(j,m)} = \int_{\Omega} \left(\nabla \mathcal{N}_i e^{\mathrm{i}kz_n}\right) \cdot \left(\nabla \mathcal{N}_j e^{\mathrm{i}kz_m}\right) d\Omega, \tag{5.8b}$$

$$\mathbf{M}_{\Gamma(i,n)(j,m)} = h \oint_{\Gamma} \mathcal{N}_i e^{\mathrm{i}kz_n} \mathcal{N}_j e^{\mathrm{i}kz_m} d\Gamma, \tag{5.8c}$$

$$\mathbf{f}_{\Gamma(i,n)} = \oint_{\Gamma} g(t,\mathbf{x}) \mathcal{N}_i e^{\mathrm{i}kz_n} d\Gamma, \tag{5.8d}$$

$$\mathbf{f}_{\Omega(i,n)} = \int_{\Omega} f(t,\mathbf{x}) \mathcal{N}_i e^{\mathrm{i}kz_n} d\Omega, \tag{5.8e}$$

where $(i,n) \in \{1,2,\ldots,N_d\} \times \{1,2,\ldots,Q\}$ denote the row incides, and similarly (j,m) denote the column indices respectively. The matrix equations in (5.7) can be further simplified by multiplying both sides with the inverse of the mass matrix $\mathbf{M}$

$$\mathbf{M^{-1}M}\frac{d\mathbf{y}_1}{dt} = \mathbf{M^{-1}M}\mathbf{y}_2,$$

$$\frac{1}{c^2}\mathbf{M^{-1}M}\frac{d\mathbf{y}_2}{dt} = \mathbf{M^{-1}}\left(-\mathbf{K} - \mathbf{M}_{\Gamma}\right)\mathbf{y}_1 + \mathbf{M^{-1}}\left(\mathbf{f}_{\Gamma} + \mathbf{f}_{\Omega}\right),$$

which can be written in a compact form as

$$\frac{d\mathbf{y}_1}{dt} = \mathbf{y}_2, \tag{5.9a}$$

$$\frac{d\mathbf{y}_2}{dt} = \mathbf{A}\mathbf{y}_1 + \tilde{\mathbf{r}}, \tag{5.9b}$$

where $\mathbf{A} = c^2\mathbf{M^{-1}}\left(-\mathbf{K} - \mathbf{M}_{\Gamma}\right)$ and $\tilde{\mathbf{r}} = c^2\mathbf{M^{-1}}\left(\mathbf{f}_{\Omega} + \mathbf{f}_{\Gamma}\right)$, respectively. Equation (5.9) can be further simplified as the standard notation for a differential equation

$$\frac{d\mathbf{y}}{dt} = \begin{bmatrix} \mathbf{0} & \mathbf{I} \\ \mathbf{A} & \mathbf{0} \end{bmatrix} \mathbf{y} + \begin{bmatrix} \mathbf{0} \\ \tilde{\mathbf{r}} \end{bmatrix},$$

or simply,

$$\frac{d\mathbf{y}}{dt} = \mathbf{B}\mathbf{y} + \mathbf{r}. \tag{5.10}$$

It is worth noting that the matrix $\mathbf{B}$ is independent of the time variable, whereas the vector $\mathbf{r}$ depends on time. Thus, with a difference scheme adopted for time discretization, one needs only to update the right hand side term $\mathbf{r}$ in (5.10) to solve in $\mathbf{y}$ for subsequent time steps.

In this chapter, the analysis with the aid of the explicit Euler scheme to integrate in time is presented. Thus, the adopted difference equation is given as $\mathbf{y}^{n+1} = \mathbf{y}^n + \Delta t\,(\mathbf{B}\mathbf{y}^n + \mathbf{r}^n)$ where superscript n is the index of the discretized time and refers to the time instance $t = n\Delta t$, where Δt is the step-size in time. With this difference scheme, one does run into the problem of obtaining the coefficient vector $\mathbf{y}^0$ pertaining to the given initial condition. The traditional way around this problem is to either (a) use nodal quadrature method and assign exact values at the nodes at time $t = 0$ as the coefficients or (b) obtain the best approximation of the initial condition over the discritization Ω_h. To the author's best knowledge, these best approximations are generally obtained for lagrangian basis functions. In this work, let us solve a Galerkin equation to obtain the best approximation for the initial condition over Ω_h using the enriched solution space as defined in equation (5.5). The corresponding weak forms are given as

$$\int_\Omega E_h(0,\mathbf{x})\phi \; d\Omega \;=\; \int_\Omega E^0(\mathbf{x})\phi \; d\Omega, \tag{5.11a}$$

$$\int_\Omega V_h(0,\mathbf{x})\phi \; d\Omega \;=\; \int_\Omega V^0(\mathbf{x})\phi \; d\Omega. \tag{5.11b}$$

This could be written compactly as $\mathbf{M}\mathbf{y}^0 = \mathbf{f}^0_\Omega$, where $\mathbf{M}$ is the same as in equation (5.7) and $\mathbf{f}^0_\Omega$ is effectively the right hand side of (5.11). Solving this linear system of equations gives us the desired vector of coefficients $\mathbf{y}^0$ to initialize the time-stepping scheme. This procedure of decomposing the initial condition into solution coefficients is discussed in more details in chapter 7.

Note that respresenting the model problem as in (5.10) allows us to directly apply a range of available difference methods for solving the first order ODE in time, such as higher order Runge-Kutta Methods (RKM), however, such a discussion is beyond the scope of this chapter and would form the basis for a latter work presented in chapter 6.

In contrast to the assembly process associated with the proposed explicit scheme, the implicit method used for the PUFEM in [43], as discussed in chapter 3, differs in its assembly mostly in the way the integral over Ω is evaluated. For the implicit method, the $\mathbf{M}$ and the $\mathbf{K}$ terms of (5.8) are evaluated and stored as a single term, as $\mathbf{M}^{\text{Imp}} = \mathbf{M} + \mathbf{K}$. Similarly, the the right-hand side $\mathbf{f}_\Omega$ for the implicit formulation is given as

$$\mathbf{f}_\Omega^{\text{Imp}}{}_{(i,q)} = \int_\Omega \Big(2E^{n-1} - E^{n-2} + \Delta t^2 f(t_n, \mathbf{x})\Big)\Big(\mathcal{N}_i e^{\mathrm{i}kz_q}\Big)\, d\Omega, \tag{5.12}$$

where E^{n-1} and E^{n-2} are the solutions at two consecutively previous steps in time. The boundary integrals in both formulations are very similar. These differences are the direct cause of dissimilarities observed in the overall computational cost associated with the assembly process in the two methods, as discussed in subsection 5.4.3.

One of the attractive features of using an explicit integration in time is the advantage of exploiting the diagonalization of the mass matrix. As it can be seen from the system equations in (5.9), one requires only to invert the mass matrix. The process of inversion can be significantly simplified by diagonalizing the mass matrix. In the FEM, one can achieve a purely diagonal mass matrix, by simply summing up all the columns of the mass matrix along each row into the respective diagonal. The off-diagonal terms are then set to zero. The approximate mass matrix for a linear FEM following this classic row-summation thus is given as

$$\bar{\mathbf{M}}_{(i)(j)} = \begin{cases} 0, & i \neq j, \\ \sum_{l=1}^{N_d} \int_\Omega \mathcal{N}_i \mathcal{N}_l d\Omega, & i = j. \end{cases} \tag{5.13}$$

Thus, inverting this approximate mass matrix then simply requires inverting the diagonal terms, which is trivial. Since one only needs to store the diagonal terms, this also reduces the memory requirements for the mass matrix storage. Such a lumping procedure is rigorously developed for the partition of unity method, for non-negative weight functions and high-order local approximation space in [137], where the local approximation spaces are based on a mix of polynomials, singular and discontinious functions. For this thesis, let us employ this classic row-summation

for plane waves used as enrichment. Thus, in the case of the proposed PUFEM each node now contributes towards a $Q \times Q$ block in the mass matrix. Therefore let us propose to its diagonalization in the same manner as in the standard FEM, which leads to a block-diagonal mass matrix. This is achieved by simply summing up all the off-diagonal blocks along each row into the respective diagonal block. The approximate mass matrix is given as

$$\bar{\mathbf{M}}_{(i,n)(j,m)} = \begin{cases} 0, & i \neq j, \\ \sum_{l=1}^{N_d} \int_{\Omega} \mathcal{N}_i e^{\mathrm{i}kz_n} \mathcal{N}_l e^{\mathrm{i}kz_m} d\Omega, & i = j. \end{cases} \tag{5.14}$$

This lumped mass matrix is much easier to store and invert as compared to the non-diagonalized consistent mass matrix where again the inversion of the mass matrix is now reduced to the inversion of smaller non-overlapping blocks of size $Q \times Q$. The total number of such blocks depends on the total number of nodes in the spatial mesh. In the following sections, the performances of the proposed methods are analysed. Henceforth, the PUFEM with explicit time integration, is mentioned as PUFEM-E and its lumped mass matrix counterpart as PUFEM-BD. The results are also compared to the PUFEM with implicit time integration PUFEM-I. The relative error is evaluated in L^1-norm percentage as

$$\text{Error} = \frac{\|E_h - E\|_{\mathrm{L}^1(\Omega)}}{\|E\|_{\mathrm{L}^1(\Omega)}} \times 100\%, \tag{5.15}$$

where E_h is the numerical solution obtained with each method while E is the exact solution.

5.4 Example of radial wave

First, let us consider a circular wave with the source located at the system origin as studied in chapter 3. The analytical solution is given by

$$E(t, x, y) = e^{\mathrm{i}(kr - \omega t)},$$

$k = 20\pi$, $Q = 27$			
Δt	PUFEM-I	PUFEM-E	PUFEM-BD
0.01	1.32	0.80	2.99
0.005	1.12	0.84	2.91
0.001	0.98	0.92	2.86
$k = 40\pi$, $Q = 57$			
Δt	PUFEM-I	PUFEM-E	PUFEM-BD
0.01	1.01	0.47	2.01
0.005	1.44	0.38	1.90
0.001	29.87	0.44	1.84
$k = 80\pi$, $Q = 97$			
Δt	PUFEM-I	PUFEM-E	PUFEM-BD
0.01	0.79	0.57	4.08
0.005	0.68	0.46	3.96
0.001	4.72	0.46	3.88

Table 5.1: Convergence with refined timestep size in the three considered time integration schemes for the example of radial wave at final time $t = 1$ and uniform mesh of 4×4 elements. The relative percentage errors are shown in columns corresponding to PUFEM-I, PUFEM-E and PUFEM-BD methods respectively.

where $r = \sqrt{x^2 + y^2}$. A unit square computational domain is assumed $\Omega = [0.1, 1.1] \times [0.1, 1.1]$. The analytical solution is imposed on the domain boundary using (5.1b) and also used to evaluate the initial conditions (5.1c) and (5.1d). Three different wavenumbers are considered $k = 20\pi$, $k = 40\pi$ and $k = 80\pi$ with the angular frequency fixed at $\omega = 1$.

5.4.1 Timestep convergence

The first aim in this example is to evaluate the convergence of the PUFEM using explicit time integration where the mass matrix is lumped or full. The domain is discretized into a uniform mesh of 4-noded square elements. Hence, the number of elements is 4 in each direction and the total number of elements is 16 while the total number of nodes is 25. For $k = 20\pi$ we enrich the PUFEM with $Q = 27$, whereas for $k = 40\pi$ and $k = 80\pi$, the chosen number of enrichment functions is $Q = 57$ and 97, respectively. Table 5.1 compares the errors of PUFEM-I, PUFEM-E and PUFEM-BD methods, for three different time steps Δt. The errors are displayed at time $t = 1$ for the three methods.

It is clear that both PUFEM-E and PUFEM-BD methods converge with respect to

the timestep refinement where smaller errors are obtained with smaller values of Δt. For $k = 20\pi$, both PUFEM-E and PUFEM-I methods give practically similar accuracy, whereas PUFEM-BD method leads to larger errors due to the approximation of the block diagonalization of the mass matrix. However, as a higher wavenumber is considered with a higher Q, PUFEM-I method shows significant increase in the error for the smallest considered timestep $\Delta t = 0.001$. The results suggest that PUFEM-I method is less stable than PUFEM-E and PUFEM-BD methods for the accumulation of the round-off errors while for the smallest Δt the solution requires 1000 steps to achieve the final time $t = 1$. PUFEM-I method seems also more sensitive to the ill-conditioning issue often observed at higher number of enrichment functions, see for instance [95, 110].

An explicit scheme is conditionally stable and usually requires the CFL number to be less than 1. On the other hand an implicit scheme is unconditionally stable and thus in general can tolerate a larger Δt. In a typical finite difference scheme, the CFL number is of the order $\sim \frac{u_m \Delta t}{h}$ where u_m is the maximum value of the wave speed present in the analytical solution and h and Δt are the space and time discretization constants, respectively. Heuristically speaking, the CFL number provides a measure of how fast the numerical value is calculated as opposed to the rate of change of the analytical solution on a given space-time grid. Hence, for the stability of the explicit approach a smaller Δt is required for a smaller space discretization. This can be a major issue for wave problems where highly refined meshes are necessary at high wavenumbers. However, thanks to the enrichment, it is shown in this example that the same coarse mesh grid can be retained also when higher wavenumbers are considered. The coarse meshes are associated with relatively large values of the spatial step h. The CFL condition in this case becomes a trivial requirement unless Δt is significantly large. Hence, the sensitivity of the proposed explicit methods against Δt is quite similar to that of the reference implicit method PUFEM-I. This, allows utilizing the benefits of the explicit scheme (such as mass lumping and distributed computation) without compromising on the time step Δt for numerical stability.

5.4.2 Number of enrichment convergence

The next aim in this example is to compare the convergence of the three methods when increasing the number of plane wave enrichments, which is often mentioned as the q-convergence, see for instance [139]. It is well known that the PUFEM suffers from ill-conditioning issues as we increase the number of enrichment functions, for example see [98, 137]. The idea here is to use a small timestep Δt to ensure accuracy while we increase the number of plane wave enrichments until the considered three time integration schemes start to diverge due to the round-off errors and the ill-conditioning issue. The time step $\Delta t = 0.001$ is fixed, and used to simulate a total of 1000 steps to reach the final time of $t = 1$. The same mesh from the previous study is also retained. Table 5.2 summarizes the numerical accuracy of the three time integration schemes obtained at $t = 1$ for the considered wavenumbers $k = 20\pi, 40\pi,$ and 80π.

From the results in Table 5.2, it is evident that for all the methods, the increase in the number of plane waves leads to a better error and that the higher the wavenumber being solved for, the higher is the Q required to achieve a converged numerical solution. It can also be seen that after a certain number of enrichment functions, the PUFEM-I and PUFEM-E methods fail to produce any good result (entries marked with a '–' in the table), whereas the PUFEM-BD method still produces meaningful results. This suggests that PUFEM-BD method is more stable to increasing Q as compared to PUFEM-I and PUFEM-E methods. To some extent this could be understood with the aid of the condition numbers of the system matrices produced by each of the methods. As can also be seen in Table 5.2, the condition number related to the matrix produced by PUFEM-BD method is generally lower than that of the other two schemes, especially for lower values of Q. Obviously, increasing Q further will also lead to divergence in the PUFEM-BD method.

To have more insight into the results let us also plot in Figure 5.1 the errors and the associated condition numbers obtained using the considered time stepping schemes for $k = 80\pi$ against increasing values of Q. One can see in this figure that in general PUFEM-E and PUFEM-I methods lead to similar errors and condition numbers but the latter diverges earlier. Although the PUFEM-BD method leads to an order of magnitude higher errors for the same values of Q as the other two methods

k	Q	Error (%)			Condition number		
		PUFEM-I	PUFEM-E	PUFEM-BD	PUFEM-I	PUFEM-E	PUFEM-BD
20π	21	1.84	1.81	7.64	6.13E+04	6.36E+04	1.34E+02
	31	2.17	0.89	1.61	5.65E+07	6.81E+07	9.40E+06
	41	–	–	1.20	6.43E+08	7.10E+08	2.94E+07
40π	37	3.79	3.78	10.92	3.56E+04	3.61E+04	5.93E+01
	47	0.8	0.76	4.67	9.8E+05	3.67E+06	1.72E+04
	57	–	0.43	1.84	2.09E+07	1.98E+08	1.43E+07
	67	–	–	1.00	3.47E+07	3.37E+07	1.66E+08
80π	71	3.89	3.89	11.84	9.68E+05	1.40E+06	0.65E+01
	81	1.34	1.33	7.73	7.77E+07	2.71E+06	1.17E+03
	91	0.74	0.71	5.10	2.33E+07	1.74E+07	3.90E+05
	101	–	0.37	3.20	2.91E+08	2.48E+07	1.64E+07
	111	–	–	1.94	5.11E+07	6.11E+07	2.56E+07

Table 5.2: The q-convergence for the three time integration schemes considered for the example of radial wave. Note that here a '–' replaces the results of a diverged case.

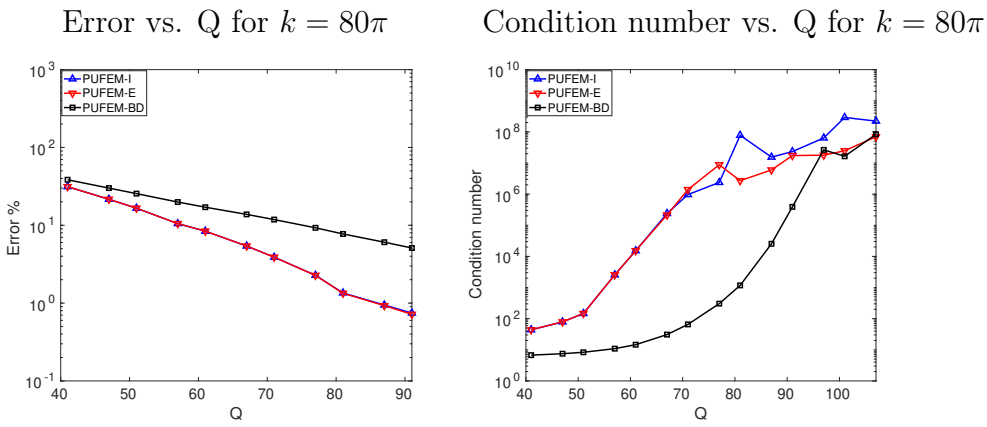

Figure 5.1: The q-convergence plots (left) and condition number plots (right) obtained using the three methods considered for the example of radial wave, for $k = 80\pi$.

Time iteration	Method	
	Explicit	Implicit
$n = 1$	$\mathbf{M}, \mathbf{K}, \mathbf{M}_\Gamma$	$\mathbf{M}^{\text{Imp}}, \mathbf{M}_\Gamma$
	$(-\mathbf{K} - \mathbf{M}_\Gamma)\,\mathbf{y}_1, \mathbf{f}_\Omega, \mathbf{f}_\Gamma$	$\mathbf{f}_{\mathbf{\Omega}}^{\text{Imp}}, \mathbf{f}_\Gamma$
$n > 1$	$(-\mathbf{K} - \mathbf{M}_\Gamma)\,\mathbf{y}_1, \mathbf{f}_\Omega, \mathbf{f}_\Gamma$	$\mathbf{f}_{\mathbf{\Omega}}^{\text{Imp}}, \mathbf{f}_\Gamma$

Table 5.3: Different terms evaluated for the assembly of the finite element linear system of equations using explicit or implicit time integration schemes, at the n^{th} iteration in time.

but the condition numbers associated with PUFEM-BD method are several orders of magnitude smaller. As Q increases beyond a certain threshold i.e. $Q \approx 111$, all three methods are affected with ill conditioning property. This could be explained in terms of the proximity of the direction of propagation of the plane wave enrichment functions, as one increases Q. The more closely packed plane waves push the system matrix closer to being singular.

5.4.3 Computational cost

The main advantage of explicit methods is often considered to be their lower computational costs when compared to implicit ones. In this subsection the aim is to compare the performance metrics of a computer CPU with PUFEM-E, PUFEM-BD and PUFEM-I methods. All the methods are implemented as a sequentially running code in Fortran. The computations are performed on a cluster running CentOS Linux 7 (Core) with an AMD Opteron$^{\text{TM}}$ CPU 6348 @ 1400 MHz $\times$ 24

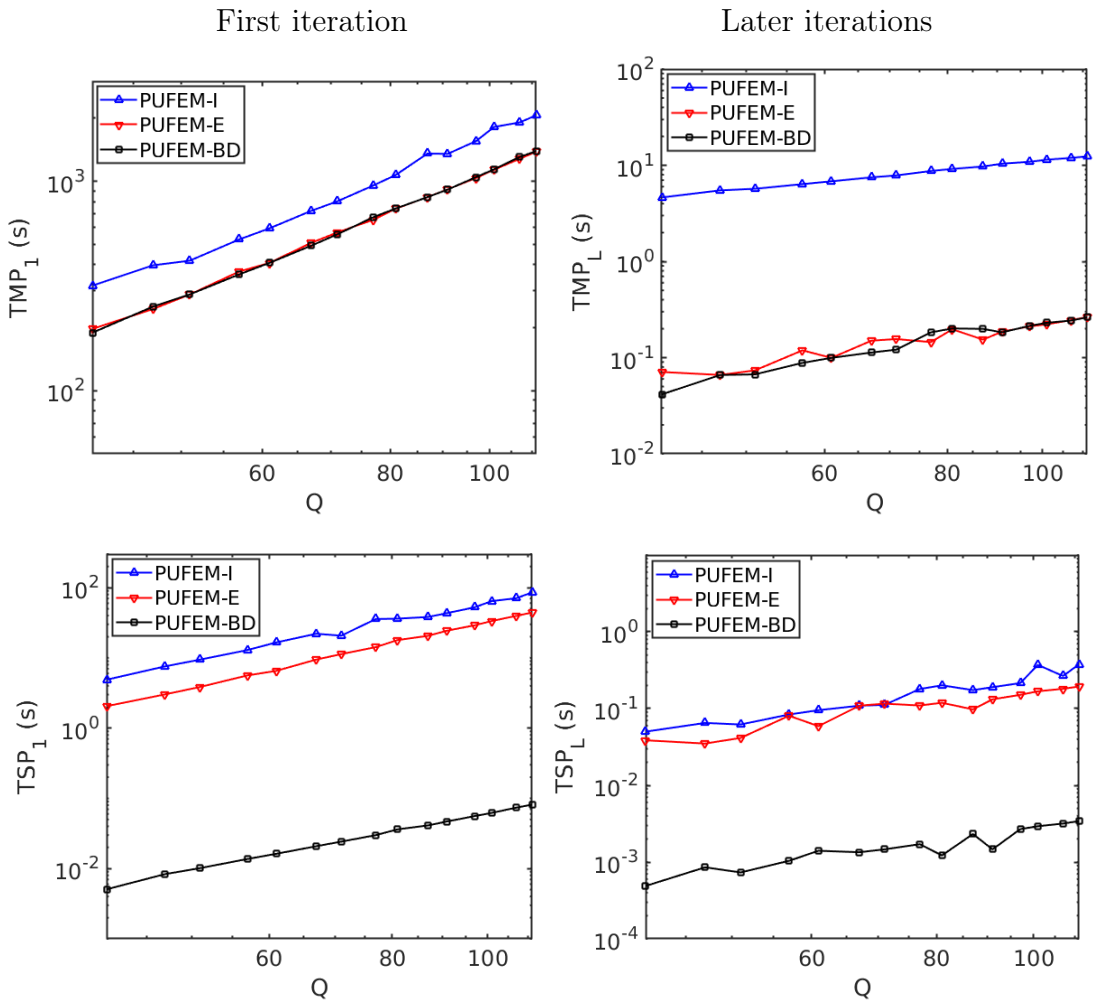

Figure 5.2: Comparison of the CPU time (in seconds) needed for assembly (top row) and solution (bottom row) for first (left column) and later iterations (right column) against degrees of freedom per node.

and 264 GB of RAM. The computational cost, for each iteration in time, is divided into the CPU time spent on the assembly of the linear system and the solution of the linear system. The assembly time is defined as the time taken by the CPU to compute the system matrices and vectors, say matrix $\mathcal{A}$ and vector $\mathbf{b}$ of the linear system of equations $\mathcal{A}\mathbf{x} = \mathbf{b}$. The solution time is the time taken by the CPU to solve this linear system i.e. to obtain the vector $\mathbf{x}$. Furthermore, the assembly and the solution times are compared in the first timestep separately from the subsequent timesteps. The reason for this breakdown in the analysis is to consider the fact that the first iteration in time takes the longest amount of CPU time to complete, for all the three methods. This step involves assembly of the mass and stiffness matrices which are saved and recycled for their usage later on. Also, the inversion of matrix $\mathcal{A}$ takes place in the first step only, using LU decomposition. Thus, both assembly and solution costs are considerably higher for the first time step, as compared to subsequent time steps. Starting from the second step in time onwards, the total CPU time required for the completion of a full iteration in time associated with each of the considered methods is practically constant. In other words, the variance in the total run-time for the n^{th} iteration in time is negligible for $n > 1$, for all the considered methods. Thus, it is sufficient to observe the trends in the first and the second iterations in time to get an overview of the relative performance of the three methods.

Table 5.3 provides a summary of the different terms evaluated over Ω and Γ in the explicit and implicit methods in order to assemble the system. The terms evaluated on the boundary Γ are very similar for both explicit and implicit methods, and hence do not contribute to any significant differences in their assembly or solution times. The CPU time comparisons are studied for $k = 80\pi$ considering again the same cases displayed in Figure 5.1. Figure 5.2 shows a comparison of the CPU times (in seconds) against an increased number of enrichment functions Q for each of the three methods i.e. PUFEM-I, PUFEM-E and PUFEM-BD. In this figure, the assembly time required by each method at the first and the later timesteps referred to by TMP_1 and TMP_L, respectively is plotted at the top row whereas the solution times required at the first and later time steps referred to by TSP_1 and TSP_L, respectively at the bottom row.

The results exhibited in Figure 5.2 show that, using the explicit approach it is possible to significantly reduce the CPU time needed to build the linear system at the first timestep compared to the implicit approach. However, the CPU time for both approaches remains of the same order for the range of Q considered in this study. This can be explained by noting that in the explicit method, the matrices $\mathbf{M}$ and $\mathbf{K}$ are stored in separate variables, whereas in the case of the implicit method, the mass and the stiffness components are added and stored in a single variable ($\mathbf{M}^{\text{Imp}}$). Even though algorithmically, the assembly in the first time step in both implicit and explicit methods requires exactly the same amount of loops, the extra access to memory for storage of two variables instead of one, costs the explicit methods more CPU time. It is noteworthy that, this overhead due to access to memory locations may vary depending on the traffic and type of other processes running concurrently on the CPU node. However, the explicit approach is still intrinsically more efficient because it does not require the calculation of the solution from the previous two time steps, as is required by the considered implicit method while integrating over Ω to compute $\mathbf{f}_{\mathbf{\Omega}}^{\text{Imp}}$. The equivalent expression computed in case of the explicit approach is $(-\mathbf{K} - \mathbf{M}_{\Gamma})\,\mathbf{y}_1$, which is much faster to evaluate since it does not require spatial integrations, and instead is just a vector to matrix multiplication. From second timestep onward the matrices $\mathbf{M}$ and $\mathbf{K}$ are only reused. Hence, the CPU time for the assembly in the case of explicit approach becomes much faster than implicit. It should be also noted that both PUFEM-E and PUFEM-BD methods require practically similar CPU time for the assembly as they involve evaluating the same terms.

Similarly, lets us compare the solution processing times required by the three methods against the number of enrichment functions Q. Figure 5.2 shows the comparisons for the first and the later time steps. As expected, the CPU time for solving the resulting system is practically similar for both PUFEM-I and PUFEM-E methods, since both these methods produce similar system matrices. Obviously with increasing Q the CPU time increases for both PUFEM-I and PUFEM-E methods. On the other hand as delineated from the plots PUFEM-BD provides much better cost effectiveness for increasing Q. For the entire considered range the CPU time remains practically constant at around 0.001 seconds. The reason behind this is the fact that

in the case of PUFEM-E and PUFEM-I methods, the size of the inverted matrix is $m^2Q \times m^2Q$ where m^2 is the total number of nodes in the given computational mesh. Whereas, PUFEM-BD method requires the inversion of m^2 non-overlapping blocks of smaller matrices each of size $Q \times Q$, and hence is much faster. It is of interest to note here that the blocks of matrices along the diagonal of the mass matrix in the PUFEM-BD method have no overlap and thus can be inverted simultaneously with distributed computing, for example over different nodes of a cluster, which could further accelerate the performance of the PUFEM-BD method.

5.5 Example of Gaussian pulse

In this section let us study the performance of PUFEM-BD method when applied to recover a transient Gaussian pulse. This problem does not include any wavenumbers that could be used to chose the enrichment, which presents a challenge for enrichment approaches. The considered computational domain is $\Omega = [1, 2] \times [1, 2]$. The analytical solution of the pulse is

$$E(t, x, y) = e^{-a(\beta + r - ct)^2},$$

where $r = \sqrt{x^2 + y^2}$ is the radial position, β is the offset that controls the onset of the pulse at the origin, a controls the width of the pulse, and c is the speed at which the pulse propagates. Again the analytical solution is imposed on the wave equation (5.1) through the initial and boundary conditions. The analyses are carried out with the parameter $\beta = 1$ kept fixed. Three widths are considered, namely, $a = 8, 16$ and 64. The speed of the pulse for all the widths is kept constant at $c = \frac{1}{8\pi}$ with the angular frequency fixed at $\omega = 1$. The simulation is carried out for the time span $t \in]0, 120]$ with the timestep size $\Delta t = 0.001$ where the total number of the computed timesteps is 120000. For the given wave speed this time span allows to analyze the transit of the pulse through the entire spatial domain. At the start of the simulation, the solution is very close to zero in the entire domain. Evaluating the error as in expression (5.15) will involve division by numbers close to zero. To

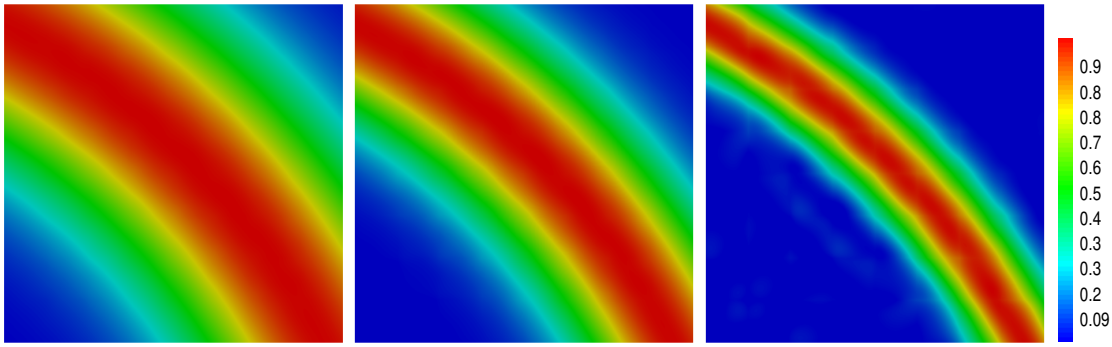

Figure 5.3: Snapshots of solution obtained with PUFEM-BD method for the example of Gaussian pulse with widths corresponding to $a = 8$, 16 and 64 (left to right) at time $t = 80$. These problems were solved on a uniform mesh with 81 nodes and 64 elements. For each of them the enrichment wavenumber is $k = 4\pi$ and number of enrichment functions is $Q = 9$.

remedy this let us redefine the relative error percentage as

$$\varepsilon = \frac{\|E_h - E\|_{\mathrm{L}^1(\Omega)}}{\|E_{\max}\|_{\mathrm{L}^1(\Omega)}} \times 100\%, \tag{5.16}$$

where $E_{\max}$ is the magnitude of the exact value of the pulse at its maximum, which is unity in this case.

To evaluate the enrichment wavenumber choice lets us study the performance of PUFEM-BD method for the Gaussian pulse as the pulse width is changed. The impact of the spatial discretization on PUFEM-BD method's accuracy is studied for a range of spatial discretizations. For this study four different meshes are used. The meshes are characterised by the chosen number of nodes in one direction $m = \{3, 5, 7, 9\}$. The considered number of enrichment functions are $Q = \{5, 9, 13, 17\}$ and the enrichment wavenumbers are $k = \{2\pi, 4\pi, 8\pi\}$ along with the three different widths corresponding to $a = \{8, 16, 64\}$. The resulting total number of studied cases is 144. The errors for all these cases at the time instance $t = 60$ and at the end of the simulation $t = 120$ are shown in tables 5.4 and 5.5, respectively. In these tables the '–' replaces the errors for the cases where the solution diverges. For illustration purposes Figure 5.3 shows the solutions obtained with PUFEM-BD method at $t = 80$ for the three considered widths.

Table 5.4 shows that increasing m for each of the 3 widths will always lead to an improved error. In general for a given m, increasing Q also improves the errors. This improvement seems less significant for $k = 8\pi$. The results in Table 5.5 again show

that increasing m improves the error. For a given m, increasing Q improves the error for the enrichment wavenumber $k = 4\pi$ in all the cases. For the wavenumbers $k = 2\pi$ the error improves for increasing Q for $a = 8$ and 16 while for $a = 64$ the error increases for $m = 3$ by increasing the number of enrichment functions to $Q = 13$. For the case $k = 8\pi$ the error seems to stay practically unchanged for an increasing Q and for all values of a. This suggests that the enrichment has limited contribution to the finite element approximation for $k = 8\pi$ in all considered widths, and for $k = 2\pi$ only in $a = 64$. The FEM approximation in this case is mainly dependent on the element size where only refining the mesh improves the error. Also as the pulse width becomes smaller at $a = 64$ the error becomes larger. This is expected as a finer mesh is needed to capture a narrower pulse.

To understand why the wavenumber $k = 4\pi$ seems to be more suitable for the considered widths, one may link the pulse width to the wavelength of the enrichment functions. For a given value of a, the pulse width could be calculated as $\frac{\sqrt{2\ln 2}}{\sqrt{2a}}$. The related enrichment wavelength will then be twice this number. Thus, for the given values of $a = \{8, 16, 64\}$, the width roughly varies between 0.3, 0.2 and 0.1. These widths will be comparable to the enrichment wavelengths that correspond to the wavenumbers 3.4π, 4.8π and 9.6π. The best results for the given parametric study are found for an enrichment wavenumber of 4π, which is close to the two wavenumbers 3.4π and 4.8π. The errors achieved in this case with $m = 9$ and $Q = 9$ are $\varepsilon = 0.3\%$ and 0.4%. It is well known that the PUFEM suffers from ill-conditioning and stability issues if the characteristic mesh size is not multiple times larger than the enrichment wavelength [29]. These issues become more evident as one increases Q in the sense that the plane waves in the basis are more closely packed together. This explains the instability and the larger errors associated with the PUFEM-BD method, especially observed at higher values of m and smaller values of wavenumber k as we increase Q, as is seen in the tables 5.4 and 5.5.

The final aim in this example is to evaluate the effect of approximation due to the lumping of the mass matrix by comparing the performance of the PUFEM-BD method to that of the PUFEM-E method. A relatively wide width pulse is considered with $a = 1$. The pulse speed is again fixed at $c = \frac{1}{8\pi}$. The problem is solved on a relatively coarse mesh, namely, $m = 5$ and for an increased Q where

		$a=8$				$a=16$				$a=64$			
		m				m				m			
	Q	3	5	7	9	3	5	7	9	3	5	7	9
$k=2\pi$	5	1.31	0.26	–	–	1.30	0.26	–	–	0.83	0.24	–	–
	9	0.55	0.07	–	–	0.59	0.09	–	–	0.41	0.11	–	–
	13	0.44	–	–	–	0.52	–	–	–	0.30	–	–	–
$k=4\pi$	5	4.79	1.07	0.34	0.14	2.84	0.64	0.20	0.08	0.99	0.30	0.11	0.06
	9	3.57	0.40	0.07	0.01	2.17	0.24	0.05	0.02	0.76	0.14	0.04	0.02
	13	3.56	0.38	–	–	2.02	0.23	–	–	0.54	0.12	–	–
$k=8\pi$	5	4.05	1.45	0.71	0.41	3.07	1.29	0.61	0.35	1.33	0.63	0.30	0.13
	9	4.08	1.45	0.52	0.19	3.17	1.19	0.37	0.14	1.40	0.48	0.14	0.05
	13	4.13	1.36	0.50	0.20	3.12	1.10	0.36	0.14	1.34	0.44	0.13	0.05

Table 5.4: The q-refinement with PUFEM-BD method for the example of Gaussian pulse for widths corresponding to $a = 8, 16$, and 64 at time $t = 60$.

		$a=8$				$a=16$				$a=64$			
		m				m				m			
	Q	3	5	7	9	3	5	7	9	3	5	7	9
$k=2\pi$	5	14.9	3.8	–	–	21.3	8.5	–	–	20.3	16.4	–	–
	9	3.8	0.4	–	–	8.9	1.8	–	–	15.5	13.8	–	–
	13	2.6	–	–	–	8.1	–	–	–	22.4	–	–	–
$k=4\pi$	5	22.2	6.9	10.3	5.6	20.2	12.1	10.3	5.0	16.7	18.0	13.1	8.8
	9	14.3	6.4	1.0	0.3	15.9	8.6	1.7	0.4	17.7	11.0	4.6	2.3
	13	14.2	3.2	–	–	12.7	3.5	–	–	15.6	8.1	–	–
$k=8\pi$	5	17.5	18.5	12.5	7.1	14.4	20.5	18.0	10.9	9.8	17.4	20.3	16.8
	9	17.8	13.2	5.0	2.2	15.0	16.4	9.4	4.0	11.6	18.9	13.7	7.3
	13	16.8	17.5	4.8	3.8	14.2	21.2	6.3	7.9	11.9	22.2	6.3	10.7

Table 5.5: The q-refinement with PUFEM-BD method for the example of Gaussian pulse for widths corresponding to $a = 8, 16$, and 64 at time $t = 120$.

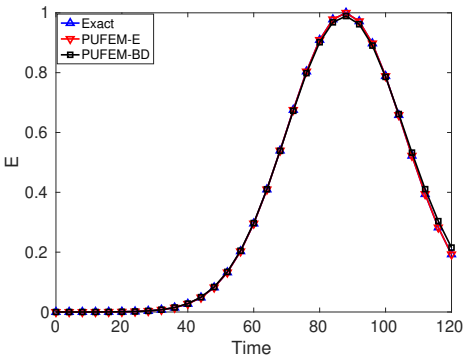

Figure 5.4: Time evolution of the exact and numerical values of the Gaussian pulse for width $a = 1$, obtained at a spatial point (1.99,1.49) on the computational domain with PUFEM-E and PUFEM-BD methods. Both solutions are obtained over a uniform mesh with 25 nodes and 16 elements, and $Q = 5$ with $k = 2\pi$).

the wavenumber of the enrichment plane waves is set as 2π. This choice of k is based on the pulse width which is 0.83 in this case. The timestep size is fixed at $\Delta t = 0.001$. For $Q = 5$ the errors at $t = 60$ are 0.002% and 0.14% with the PUFEM-E method and the PUFEM-BD method, respectively. At the end of the simulations i.e. at $t = 120$, the error increases to 0.004% with the PUFEM-E method and to 1.63% with the PUFEM-BD method. When the number of enrichment functions is increased to $Q = 9$, it is observed that the PUFEM-E method becomes unstable and fails to produce any results whereas the errors with the PUFEM-BD method improve to 0.02% at $t = 60$ and 0.04% at $t = 120$. This result confirms the trends observed in subsection 5.4.2. The error associated with the PUFEM-BD method is again larger than that of the PUFEM-E method, which is expected because of the approximation due to mass lumping. Also to be seen here is that the PUFEM-BD method is more resilient to increasing Q than the PUFEM-E method. In Figure 5.4 let us plot a comparison of the numerical solutions obtained with the two considered explicit methods, as they evolve in time at a fixed spatial point on the computational domain. For illustration, snapshots of the numerical solution for the pulse recovered with PUFEM-E method for $Q = 5$ at different time instances, are shown in Figure 5.5.

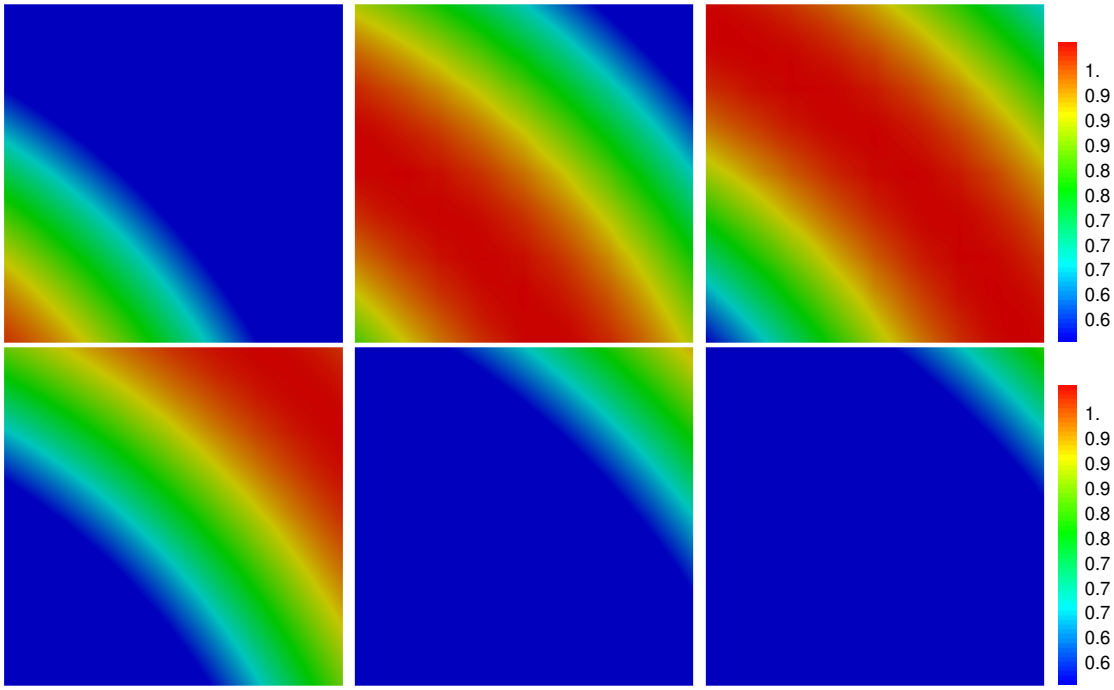

Figure 5.5: Time evolution of the Gaussian pulse (width corresponding to $a = 1$) in time, solved using PUFEM-E method, for $Q = 5$ and $k = 2\pi$ over a uniform mesh of 16 elements. Snapshots were taken at time $t = 56, 72, 80, 92, 104$, and 108 arranged in the figure from left to right and top to bottom.

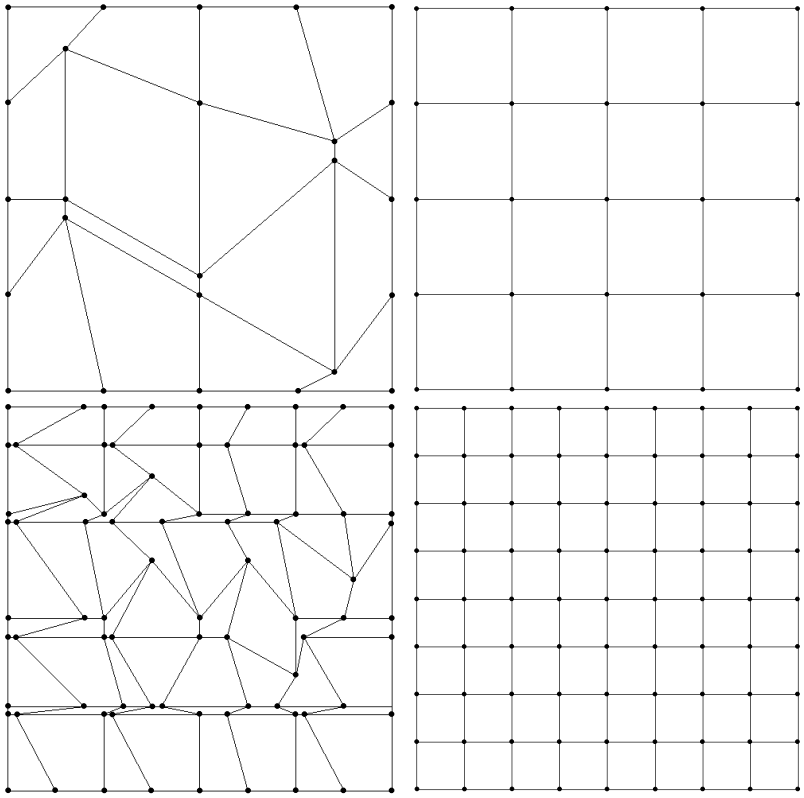

Figure 5.6: Uniform meshes and their distorted counterparts, used in the example of transient envelope wave.

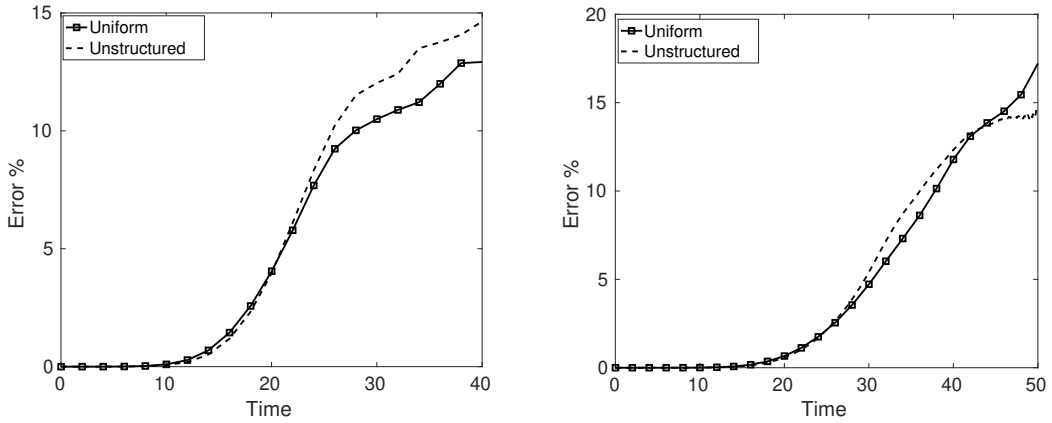

Figure 5.7: Comparison of errors associated with numerical solutions for the example of transient envelope wave, obtained using the PUFEM-BD method over uniform and unstructured meshes respectively. The plots are for $k = 4\pi$ (left) and $k = 8\pi$ (right), for $Q = 13$ and $Q = 17$, respectively.

5.6 Example of transient envelope wave

In this numerical example let us recover a transient envelope wave which is described in chapter 3. The analytical solution of the problem is given as

$$E(t, x, y) = Ae^{\mathrm{i}\omega f_L(t,x,y)},$$

where f_L is a propagator function that controls the initial condition of the problem. Here let us use the F_2 propagator, described in details in the reference appendix A.1 and A.2. The propagator implies a gradual increase in the amplitude of the wave expanding symmetrically around the coordinate origin. Two different wavenumbers, namely, $k = 4\pi$ and $k = 8\pi$ are considered.

The aim in this example is to evaluate the impact of using an unstructured mesh on the approximation levied upon by the lumped mass approach. To this end let us consider two sets of meshes, first with uniform elements similar to the meshes considered in the previous studies, and second with distorted elements. The unstructured meshes of the distorted elements are obtained by randomly displacing the nodes of the uniform meshes. It should be stressed that only the locations of the nodes, are displaced so that the distorted meshes include the same number of nodes and elements as their uniform counterparts but the elements are no longer square in shape. Furthermore, the distortion of the meshes is performed to produce

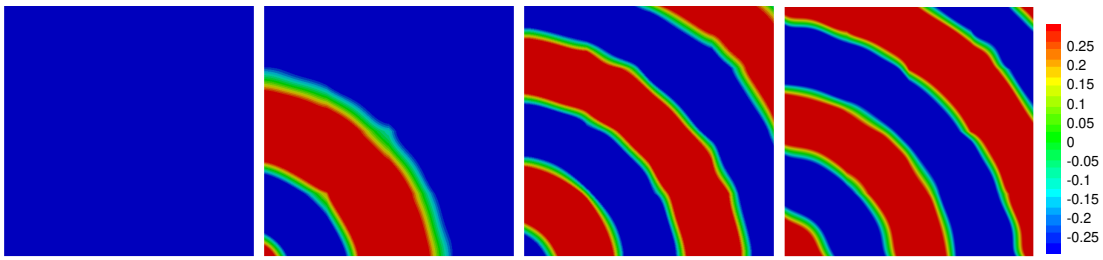

Figure 5.8: Snapshots of numerical solutions obtained with the PUFEM-BD method for the example of transient envelope wave, solved on a uniform grid with 16 elements and $Q = 13$ with $k = 4\pi$. These snapshots correspond to time t=10, 20, 30 and 40 (left to right).

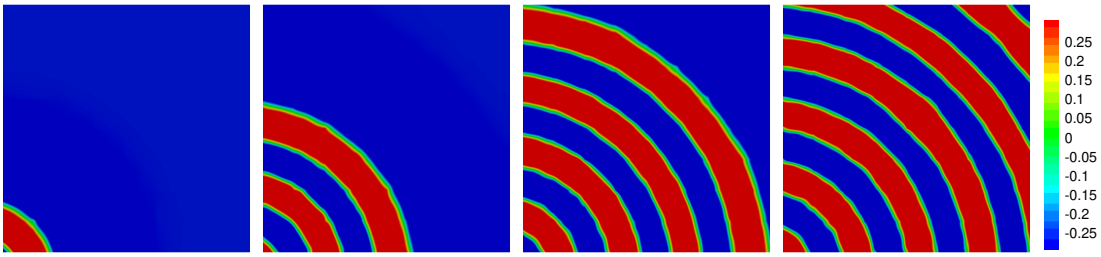

Figure 5.9: Snapshots of numerical solutions obtained with the PUFEM-BD method for the example of transient envelope wave, solved on a uniform grid with 64 elements and $Q = 17$ with $k = 8\pi$. These snapshots correspond to time t=20, 30, 40 and 50 (left to right).

severely poor quality elements. Figure 5.6 shows the two uniform meshes considered in this study alongside the unstructured meshes. The coarse meshes composed of 25 nodes and 16 elements, are then enriched using $Q = 13$ to solve the problem for $k = 4\pi$. Similarly the fine meshes composed of 81 nodes and 64 elements are enriched with $Q = 17$ and used to solve for $k = 8\pi$. The step-size in time in both the cases is kept constant at $\Delta t = 0.01$. The simulation is completed at $t = 40$ for $k = 4\pi$ and $t = 50$ for $k = 8\pi$, respectively, allowing the waves to spread into the entire computational domain. It is noteworthy that the angular frequency in time is kept constant at 1, thus for a higher wavenumber, the wave moves slower. The time evolution of the errors associated with the PUFEM-BD method for the considered two wavenumbers are then displayed in Figure 5.7. Figures 5.8 and 5.9 show the numerical solutions obtained with the PUFEM-BD method for the two considered wavenumbers, respectively, at different time instances. The results are very similar to that obtained with the reference implicit method in chapter 3.

The results in Figure 5.7 show that the errors are relatively similar if using a structured or an unstructured mesh for the start of the simulation. For example for

$k = 4\pi$ both meshes lead to similar errors up to time $t \approx 19$, while for $k = 8\pi$ up to time $t \approx 25$. Thereafter, the unstructured meshes cause a significant deviation in the error evolution. To compare this behavior to the explicit time integration scheme without lumping, the problem is solved again using the PUFEM-E method on the same meshes shown in Figure 5.6. On the uniform meshes, the errors in numerical solution at the end of the simulation with the PUFEM-E method are 5.97% for $k = 4\pi$ on the coarse uniform mesh with $Q = 7$, and is 7.64% for $k = 8\pi$ on the fine uniform mesh with $Q = 11$. These errors are compared to 12.91% for $k = 4\pi$ with $Q = 13$ and 17.21% for $k = 8\pi$ with $Q = 17$, using the PUFEM-BD method. However if one increases Q any further, the PUFEM-E method becomes unstable for both the wavenumbers considered. Moreover, the PUFEM-E method fails to produce any results when distorted meshes are used. This shows that the lumping approach is more stable not only for an increased Q, as is also seen in the previous test cases, but also is more stable when using unstructured meshes.

5.7 Conclusions

In this chapter it is proposed to use explicit time integration scheme with block diagonal lumping of the mass matrix for the partition of unity finite element solution of time domain wave problems. The convergence of the solution for refined temporal and spatial discretizations is studied. The results obtained with the explicit scheme both lumped and full, are compared to the results obtained with an implicit time integration scheme. The results presented herein show major advantages for the explicit approach with a lumped mass matrix. The advantages are related to significant reduction in the CPU time as well as better conditioned linear system of equations.

The work also investigates the partition of unity solution of a transient Gaussian pulse which does not involve a specific wavenumber. A parametric study shows that the plane wave enrichment can still be used for the solution. Better errors are achieved for the cases where the wavelength of the enrichment functions is close to the pulse width. More rigorous methods could be developed for isolating the spatial frequencies present in the solution, albeit that would form the basis of future work

in developing the techniques presented in this work.

Inherently, the explicit time integration schemes, as opposed to their implicit counterparts, are only conditionally stable. The CFL condition must be satisfied to ensure their numerical stability. This condition essentially requires that the problem is solved numerically on a fine enough discretization in both space and time, such that the numerical solver is able to capture the fastest of the wave components present in the actual solution. The oscillatory nature of the enrichment functions used to improve the finite element basis allows to use significantly coarse meshes even for high wavenumbers. The coarse spatial mesh in turn facilitates utilizing the benefits of an explicit scheme without the need for a fine step-size in time. The discussed numerical results show that the step-size used with the considered implicit scheme is very similar to that used with the proposed explicit counterparts.

The PUFEM is known to produce ill-conditioned linear system of equations with an increased nodal density of the enrichment functions. The results discussed in this chapter show that the lumped mass approach improves the conditioning of the PUFEM system matrix by several orders of magnitude. Furthermore, the resulting block diagonal system matrix is much faster to invert, and can be stored much more efficiently as compared to the full matrix for the non-lumped approach. The results also suggest that lumping the mass matrix makes the PUFEM more stable against poor quality distorted elements used to discretize the spatial mesh. Although the block diagonal lumping of the mass matrix is only tested for the partition of unity method, and in the context of wave propagation problems, the approach could also be used for other enrichment techniques such as the generalized finite element method when solving time-domain problems.

Chapter 6

Higher order integration schemes in time

6.1 Overview

In the previous chapters, first order implicit and explicit integration schemes are investigated to discretize the time variable, in conjunction with plane wave enrichment functions used for spatial approximation. This chapter further extends the research into using higher order integration schemes available in the Runge-Kutta family to facilitate the usage of coarse step-size in time. The numerical solutions obtained with the higher order time integration models are tested against the previously established low order schemes, and the results are compared.

6.2 Semi-discrete formulation

Previously we have seen the discretization, using a fully-implicit difference scheme with respect to the time variable using low order implicit backward Euler, along with a semi-discrete Galerkin method with plane wave enrichment functions, with respect to the space variable, in Chapter 3. Similarly, the first order explicit forward Euler integration scheme for the time variable is investigated in Chapter 5. The solution space investigated in this research, is constructed using functions of the form

$$E_h(t, \mathbf{x}) = \sum_{j=1}^{N_d} \sum_{q=1}^{Q} \hat{E}_j^q(t) \mathcal{E}_q(\mathbf{x}) \mathcal{N}_j(\mathbf{x}), \tag{6.1}$$

where the bump functions $\mathcal{N}_j(\mathbf{x})$ provide the locality and global regularity to the solution, the enrichment functions $\mathcal{E}_q(\mathbf{x})$ provide the information about the kernel of the governing PDE, and the scaling coefficient $\hat{E}_j^q(t)$ provides the time dependence for the solution space. This separation of the space and time variables, permits semi-discrete time dependent analysis for the wave equation. Consider the scalar wave equation $\ddot{E} - c^2\nabla^2 E = c^2 f$, arranged as follows

$$\begin{bmatrix} \dot{E} \\ \dot{V} \end{bmatrix} = \begin{bmatrix} 0 & I \\ c^2\nabla^2 & 0 \end{bmatrix} \begin{bmatrix} E \\ V \end{bmatrix} + \begin{bmatrix} 0 \\ c^2 f \end{bmatrix}, \tag{6.2}$$

where the dot notation implies the time derivative, I is the identity matrix, c is the wave speed, f is the source, E is the scalar field and $V = \dot{E}$. The field values and the source are all functions of time t defined over the space Ω, just as seen in previous chapters. Next, obtain the semi-discrete form

$$\begin{bmatrix} \mathbf{M}\dot{\mathbf{y}}_1 \\ \mathbf{M}\dot{\mathbf{y}}_2 \end{bmatrix} = \begin{bmatrix} 0 & \mathbf{M} \\ -c^2\mathbf{K} & 0 \end{bmatrix} \begin{bmatrix} \mathbf{y}_1 \\ \mathbf{y}_2 \end{bmatrix} + \begin{bmatrix} 0 \\ c^2\mathbf{f}_\Gamma + c^2\mathbf{f}_\Omega \end{bmatrix}, \tag{6.3}$$

by integrating over Ω, on both sides of equation (6.2). Here, $\mathbf{y}_1$ and $\mathbf{y}_2$ are coefficient vectors, $\mathbf{M}$ is the mass matrix, $\mathbf{K}$ is the stiffness matrix, $\mathbf{f}_\Gamma$ is the boundary condition dependent integral and $\mathbf{f}_\Omega$ is the source dependent integral, as defined in section 5.3 of Chapter 5. Applying the inverse of the mass matrix on both sides of this weak form produces the system of first order ordinary differential equations of the form

$$\dot{\mathbf{y}} = \begin{bmatrix} \mathbf{0} & \mathbf{I} \\ \mathbf{A} & \mathbf{0} \end{bmatrix} \mathbf{y} + \begin{bmatrix} \mathbf{0} \\ \tilde{\mathbf{r}} \end{bmatrix}, \tag{6.4}$$

where $\mathbf{y} = \{\mathbf{y}_1, \mathbf{y}_2\}^\top$, $\mathbf{A} = -c^2\mathbf{M}^{-1}(\mathbf{K})$, $\tilde{\mathbf{r}} = c^2\mathbf{M}^{-1}(\mathbf{f}_\Omega + \mathbf{f}_\Gamma)$ and $\mathbf{I}$ is the identity matrix. This could be further simplified as

$$\dot{\mathbf{y}} = \mathbf{B}\mathbf{y} + \mathbf{r}, \tag{6.5a}$$

$$\Rightarrow \dot{\mathbf{y}} = S(\mathbf{y}, t), \tag{6.5b}$$

where $S(\mathbf{y}, t)$ is generally referred to as the slope. Note that the operator

$$\mathbf{B} = \begin{bmatrix} \mathbf{0} & \mathbf{I} \\ \mathbf{A} & \mathbf{0} \end{bmatrix},$$

is independent of the time variable. The form $\dot{\mathbf{y}} = S(\mathbf{y}, t)$, is suitable to apply a range of available integration schemes for the time variable. In the following sections, different schemes from the Runge-Kutta family of methods are investigated.

6.3 Explicit Runge-Kutta methods

For a first order ordinary differential equation of the form $\dot{\mathbf{y}} = S(\mathbf{y}, t)$, the Runge-Kutta methods (RKMs) could be applied given the initial condition $\mathbf{y}(0) = \mathbf{y}_0$. In this section, several explicit schemes in the RKM family are investigated. For an explicit formulation, given the value of the coefficient vector $\mathbf{y}^n$ at time $t_n = n\Delta t$, where Δt is the step-size in time and integer n is the time index, the value of the coefficient vector for the next time index is given as

$$\mathbf{y}^{n+1} = \mathbf{y}^n + (\Delta t) \sum_{i=1}^{s} b_i \mathbf{k}_i, \tag{6.6a}$$

$$\mathbf{k}_i = S\left(\mathbf{y}^n + (\Delta t) \sum_{j=1}^{p} a_{ij} \mathbf{k}_j, t_n + c_i \Delta t \right), \tag{6.6b}$$

where b_i and c_i are the weights and nodes of the RKM integration scheme, and a_{ij} are the elements of the RKM matrix. These values are generally available for different

c_i	a_{ij}
	b_i

Table 6.1: The Butcher tableau for a generic RKM.

schemes in a tabular form, often termed as the Butcher tableau, represented as shown in Table 6.1. In equation (6.6) s is the number of intermediate steps computed for the RKM scheme which also defines its order. Also for explicit schemes, the value of $p = (i - 1)$ in (6.6), whereas for implicit schemes, the value of $p = s$.

6.3.1 First order explicit RKM

The Butcher tableau for the simplest first order method of

0	0
	1

Table 6.2: The Butcher tableau for forward Euler.

the explicit RKM family is shown in Table 6.2. Using this table, the difference scheme for the semi-discrete wave equation (6.5) can be written as

$$\mathbf{y}^{n+1} = \mathbf{y}^n + (\Delta t)\mathbf{k}_1, \tag{6.7a}$$

$$\mathbf{k}_1 = S\left(\mathbf{y}^n, t_n\right). \tag{6.7b}$$

Simplifying this difference scheme, we get $\mathbf{y}^{n+1} = \mathbf{y}^n + \Delta t\left(\mathbf{B}\mathbf{y}^n + \mathbf{r}^n\right)$. This is exactly the same forward Euler scheme as used in Chapter 5. In this scheme, the coefficient vectors $\mathbf{y}_1$ and $\mathbf{y}_2$ are evaluated as

$$\mathbf{y}_1^{n+1} = \mathbf{y}_1^n + (\Delta t)\mathbf{y}_2^n, \tag{6.8a}$$

$$\mathbf{y}_2^{n+1} = \mathbf{y}_2^n + (\Delta t)\mathbf{A}\mathbf{y}_1^n + (\Delta t)\tilde{\mathbf{r}}^n. \tag{6.8b}$$

The equations (6.8a) and (6.8b) are solved simultaneously. However, one can also modify the algorithm to first solve for $\mathbf{y}_1^{n+1}$ and then use this to solve $\mathbf{y}_2^{n+1} = \mathbf{y}_2^n + (\Delta t)\mathbf{A}\mathbf{y}_1^{n+1} + (\Delta t)\tilde{\mathbf{r}}^n$. Such modifications are investigated in the domain of symplectic RKM family [18, 135]. As compared to nonsymplectic counterparts, the symplectic methods are argued to provide better accuracy in numerical solutions for long-term time evolution of energy preserving physical systems *e.g.* planetary systems and systems of charged particles in electromagnetic fields [65, 132]. Such techniques are not investigated in this thesis.

6.3.2 Second and higher order explicit RKM

The generic second order explicit RKM is defined with its

0	0	0
α	α	0
	$1 - \frac{1}{2\alpha}$	$\frac{1}{2\alpha}$

Table 6.3: The Butcher tableau for generic second order explicit RKM.

Butucher tableau shown in Table 6.3. The value of $\alpha = \frac{2}{3}$ defines the Ralston's method. Using the Ralston's method, the difference scheme for the semi-discrete wave equation (6.5) is given as

$$\mathbf{y}^{n+1} = \mathbf{y}^n + (\Delta t)\left(\frac{\mathbf{k}_1}{4} + \frac{3\mathbf{k}_2}{4}\right), \tag{6.9a}$$

$$\mathbf{k}_1 = S\left(\mathbf{y}^n, t_n\right), \tag{6.9b}$$

$$\mathbf{k}_2 = S\left(\mathbf{y}^n + (\Delta t)\frac{2\mathbf{k}_1}{3}, t_n + \frac{2}{3}\Delta t\right). \tag{6.9c}$$

Simplifying the above difference scheme for the generic case, we get

$$\mathbf{k}_1 = \mathbf{B}\mathbf{y}^n + \mathbf{r}^n = \begin{bmatrix} \mathbf{y}_2^n \\ \mathbf{A}\mathbf{y}_1^n + \tilde{\mathbf{r}}^n \end{bmatrix} = \begin{bmatrix} \mathbf{k}_1^u \\ \mathbf{k}_1^l \end{bmatrix}, \tag{6.10a}$$

$$\begin{aligned} \mathbf{k}_2 &= \mathbf{B}\left(\mathbf{y}^n + (\Delta t)a_{21}\mathbf{k}_1\right) + \mathbf{r}^{(n+c_2)} \\ &= \begin{bmatrix} \mathbf{y}_2^n + (\Delta t)a_{21}\mathbf{k}_1^l \\ \mathbf{A}\left(\mathbf{y}_1^n + (\Delta t)a_{21}\mathbf{k}_1^u\right) + \tilde{\mathbf{r}}^{(n+c_2)} \end{bmatrix} = \begin{bmatrix} \mathbf{k}_2^u \\ \mathbf{k}_2^l \end{bmatrix}, \end{aligned} \tag{6.10b}$$

where the symbols $\mathbf{k}_i^u$ and $\mathbf{k}_i^l$ are introduced to denote intermediate increments computed for the RKM. Also note that in equations (6.10), the short-hand notation $(n + c_2)$ represents the index for time $t = t_n + c_2\Delta t$. Using the notations as defined

in equations (6.10), the coefficient vectors $\mathbf{y}_1$ and $\mathbf{y}_2$ are evaluated as

$$\mathbf{y}_1^{n+1} = \mathbf{y}_1^n + (\Delta t)\sum_{i=1}^{2} b_i \mathbf{k}_i^u, \tag{6.11a}$$

$$\mathbf{y}_2^{n+1} = \mathbf{y}_2^n + (\Delta t)\sum_{i=1}^{2} b_i \mathbf{k}_i^l. \tag{6.11b}$$

Equivalent forms of equations (6.10) and (6.11) could be developed for higher order

0	0			
1/2	1/2			
1/2	0	1/2		
1	0	0	1	
	1/6	1/3	1/3	1/6

Table 6.4: The Butcher tableau for fourth order explicit RKM.

RKMs. Consider the Butcher tableau as shown in Table 6.4, which defines the classic fourth order RKM. For this tableau, the time stepping scheme is formulated as

$$\mathbf{y}^{n+1} = \mathbf{y}^n + (\Delta t)\sum_{i=1}^{4} b_i \mathbf{k}_i, \tag{6.12a}$$

$$\mathbf{k}_i = \begin{bmatrix} \mathbf{k}_i^u \\ \mathbf{k}_i^l \end{bmatrix} = \begin{bmatrix} \mathbf{y}_2^n + (\Delta t)\sum_{j=1}^{i-1} a_{ij}\mathbf{k}_j^l \\ \mathbf{A}\left(\mathbf{y}_1^n + (\Delta t)\sum_{j=1}^{i-1} a_{ij}\mathbf{k}_j^u\right) + \tilde{\mathbf{r}}^{(n+c_i)} \end{bmatrix}, \tag{6.12b}$$

which can be used to solve for the coefficients

$$\mathbf{y}_1^{n+1} = \mathbf{y}_1^n + (\Delta t)\sum_{i=1}^{4} b_i \mathbf{k}_i^u, \tag{6.13a}$$

$$\mathbf{y}_2^{n+1} = \mathbf{y}_2^n + (\Delta t)\sum_{i=1}^{4} b_i \mathbf{k}_i^l. \tag{6.13b}$$

The difference schemes of (6.11) and (6.13) can be implemented to solve the semi-discrete wave equation (6.5), using second and fourth order explicit RKMs. Similarly, these schemes could be well extended for other higher order RKMs using the appropriate Butcher tableau for integration weights and abscissae.

6.4 High order implicit RKM

From the previous section one can derive that the intermediate increment vectors $\mathbf{k}_i = \{\mathbf{k}_i^u, \mathbf{k}_i^l\}^\top$ for the generic s^{th} order explicit RKM are given as

$$\begin{bmatrix} \mathbf{k}_i^u \\ \mathbf{k}_i^l \end{bmatrix} = \begin{bmatrix} \mathbf{y}_2^n + (\Delta t)\sum_{j=1}^{i-1} a_{ij}\mathbf{k}_j^l \\ \mathbf{A}\left(\mathbf{y}_1^n + (\Delta t)\sum_{j=1}^{i-1} a_{ij}\mathbf{k}_j^u\right) + \tilde{\mathbf{r}}^{(n+c_i)} \end{bmatrix}, \tag{6.14a}$$

$$= \mathbf{B}\left(\mathbf{y}^n + (\Delta t)\mathbf{M}^s\mathbf{k}_i\right) + \mathbf{r}^{(n+c_i)}, \tag{6.14b}$$

where $\mathbf{M}^s$ is the $s \times s$ RKM matrix, composed of the elements a_{ij}, as defined by the Butcher tableau. Note that for the explicit RKMs, the elements in the upper triangle of $\mathbf{M}^s$, including the diagonal elements, are identically zero. However, this is not true for the implicit family of RKMs. For the sake of simplicity, only diagonally implicit RKMs are considered for the purposes of this research.

For a diagonally implicit method with a lower triangular RKM matrix, let us denote the intermediate increment vectors as $\check{\mathbf{k}}_i = \{\check{\mathbf{k}}_i^u, \check{\mathbf{k}}_i^l\}^\top$. These vectors can be evaluated as

$$\begin{bmatrix} \check{\mathbf{k}}_i^u \\ \check{\mathbf{k}}_i^l \end{bmatrix} = \begin{bmatrix} \mathbf{y}_2^n + (\Delta t)\sum_{j=1}^{i-1} a_{ij}\check{\mathbf{k}}_j^l \\ \mathbf{A}\left(\mathbf{y}_1^n + (\Delta t)\sum_{j=1}^{i-1} a_{ij}\check{\mathbf{k}}_j^u\right) + \tilde{\mathbf{r}}^{(n+c_i)} \end{bmatrix} + \begin{bmatrix} (\Delta t)a_{ii}\check{\mathbf{k}}_i^l \\ (\Delta t)a_{ii}\mathbf{A}\check{\mathbf{k}}_i^u \end{bmatrix}, \tag{6.15a}$$

$$= \begin{bmatrix} \mathbf{k}_i^u \\ \mathbf{k}_i^l \end{bmatrix} + \begin{bmatrix} \beta_i\check{\mathbf{k}}_i^l \\ \beta_i\mathbf{A}\check{\mathbf{k}}_i^u \end{bmatrix}, \tag{6.15b}$$

where $\beta_i = (\Delta t)a_{ii}$, and the values of vectors $\mathbf{k}_i^l$ and $\mathbf{k}_i^u$ are the same as computed in the case of explicit RKM in equation (6.14). Rearranging the terms in equation

(6.15), we get

$$\begin{bmatrix} \mathbf{I} & -\beta_i \\ -\beta_i \mathbf{A} & \mathbf{I} \end{bmatrix} \begin{bmatrix} \check{\mathbf{k}}_i^u \\ \check{\mathbf{k}}_i^l \end{bmatrix} = \begin{bmatrix} \mathbf{k}_i^u \\ \mathbf{k}_i^l \end{bmatrix}, \tag{6.16a}$$

$$\Rightarrow \begin{bmatrix} \mathbf{I} & -\beta_i \\ 0 & \mathbf{I} - \beta_i^2 \mathbf{A} \end{bmatrix} \begin{bmatrix} \check{\mathbf{k}}_i^u \\ \check{\mathbf{k}}_i^l \end{bmatrix} = \begin{bmatrix} \mathbf{k}_i^u \\ \mathbf{k}_i^l + \beta_i \mathbf{A} \mathbf{k}_i^u \end{bmatrix}, \tag{6.16b}$$

$$\Rightarrow \begin{bmatrix} \check{\mathbf{k}}_i^u \\ \check{\mathbf{k}}_i^l \end{bmatrix} = \begin{bmatrix} \mathbf{k}_i^u + \beta_i \check{\mathbf{k}}_i^l \\ \mathbf{D}_i \left(\mathbf{k}_i^l + \beta_i \mathbf{A} \mathbf{k}_i^u \right) \end{bmatrix}, \tag{6.16c}$$

where $\mathbf{D}_i = \left[\mathbf{I} - \beta_i^2 \mathbf{A} \right]^{-1}$. Note that $\mathbf{D}_i$ is a constant, only dependent on the diagonal elements of the RKM matrix, hence, it does not require to be computed at every step in time. Also note that in equation (6.16c) the vector $\check{\mathbf{k}}_i^l$ only depends on the values of vectors $\mathbf{k}_i^l$ and $\mathbf{k}_i^u$, and that the vector $\check{\mathbf{k}}_i^u$ can be computed after computing $\check{\mathbf{k}}_i^l$. Thus, using the form of equation (6.16c) one can easily modify an explicit algorithm to obtain a diagonally implicit model. Once we have the intermediate increment vectors, the solution vectors are computed as

$$\mathbf{y}_1^{n+1} = \mathbf{y}_1^n + (\Delta t) \sum_{i=1}^{s} b_i \check{\mathbf{k}}_i^u, \tag{6.17a}$$

$$\mathbf{y}_2^{n+1} = \mathbf{y}_2^n + (\Delta t) \sum_{i=1}^{s} b_i \check{\mathbf{k}}_i^l, \tag{6.17b}$$

for the given coefficients of any s-step diagonally implicit RKM. In this chapter, the Qin and Zhang's two-step, second order and the Crouzeix's two-step third order, diagonally implicit RKMs are used for validation purposes, which are defined by their Butcher tableau as given in Table 6.5. In the next section, some numerical tests are considered to investigate the performance of the discussed RKM schemes used in conjunction with the plane wave enrichment functions to solve the wave equation.

$$\begin{array}{c|cc} 1/4 & 1/4 & \\ 3/4 & 1/2 & 1/4 \\ \hline & 1/2 & 1/2 \end{array} \qquad \begin{array}{c|cc} \frac{1}{2}+\frac{\sqrt{3}}{6} & \frac{1}{2}+\frac{\sqrt{3}}{6} & \\ \frac{1}{2}-\frac{\sqrt{3}}{6} & -\frac{\sqrt{3}}{3} & \frac{1}{2}+\frac{\sqrt{3}}{6} \\ \hline & 1/2 & 1/2 \end{array}$$

Table 6.5: The Butcher tableaus for the diagonally implicit Qin and Zhang's method (left) and the Crouzeix's method (right).

	First time step error (%)			Final time step error (%)		
Δt	IE	IQZ	IC	IE	IQZ	IC
0.1	0.4998	0.0593	0.0589	5.5250	1.1321	1.1231
0.01	0.0571	0.0569	0.0569	1.3013	0.9318	0.9316
0.001	0.0569	0.0569	0.0569	0.9571	0.9254	0.9254

Table 6.6: The convergence of percentage L_1-norm errors associated with the numerical solutions, for $k = 20\pi$, obtained with the implicit methods. The error percentage values at the first time step ($t = \Delta t$) and the final time step ($t = T$) are shown.

6.5 Numerical tests

In this section the convergence of the aforementioned high order integration schemes with respect to the step-size in time is studied. To this end, the test example of progressive cylindrical wave problem as seen in subsection 3.6 of Chapter 3 is considered. The considered computational domain is $\Omega = [0.1, 1.1] \times [0.1, 1.1]$, and the 16 element uniform mesh used is as shown in Figure 3.1. The problem is solved for a total time $T = 1$, for three different step-sizes in time *i.e.*, $\Delta t = \{0.1, 0.01, 0.001\}$ to study temporal convergence. Three different problem wavenumbers are considered *i.e.*, $k = \{8\pi, 14\pi, 20\pi\}$. To solve for wavenumber $k = 8\pi$, the number of enrichment functions $Q = 13$ is used. Similarly, for the wavenumbers $k = 14\pi$ and $k = 20\pi$, the number of enrichment functions $Q = 23$ and $Q = 31$ are used, respectively. The L_1-norm error, as per the error definition used in the numerical examples of Chapter 3, is computed for the numerical solutions obtained with the high order explicit and implicit RKMs discussed in the previous section. The solutions obtained with the implicit Euler, the Qin and Zhang's method, and the Crouzeix's method are termed as IE, IQZ, and IC, respectively. Similarly, the solutions obtained with the explicit Euler method, the explicit Ralston's method and the classic fourth order explicit RKM are termed as XE, XR, and XC, respectively.

	First time step error (%)			Final time step error (%)		
Δt	XE	XR	XC	XE	XR	XC
0.1	0.5021	0.0584	0.0589	4.7474	1.0118	1.1184
0.01	0.0571	0.0569	0.0569	0.7730	0.9303	0.9316
0.001	0.0569	0.0569	0.0569	0.8957	0.9254	0.9254

Table 6.7: The convergence of percentage L_1-norm errors associated with the numerical solutions, for $k = 20\pi$, obtained with the explicit methods. The error percentage values at the first time step ($t = \Delta t$) and the final time step ($t = T$) are shown.

Table 6.6 shows the values of the percentage errors, associated with the numerical solutions, for the case $k = 20\pi$, obtained with the considered implicit methods. It can be seen that for all the three considered methods IE, IQZ and IC, the numerical accuracy increases with reduction in the step-size Δt. Also, for a given Δt, it can be seen from the table that the order of numerical accuracy associated with IC is greater than that of IQZ, which in turn is greater than that of IE. Moreover, the performance of the first order implicit Euler method, denoted by IE, is significantly inferior as compared to the other two higher order methods for the coarse step-size $\Delta t = 0.1$. Similarly, Table 6.7 provides the values of the percentage errors, associated with the numerical solutions, for the case $k = 20\pi$, obtained with the considered explicit methods. Again, it can be seen from Table 6.7 that the numerical accuracy associated with the first order explicit Euler method, denoted by XE, is significantly poorer as compared to the other two higher order explicit methods for the coarse step-size $\Delta t = 0.1$. Also, the numerical accuracy associated with the finest step-size $\Delta t = 0.001$ is very similar for all the three explicit methods.

In the case of explicit methods, it is noteworthy to mention that the solution obtained with XE for $\Delta t = 0.01$ is slightly better than that for $\Delta t = 0.001$. The error percentage at the final time step $t = 1$ is about 0.77% for the former, as compared to the 0.89% for the latter. However, this deterioration in error is absent when comparing the error percentages for the first time step. This could be explained as an increased accumulation of round-off errors associated with the lower step-size $\Delta t = 0.001$. Similarly, it can be seen that for the fine step-sizes in time, the performance of the higher order explicit methods suffers from accumulation of round-off errors owing to the extra calculations performed in the intermediate steps as compared to the first order explicit method.

	First time step error (%)			Final time step error (%)		
Δt	IE	IQZ	IC	IE	IQZ	IC
0.1	0.4993	0.0507	0.0501	5.8728	1.5633	1.5544
0.01	0.0461	0.0459	0.0459	1.6871	1.3309	1.3308
0.001	0.0459	0.0459	0.0459	1.3524	1.3208	1.3208

Table 6.8: The convergence of percentage L_1-norm errors associated with the numerical solutions, for $k = 14\pi$, obtained with the implicit methods. The error percentage values at the first time step ($t = \Delta t$) and the final time step ($t = T$) are shown.

	First time step error (%)			Final time step error (%)		
Δt	XE	XR	XC	XE	XR	XC
0.1	0.5014	0.0480	0.0501	4.6482	1.4383	1.5495
0.01	0.0463	0.0459	0.0459	1.1189	1.3295	1.3308
0.001	0.0460	0.0459	0.0459	1.2906	1.3208	1.3208

Table 6.9: The convergence of percentage L_1-norm errors associated with the numerical solutions, for $k = 14\pi$, obtained with the explicit methods. The error percentage values at the first time step ($t = \Delta t$) and the final time step ($t = T$) are shown.

Similar trends are observed for the other two cases, with $k = 14\pi$ and $k = 8\pi$ as well. The error values for these cases are summarized in tables 6.8, 6.9, 6.10, and 6.11. The temporal evolution of the error is plotted in Figure 6.1 for the numerical solutions obtained with the implicit as well as explicit methods for the three wavenumbers considered. The plots in this figure correspond to the case with coarse step-size $\Delta t = 0.1$. The results discussed in this section clearly show the advantage of using higher order integration schemes over the first order scheme, for both implicit as well as explicit formulations, in conjunction with the plane wave based PUFEM for solving the wave equation.

	First time step error (%)			Final time step error (%)		
Δt	IE	IQZ	IC	IE	IQZ	IC
0.1	0.5168	0.1515	0.1512	6.7621	2.6570	2.6476
0.01	0.1473	0.1472	0.1472	2.6799	2.3398	2.3397
0.001	0.1472	0.1472	0.1472	2.3538	2.3221	2.3221

Table 6.10: The convergence of percentage L_1-norm errors associated with the numerical solutions, for $k = 8\pi$, obtained with the implicit methods. The error percentage values at the first time step ($t = \Delta t$) and the final time step ($t = T$) are shown.

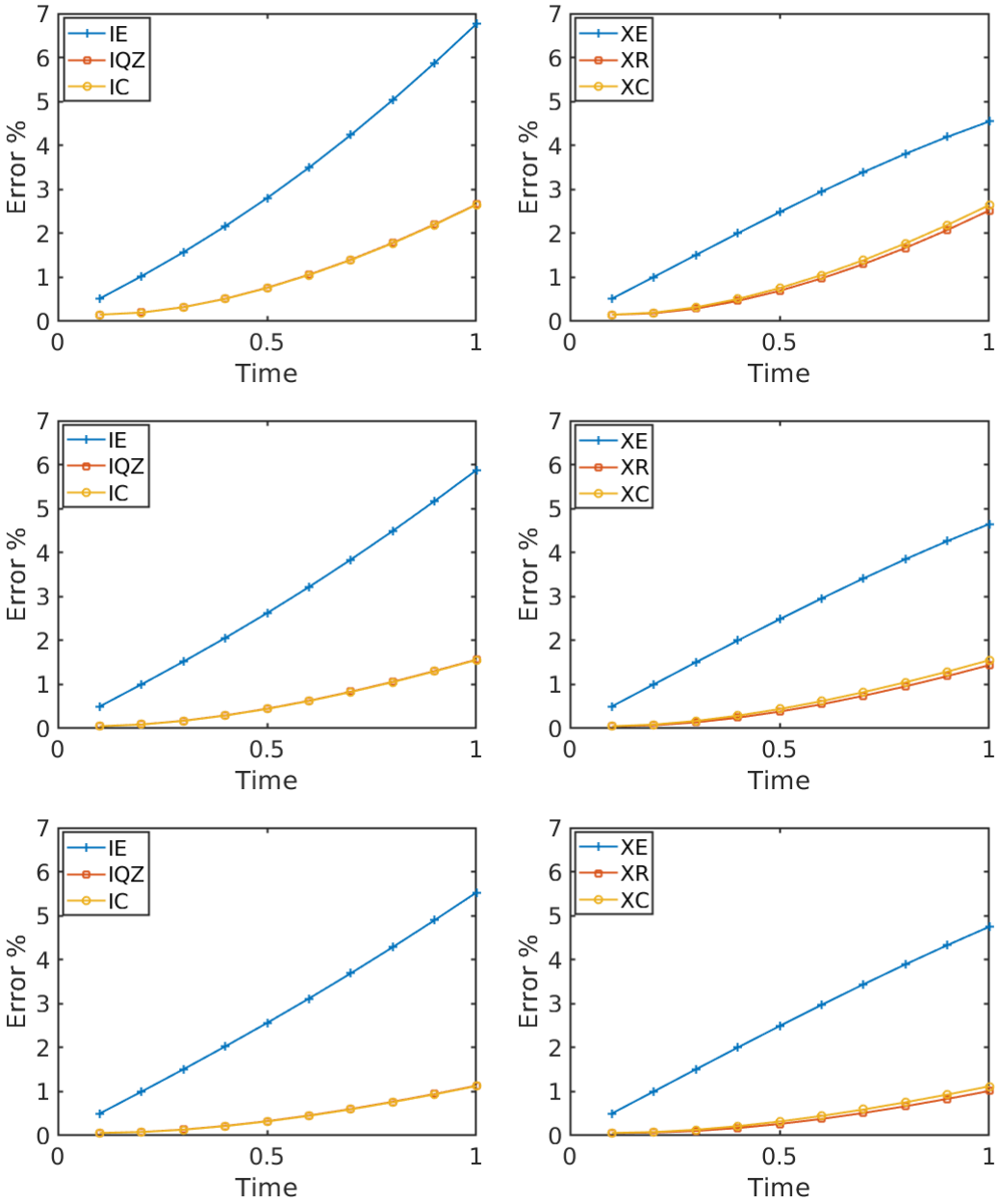

Figure 6.1: The temporal evolution of the error for the step-size $\Delta t = 0.1$. The solutions obtained with the implicit methods (left column) and the explicit methods (right column) are plotted separately. The top row corresponds to the case with wavenumber $k = 8\pi$, where as the middle and bottom rows correspond to the cases $k = 14\pi$ and $k = 20\pi$ respectively.

	First time step error (%)			Final time step error (%)		
Δt	XE	XR	XC	XE	XR	XC
0.1	0.5150	0.1493	0.1511	4.5439	2.5204	2.6423
0.01	0.1473	0.1472	0.1472	2.0797	2.3384	2.3397
0.001	0.1472	0.1472	0.1472	2.2912	2.3221	2.3221

Table 6.11: The convergence of percentage L_1-norm errors associated with the numerical solutions, for $k = 8\pi$, obtained with the explicit methods. The error percentage values at the first time step ($t = \Delta t$) and the final time step ($t = T$) are shown.

6.6 Conclusions

In this chapter, the high order integration schemes from the RKM family are used in conjunction with the plane wave based PUFEM for solving the time dependent wave equation. Both implicit as well as explicit methods are considered. The performance of the higher order schemes are compared against the first order explicit and implicit Euler schemes. Through numerical examples, it is observed that for a fine step-size Δt, the numerical accuracy associated with the low order Euler schemes is very similar to that of the high order RKMs. Moreover, for a coarse step-size in time, the first order Euler schemes are significantly less accurate as compared to the higher order counterparts. The improved accuracy for coarser step-size in time comes at the cost of storing and evaluating extra intermediate slope vectors as required for the high order RKM integration schemes. Nonetheless, low storage methods are also available, hence, their usage could be investigated to optimize run-time storage requirements associated with high order integration schemes.

Chapter 7

Algorithmic structure and numerical applications

7.1 Overview

The numerical code for implementing the finite element techniques developed through this research is coded in FORTRAN. This chapter outlines some of the aspects of the developed numerical code, such as meshing and the flowchart of the algorithm. Some technicalities are also discussed such as implementing non-homogeneous initial and boundary conditions when using plane wave basis enrichment functions. Towards the end, a couple of numerical examples are considered to motivate the relevance of this research when solving real-world problems in engineering.

7.2 Meshing

Meshing is an important aspect of the finite element algorithm. The geometrical domain is discretized into smaller chunks or patches, that provide the support for the basis functions that are used for approximating the geometry. The feature of being able to approximate any kind of geometry, is essentially a great advantage with the finite element technique as compared to the finite differences. To model complex geometries with a low order finite element scheme, one requires very small patches resulting into a fine mesh to be able to closely approximate the underlying geometry. Whereas, with higher order polynomials used as the basis for approxi-

mating the geometry, one can use relatively coarser meshes. Furthermore, one can use the same basis for approximating the geometry as well as the physical problem. Depending on the order of basis functions used for geometrical approximations and for the numerical solution space, the methodology is termed as sub-, iso-, or super-parametric. A good reference to the fundamentals of meshing could be found in several standard textbooks for the FEM such as in [160].

The process of mesh generation is complex. The difficulties involved in generating a computational mesh grows with the complexities in the geometry itself. However, it is very useful to be able to create and manipulate computational meshes in order to feed the analysis requirements. For example, one often requires to perform mesh refinement or change the order of elements used for meshing. These capabilities are very useful, *e.g.* to study numerical convergence with mesh refinement. To this end, the author employs the divide and conquer strategy. The meshing required for analysis is carried out using the open source package GMSH. The data file generated for the mesh is then read into the finite element solver program developed for this research, written in FORTRAN. The GMSH provides various formats to store the output of the generated mesh. For the purposes of this research the "SU2" format is chosen. This format provides ordered and delimited row-wise entries for element nodes and their connectivity. It also provides entries to store the nodes on domain boundaries. An example SU2 data file for the PUFEM mesh used in Figure 3.1 is provided in the Appendix B.1. The following section outlines some aspects of the meshing strategy adopted to aid the research presented in this thesis.

7.3 Quadrilateral elements and outward normals

The knowledge about the orientation of the element edges are very important when implementing finite element procedures. The sense or the direction of line integrals are pivotal to correctly calculating boundary integrals. Also, the outward normal vectors to the element edges are often used to define inter element flux quantities. The task of obtaining the direction cosines of the outward normal vector could become very complex when using non-trivial geometries. To this end, a simple procedure is devised to automate the computation of the outward normal vectors at

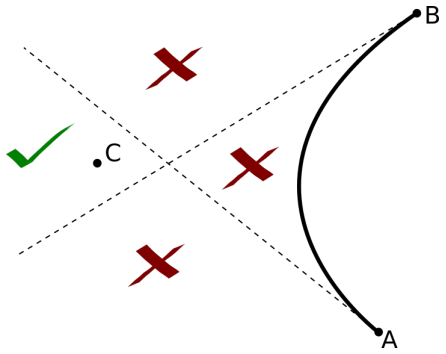

Figure 7.1: The sketch shows the allowed quadrant (with the check mark) for the centre (C) of an element with respect to two consecutive nodal points (A and B) on the element boundary. The forbidden quadrants for the centre of the element are marked with crosses.

any given boundary point for two dimensional elements. The numerical recipe is as follows:

1. Compute the Jacobian matrix for the local element transformation.
2. Use the Jacobian matrix to obtain the slope of the tangent to the element edge at the given boundary point. Let this slope be denoted as m.
3. Compute the slope of the line joining the given boundary point to the centre of the element. Let this slope be denoted as m_0.
4. Compute a temporary normal vector at the given boundary point. This vector, denoted as $\tilde{n}$ is given as

$$\tilde{n} = \begin{cases} (1,0) & , m \to \infty, \\ \left(\frac{m}{\sqrt{1+m^2}}, \frac{-1}{\sqrt{1+m^2}}\right) & , \text{otherwise.} \end{cases} \tag{7.1}$$

5. Calculate the actual normal vector n at the given boundary point as

$$n = \begin{cases} \tilde{n} & , \tilde{n} \cdot m_0 < 0, \\ -\tilde{n} & , \tilde{n} \cdot m_0 > 0. \end{cases} \tag{7.2}$$

The Jacobian matrix referred to in the above recipe, is the matrix given as

$$J_{\mathcal{D}} = \begin{bmatrix} \frac{\partial x}{\partial \xi} & \frac{\partial x}{\partial \eta} \\ \frac{\partial y}{\partial \xi} & \frac{\partial y}{\partial \eta} \end{bmatrix}, \tag{7.3}$$

for the transformation $\mathcal{D} : \mathbb{R}^2 \rightarrow \mathbb{R}^2$, that maps the local coordinates (ξ, η) to the global coordinates (x, y). The slope $m = \frac{\partial y}{\partial x}$ at a given boundary point could then be computed using the entries of the Jacobian matrix. This slope $m \rightarrow \infty$ depending on $\frac{\partial x}{\partial \xi} \rightarrow 0$ or $\frac{\partial x}{\partial \eta} \rightarrow 0$, which is easily verifiable on corresponding element edges. Note that the computation of the slope m only relies on the entries of the Jacobian matrix. Thus, the same recipe is used to calculate the outward normal vectors, independent of the order of the elements used for meshing. The centre of the element referred to in the recipe corresponds to the global point given by the transformation $\mathcal{D}(\xi = 0, \eta = 0)$. Note that, as seen from equation (7.2), this recipe would work only for the cases where the outward normal at a given boundary point, is never at an acute angle with the line joining the given point to the center of the element. In other words, the inner product $n \cdot m_0$ should always be strictly negative. Such an example case is shown in Figure 7.1. This recipe is thus suitable for quadrilateral elements of any order, with sufficiently small arcs between any two consecutive nodes on the element boundary. The elements used for the purposes of this research are only two dimensional quadrilaterals. However, similar strategies could be developed for triangular elements.

7.4 Flowchart and overview of the algorithm

Figure 7.2 shows the flowchart for the implementation algorithm for the numerical solver developed in this research. As can be seen, there are two main loops in the algorithm, separated by the block that reads "Method/Problem based modifications" (depicted with the blue oval in Figure 7.2). The "Data_read" section imports the input data generated with GMSH. This data is then used to allocate the required memory to store various data types used for the numerical calculations. The memory is allocated dynamically, and the code is scalable to the problem at hand defined by the input data. The code then encounters the first loop. In this upper loop, the mass matrix, the stiffness matrix and the load vector are populated and assembled, to build the system of equations

$$\mathcal{A}\mathcal{X} = \mathcal{B}, \tag{7.4}$$

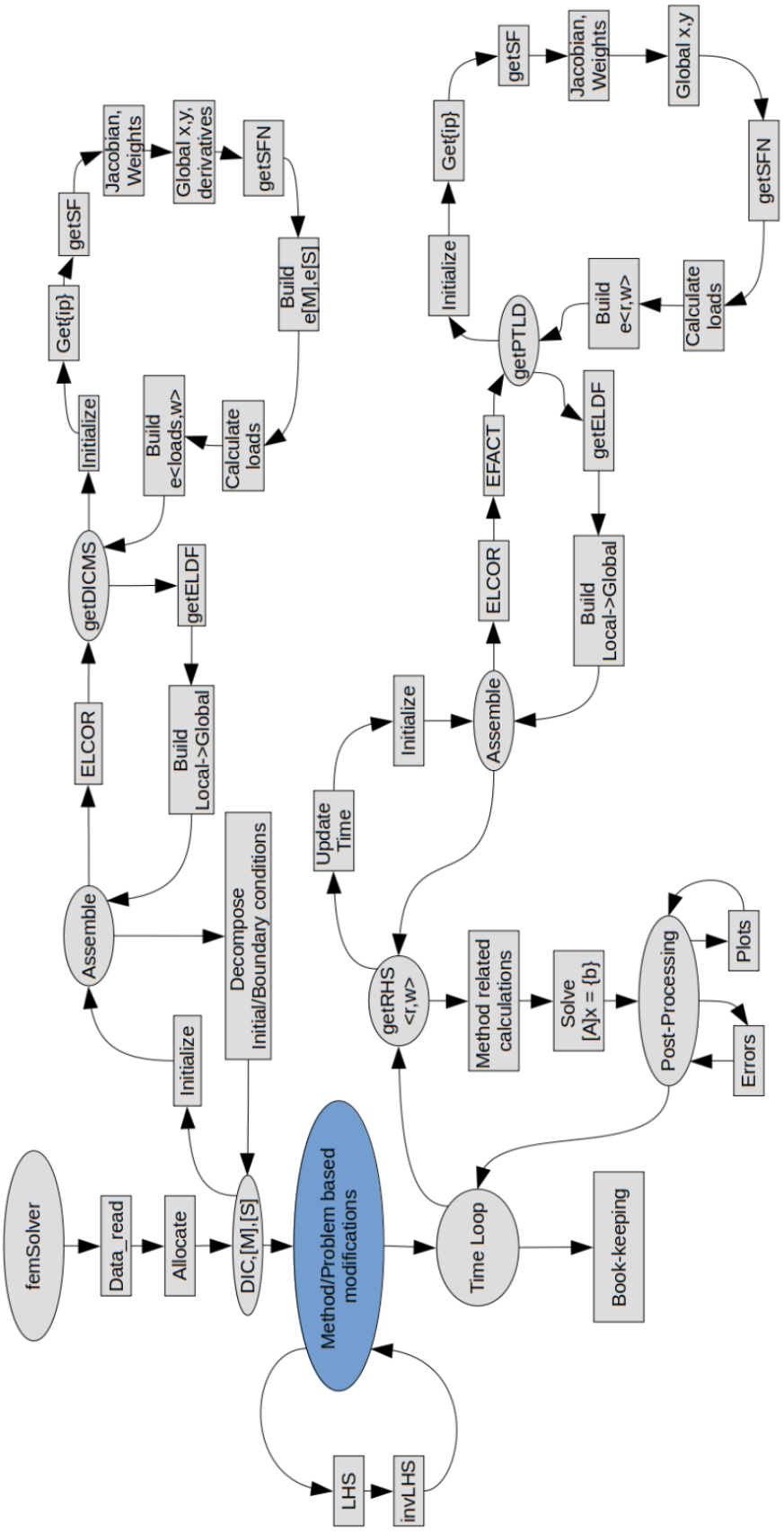

Figure 7.2: Flowchart for the PDE solver.

where $\mathcal{A}$ is the system matrix, $\mathcal{X}$ is the vector that contains the unknown coefficients for the numerical solution, and $\mathcal{B}$ is the load vector. The inversion of the system matrix takes place in the "Method/Problem based modifications" section. To compute the inverse $\mathcal{A}^{-1}$ of the system matrix, the code uses the ZGESV subroutine, openly available under the LAPACK library for linear algebra. The subroutine uses LU decomposition with partial pivoting and row interchanges to factor the system matrix. Next, a time loop is encountered, which updates the load vector $\mathcal{B}$ at each time step to incorporate boundary and source terms. In this section, the product of the inverse $\mathcal{A}^{-1}$ of the system matrix with the updated load vector provides the solutions to the governing PDE. Within this loop, the program also performs post-processing tasks, such as computing error values and saving numerical data for plots. Towards the end of the time loop, the program performs some book-keeping to register all the outputs of the simulation in various log files, and discard any temporary files created during the run.

7.5 Initial and boundary conditions

When working on novel numerical techniques to solve PDEs, it is common to construct simple problems for the purpose of testing and validating. For instance, the initial and boundary conditions are often assumed to be homogeneous when studying wave problems. However, in real-world applications, it may not be always possible to circumvent the necessity to deal with non-homogeneous conditions. This section addresses, the challenges encountered in employing plane wave enrichment functions into the solution basis, when dealing with non-homogeneous initial/boundary value wave problems.

Consider a scalar field E defined on a two-dimensional open bounded domain Ω, given as

$$E(t, \mathbf{x}) = f(t, \mathbf{x}), \quad (t, \mathbf{x}) \in [0, T[\times\Omega \,, \tag{7.5}$$

where $\mathbf{x} = (x, y)^\top$ are the Cartesian coordinates, t is the time variable, and $f(t, \mathbf{x})$ is the non-zero closed-form expression that defines the scalar field E on Ω, as a

function of t and $\mathbf{x}$. Next, consider a linear form

$$\mathcal{L}(\phi) = \int_{\Omega} E(t, \mathbf{x})\ \phi(\mathbf{x})\ d\Omega\ , \tag{7.6}$$

defined for all functions $\phi(\mathbf{x}) \in V_h$, for some finite element space V_h defined over the partition $\Omega_h \subseteq \Omega$. The linear form of equation (7.6) arises frequently when solving variational problems. One way to calculate this linear form is to obtain an approximate numerical integration using a suitable quadrature scheme. Another way is to approximate the linear form with a bilinear form given as

$$\mathcal{B}(E_h, \phi) = \int_{\Omega} E_h(t, \mathbf{x})\ \phi(\mathbf{x})\ d\Omega\ . \tag{7.7}$$

Here, E_h is the trial function such that it satisfies $\mathcal{B}(E_h, \phi) = \mathcal{L}(\phi)$ for all test functions $\phi(\mathbf{x}) \in V_h$. In other words, E_h is the best approximation for the scalar field E over Ω_h. Using the FEM, the approximation E_h could be written as

$$E_h(t, \mathbf{x}) = \sum\nolimits_{j=1}^{N_d} E_j(t) \mathcal{N}_j(\mathbf{x}), \tag{7.8}$$

where N_d is the total number of nodal points in the partition, $\mathcal{N}(\mathbf{x}) = (\mathcal{N}_1, \cdots, \mathcal{N}_{N_d})^\top$ are the local basis functions, and $E_j(t)$ are the nodal values of the global function $E_h(t, \mathbf{x})$. To obtain these coefficients, one has to solve the system of equations given by the weak form

$$\int_{\Omega} E_h(t, \mathbf{x})\ \phi(\mathbf{x})\ d\Omega \ = \ \int_{\Omega} f(t, \mathbf{x})\ \phi(\mathbf{x})\ d\Omega\ , \tag{7.9a}$$

$$\Rightarrow \mathbf{M}\mathbf{\Psi}(t) \ = \ \mathcal{L}(\phi)\ , \tag{7.9b}$$

where the matrix $\mathbf{M}$ is often termed as the mass matrix, and the vector $\mathbf{\Psi}(t) = \{E_1(t), E_2(t), \ldots, E_{N_d}(t)\}^\top$ stores the nodal coefficients of the approximation E_h.

7.5.1 Non-homogeneous initial condition

The utility of using the bilinear form instead of the linear form becomes more clear when we consider the system of ordinary differential equations

$$\frac{d\mathbf{y}}{dt} = \mathbf{B}\mathbf{y} + \mathbf{r}, \tag{7.10}$$

as obtained in Chapter 5 for the semi-discretized wave equation. The above form of ordinary differential equations is suitable for applying various explicit as well as implicit integration schemes for the time variable. However, for using high order integration schemes, for instance the Runge-Kutta family of methods, one requires the knowledge of the vector $\mathbf{y}(t)$ at time $t = 0$. Often this information is available only in a closed-form expression, such as in equation (7.5), defined as an initial condition. Thus, it becomes necessary to obtain the coefficients of the solution vector at $t = 0$, by solving a Galerkin equation of the form (7.9). This process of obtaining initial value coefficients becomes trivial in the case of polynomial based finite element techniques, by using special integration schemes such as the Gauss-Lobato [151] quadrature rule. Using special quadrature schemes, the mass matrix $\mathbf{M}$ of equation (7.9) becomes diagonal for high order polynomial basis. Such a diagonalization of the mass matrix is not trivial in the case of plane wave based PUFEM. One can perhaps try using the Gram-Schmidt process to orthonormalize the plane wave basis functions used in the PUFEM, under the inner product defined as the bilinear form of equation (7.7). However, such a method is not available for the proposed PUFEM, to the best knowledge of the author. Thus, for the purposes of this thesis, the author solves the variational form of equation (7.9) to obtain the initial value coefficients for the PUFEM. Examples of using this approach to implement the non-homogeneous initial condition are considered in previous chapters.

7.5.2 Non-homogeneous boundary condition

This approach is also useful for implementing non-homogeneous Dirichlet boundary conditions, when using the PUFEM. Consider the system of equations obtained in

(7.4) and rearrange the rows as

$$\begin{bmatrix} \mathcal{A}_{11} & \mathcal{A}_{12} \\ \mathcal{A}_{21} & \mathcal{A}_{22} \end{bmatrix} \begin{bmatrix} \mathcal{X}_1 \\ \mathcal{X}_2 \end{bmatrix} = \begin{bmatrix} \mathcal{B}_1 \\ \mathcal{B}_2 \end{bmatrix}, \tag{7.11}$$

such that $\mathcal{X}_1$ is a vector containing all the QN_1 non-boundary coefficients and $\mathcal{X}_2$ is a vector containing all the QN_2 boundary coefficients, for a total of $N_1 + N_2$ nodes in the computational mesh, using a total of Q enrichment functions per node. Similarly, $\mathcal{A}_{11}$ is a $QN_1 \times QN_1$ matrix and $\mathcal{A}_{22}$ is a $QN_2 \times QN_2$ matrix, where QN_1 and QN_2 are the total degrees of freedom associated with non-boundary coefficients and boundary coefficients respectively. For solving problems with Dirichlet boundary condition, the procedure is to

1. Obtain the boundary coefficients $\mathcal{X}_2$, pertaining to the given Dirichlet boundary condition.
2. Eliminate the rows from the system matrix that correspond to the boundary coefficients. Thus, obtain a reduced system of equations given as

$$\mathcal{A}_{11}\mathcal{X}_1 + \mathcal{A}_{12}\mathcal{X}_2 = \mathcal{B}_1.$$

3. Solve the reduced system $\mathcal{A}_{11}\mathcal{X}_1 = \mathcal{B}_1 - \mathcal{A}_{12}\mathcal{X}_2$, to obtain the unknown non-boundary coefficients $\mathcal{X}_1$.
4. Repeat from above, for every step in time.

For the case of PUFEM, to obtain the boundary coefficients for non-homogeneous Dirichlet boundary conditions, is not trivial. To this end, a bilinear form similar to equation (7.7) is defined on the Dirichlet boundary, to solve for the boundary coefficients. Let us consider a test example for further clarity. Let a wave problem

be defined as

$$\frac{1}{c^2}\frac{\partial^2 E}{\partial t^2} - \nabla^2 E = 0, \qquad (t,\mathbf{x}) \in [0,T[\times\Omega, \tag{7.12a}$$

$$E(t,\mathbf{x}) = 0, \qquad (t,\mathbf{x}) \in [0,T[\times\Gamma_1, \tag{7.12b}$$

$$E(t,\mathbf{x}) = f(t,\mathbf{x}), \qquad (t,\mathbf{x}) \in [0,T[\times\Gamma_2, \tag{7.12c}$$

$$\frac{\partial E(t,\mathbf{x})}{\partial t} = \frac{\partial f(t,\mathbf{x})}{\partial t}, \qquad (t,\mathbf{x}) \in [0,T[\times\Gamma_2, \tag{7.12d}$$

$$E(0,\mathbf{x}) = \frac{\partial E(0,\mathbf{x})}{\partial t} = 0, \qquad \mathbf{x} \in \Omega, \tag{7.12e}$$

where $f(t,\mathbf{x}) = \sin(k(x-0.1))\sin(\omega t)$. This model problem defines homogeneous initial condition with non-homogeneous Dirichlet boundary conditions as given with equations (7.12c) and (7.12d). The considered domain is rectangular, $\Omega = [0.1, 1.1]\times[0.1, 5.1]$, with two boundaries Γ_1 and Γ_2. Here $\Gamma_2 = [0.1, 1.1]$, and Γ_1 consists of the rest of the three edges of the rectangle. For this test example, the wave speed is $c = \omega/(2k)$, with $\omega = k = \pi$. The total time is $T = 5$. To obtain the boundary coefficients for the field $E(t,\mathbf{x})$ and its time derivative as given in (7.12), solve the following extra bilinear forms

$$\int_{\Gamma_2} E_h(t,\mathbf{x})\ \phi(\mathbf{x})\ d\Gamma = \int_{\Gamma_2} f(t,\mathbf{x})\ \phi(\mathbf{x})\ d\Gamma, \tag{7.13a}$$

$$\int_{\Gamma_2} \frac{\partial E(t,\mathbf{x})}{\partial t}\ \phi(\mathbf{x})\ d\Gamma = \int_{\Gamma_2} \frac{\partial f(t,\mathbf{x})}{\partial t}\ \phi(\mathbf{x})\ d\Gamma, \tag{7.13b}$$

at every time step.

For numerical solution of this model problem, the used enrichment wavenumber is the same as the problem wavenumber. Five different uniform meshes, named here as mi for $i = \{1,2,3,4,5\}$, with a total of 45, 115, 217, 351, and 517 number of nodes respectively are used. Three different number of enrichment functions $Q = \{3,5,7\}$ are used for analysis, amounting to a total of 15 test cases. The numerical solutions, obtained with the forward Euler explicit time integration scheme, in this section are termed as XPL-miQj for the i^{th} mesh using j^{th} number of nodal enrichment functions. The step-size in time is $\Delta t = 0.001$. The mesh refinement results, for the

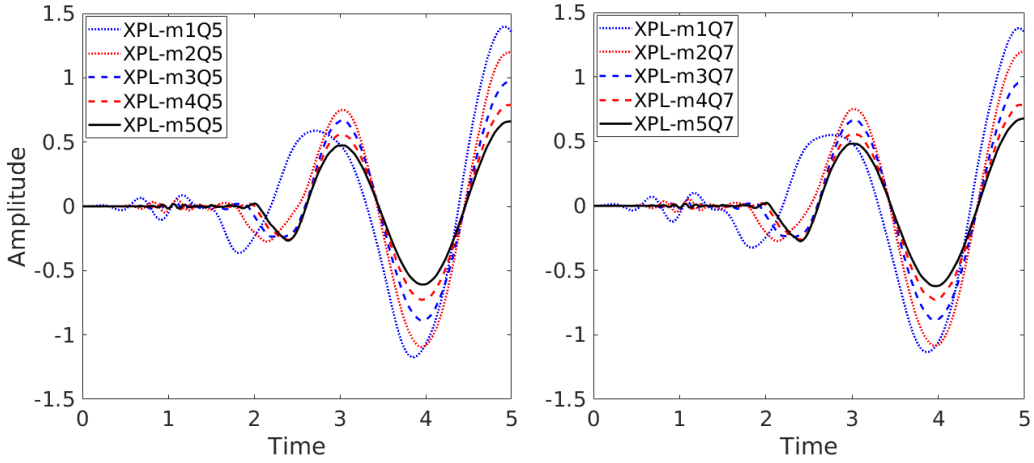

Figure 7.3: Evolution of the numerical solution recorded at the point (0.6,1.25) in the domain. The plots show mesh refinement for $Q = 5$ (left) and $Q = 7$ (right), using explicit time integration scheme.

values of $Q = 5$ and $Q = 7$ are shown in Figure 7.3. In this figure, the amplitude of the numerical solution recorded at a point (0.6,1.25) in the domain is plotted against the time axis, showing a clear convergence of the solution with increasing number of nodes in the mesh. The time evolution of the converged solution for the case m5Q7 is shown in Figure 7.4.

Similar results are obtained with the lumped mass approach. The numerical solutions obtained with the lumped mass and the consistent mass methods are compared in Figure 7.5 for the case m5Q7. It can be seen from the plot that both the solutions are practically the same. Also, for a coarser time step, $\Delta t = 0.01$ using the fourth order Runge-Kutta method, in conjunction with both consistent as well as lumped mass methods, produces similar results as compared to the first order explicit method. As an example, Figure 7.5 shows the numerical results obtained for the lumped mass approach using the forward Euler scheme (BD-m5Q7 data in the graph) and the fourth order scheme (BD-RKM4 data in the graph). However, it is noted that a further dilation of the time step to $\Delta t = 0.1$ results in unstable numerical solutions. To see the time evolution of the numerical solution at a point much closer to the Dirichlet boundary, another plot is shown in Figure 7.6. The plot shows the amplitude of the recovered solution at the point (0.6,0.426087) in the computational domain. Clearly, both the methods *i.e.*, with and without the mass lumping, produce stable solutions.

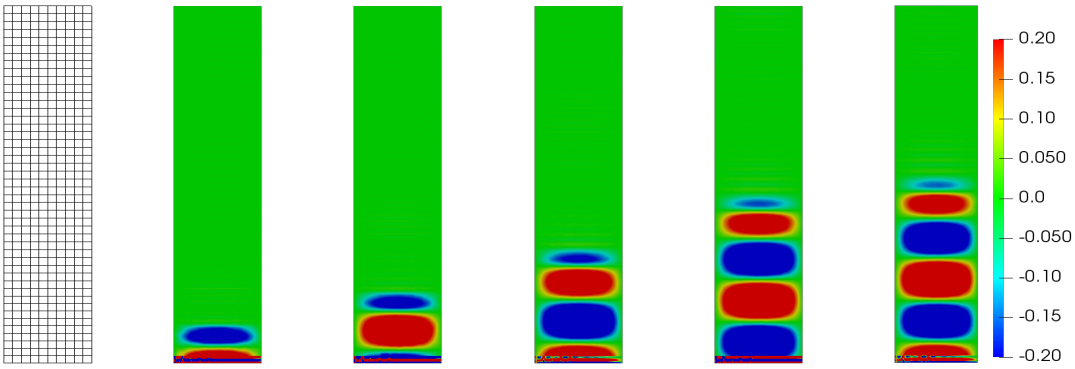

Figure 7.4: The computational mesh (far left) and the snapshots of the converged numerical solution obtained with the first order explicit time scheme with consistent mass approach. The snapshots correspond to time t=0.9, 1.8, 3, 4.5, and 5 from left to right.

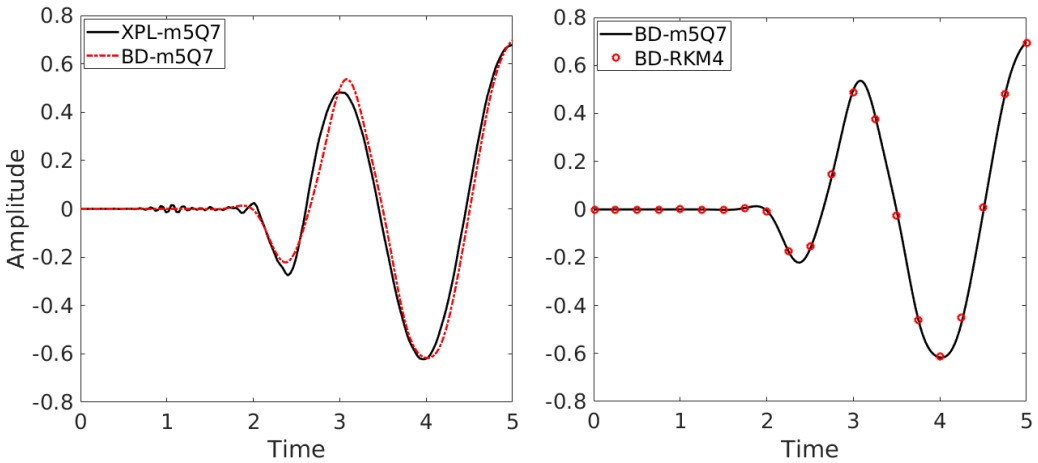

Figure 7.5: The plot on the left shows comparison of lumped mass (BD-m5Q7 data) and consistent mass (XPL-m5Q7 data) approaches for the converged case m5Q7. The plot on the right compares the first order and the fourth order explicit time integration schemes for the lumped mass approach.

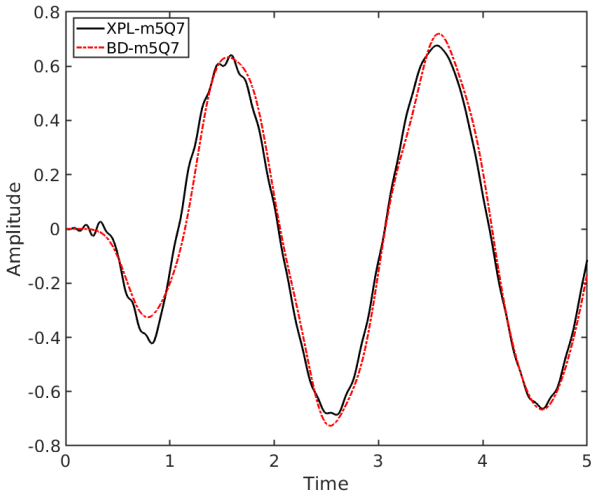

Figure 7.6: Evolution of the numerical solution recorded at the point (0.6,0.426087) in the domain, which is much closer to the Dirichlet boundary.

It would be beneficial to study the stability conditions for the time integration schemes in the context of the PUFEM, albeit this would form the basis for future work. Moreover, the mass matrix used for solving the Galerkin equations of (7.9) may not always be invertible, owing to the poor conditioning when using enriched functions as basis. The conditioning of this mass matrix is further deteriorated especially when solving for the boundary coefficients, since the line integrals are one dimension less than the two dimensional domain integrals used when solving for initial value coefficients. Furthermore, the interpolation of the numerical solution in the elements that contain the Dirichlet boundary may result into spurious oscillations inside those elements. This is because such elements consist of nodes which solve not the same variational problem. Thus, a further research into developing better integration quadrature schemes for diagonalizing the mass matrix associated with enriched techniques could be beneficial.

7.6 Numerical examples for real-world problems

In this section we study the solution of the wave equation subjected to homogeneous boundary and initial conditions, with a non-zero source inside the domain. Such problems arise in many real world applications, such as in electromagnetic compatibility analysis and modal analysis for waveguides [97, 129]. In particular,

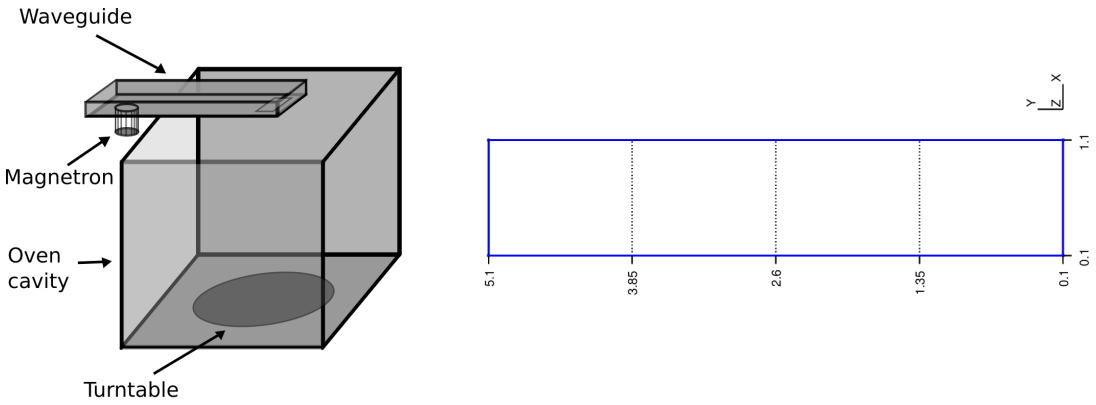

Figure 7.7: Rectangular waveguide inside a microwave oven (left) and modelled waveguide geometry used for analysis (right).

this section considers two different areas of applications, as shown in Figures 7.7 and 7.11. In the first application consider a waveguide that is typically used inside a microwave oven to illuminate the oven chamber with electromagnetic radiation [128]. The four walls of the waveguide create a resonant cavity that reflects the inbound radiation inside it. The second application is for a circular cross-section of a high voltage insulated steel armoured electrical cable. The steel armour, that is used to provide sustenance for the high voltage electrical cables to endure mechanical stress as they are buried underground, also traps electromagnetic disturbances occurring inside the cable due to current imbalances and material defects [133]. The solution of the wave equation inside these geometries provides the distribution of the electromagnetic energy within the material, which then could be coupled with the diffusion equation to analyse various thermal properties [6, 33]. Owing to the increase in power demands both for industrial and household usage, such analyses are deemed useful to evaluate performance and prevent ageing of cables. For the purpose of this research, we define a model problem as

$$\frac{1}{c^2}\frac{\partial^2 E}{\partial t^2} - \nabla^2 E = f(t,\mathbf{x}), \qquad (t,\mathbf{x}) \in [0,T[\times\Omega, \tag{7.14a}$$

$$E(t,\mathbf{x}) = 0, \qquad (t,\mathbf{x}) \in [0,T[\times\Gamma, \tag{7.14b}$$

$$E(0,\mathbf{x}) = 0, \qquad \mathbf{x} \in \Omega, \tag{7.14c}$$

$$\frac{\partial E(0,\mathbf{x})}{\partial t} = 0, \qquad \mathbf{x} \in \Omega. \tag{7.14d}$$

To solve for the scalar field value E inside the domain Ω for a given source term $f(t, \mathbf{x})$, the domain and the source term are defined separately for the two considered geometries. Since the solution vanishes on the boundary, the weak form for this example is given as

$$\int_{\Omega'} \frac{\partial E}{\partial t}\phi \, d\Omega = \int_{\Omega'} V\phi \, d\Omega, \tag{7.15a}$$

$$\frac{1}{c^2}\int_{\Omega'} \frac{\partial V}{\partial t}\phi \, d\Omega = -\int_{\Omega'} \nabla E \cdot \nabla\phi \, d\Omega + \int_{\Omega'} f(t, \mathbf{x})\phi \, d\Omega, \tag{7.15b}$$

where $\Omega' = \{\mathbf{x} : \mathbf{x} \in \Omega \text{ and } \mathbf{x} \notin \Gamma\}$. Notice that for the homogeneous case, we do not need to solve the extra Galerkin equations of the form (7.9). The reduced system that we solve for this model problem is simply given as $\mathcal{A}_{11}\mathcal{X}_1 = \mathcal{B}_1$, referring to the notation as described in subsection 7.5.2.

7.6.1 Rectangular waveguide

For the waveguide geometry, as seen in Figure 7.7, consider

$$f(t, x, y) = \sin\left(\frac{(x-a)\pi}{0.2}\right)\sin\left(\frac{(y-a)\pi}{0.2}\right)\sin(\pi t), \tag{7.16}$$

where $(x, y) \in [a, a+0.2] \times [a, a+0.2]$ and $a = 0.55$. The considered computational domain is $\Omega = [0.1, 1.1] \times [0.1, 5.1]$, and the problem is solved for the total time period $T = 10$. The step-size in time is $\Delta t = 0.001$ and the simulation is run for a total of 10000 time steps. The wave speed $c = \frac{1}{\pi}$. To arrive at the converged solution, we adopt the same approach of mesh refinement and increasing number of nodal enrichment plane waves, as used in previous numerical examples such as in Chapter 5 for the example of a Gaussian pulse. Since for this example the angular frequency, as seen from equation (7.16), is $\omega = \pi$ we use $k = \omega/c = \pi^2$ as the wavenumber for the plane wave enrichments. Note that the phase velocity in practice is much larger than that considered for the purposes of this research. Also, the angular frequency could be much larger than that considered here. For such high variations that are dependent on the time variable, one would have to tend towards some sort of high order integration scheme in time, or perhaps would have to introduce time dependent enrichment functions in the finite element solution space. Consider three uniform

meshes, with rectangular elements, consisting of 45, 171, and 741 nodes respectively, termed here as meshes m1, m2, and m3. Subsequently for each mesh, consider three different number of enrichment functions $Q = \{5, 7, 9\}$ and solve the wave problem using the PUFEM-BD method *i.e.*, the lumped mass approach, to get a total of 9 different numerical solutions. These numerical solutions are termed as BD-miQj, where $i \in \{1, 2, 3\}$ denotes the mesh number and $j \in \{5, 7, 9\}$ denotes the number of enrichment functions used per node. The total degrees of freedom associated with these BD-miQj solutions ranges from 225 (for BD-m1Q5) to 6669 (for BD-m3Q9). For comparison, we also solve the wave problem on a very fine mesh with a total of 12561 nodes using the first order FEM, without using any nodal enrichment. Figure 7.8 compares these BD-miQj numerical solutions against the solution obtained with the non-enriched FEM. In this figure we plot the time evolution of the numerical solution recorded at the point (x=0.6,y=2.6) inside the domain Ω. It can be clearly seen that as we increase the total degrees of freedom used with the PUFEM-BD method, the solution converges towards the reference FEM solution. Here we define the percentage error as

$$\varepsilon = \frac{\|E_{num} - E_{FEM}\|_{\mathrm{L}^1(\Omega)}}{\|E_{\max}\|_{\mathrm{L}^1(\Omega)}} \times 100\%, \tag{7.17}$$

where E_{FEM} is the reference solution obtained with the non enriched FEM over a very fine mesh, and $E_{\max}$ is the magnitude of the source term at its maximum, which is unity in this case. The percentage error is plotted for individual BD-miQj solutions, recorded at the reference point (0.6,2.6), as shown in Figure 7.8. It is observed from this figure that the relative error associated with the three BD-m1Qj solutions is below 6%, and with the BD-m2Qj and BD-m3Qj solutions is below 1%, throughout the total duration of the simulation. The time evolution of the numerical solution at a point (0.6,1.35) in the computational domain which is much closer to the source term is also plotted in Figure 7.9. It can be clearly seen that the solution obtained with the PUFEM-BD is stable and is in agreement with the reference FEM solution.

We also test the performance of the PUFEM-BD method for this geometry over an unstructured mesh, as shown in Figure 7.10. The unstructured mesh consists of

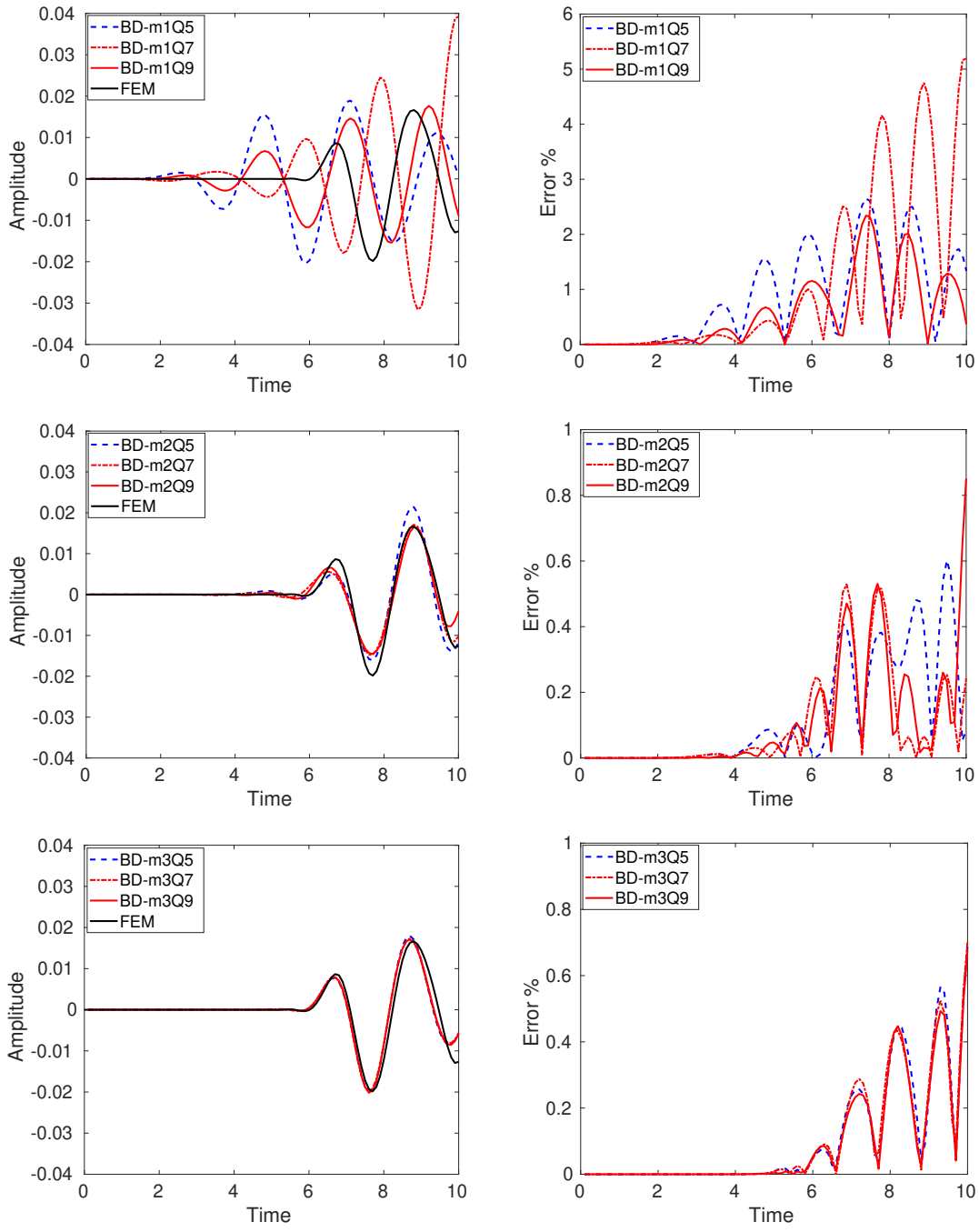

Figure 7.8: Comparison of the numerical solutions obtained with the PUFEM-BD method against the reference FEM solution, for the rectangular waveguide example. The graphs show (left column) the time evolution of the amplitude of the scalar field E at a point (0.6,2.6) inside the computational domain Ω, and (right column) the relative error in these amplitudes obtained with the PUFEM-BD solutions as compared to the fine mesh FEM solution.

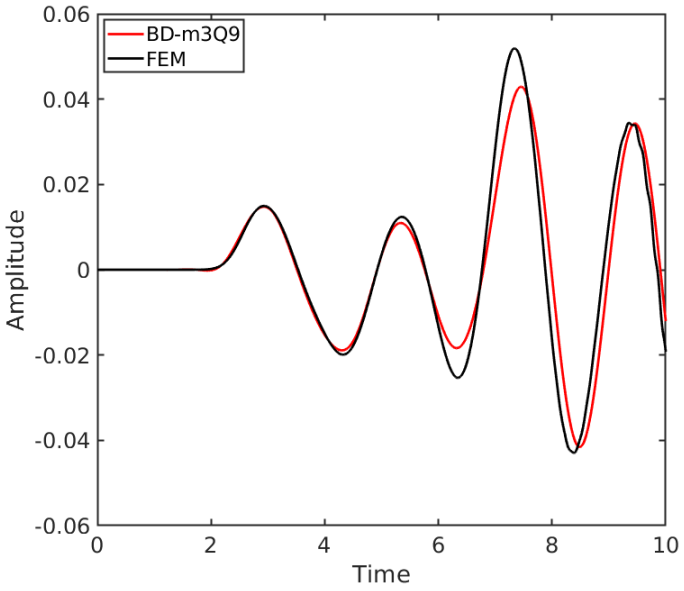

Figure 7.9: Time evolution of the numerical solution obtained with the PUFEM-BD and the reference FEM solution for the rectangular waveguide example, at a point (0.6,1.35) in the computational domain.

655 nodes, and is obtained using the open-source package GMSH. For this mesh, the number of enrichment functions $Q = 9$ is used. This resulted into a total of 5895 degrees of freedom, which is comparable to that associated with the BD-m3Q9 method. The numerical results obtained with the unstructured mesh are also shown in Figure 7.10, along with the BD-m3Q9 solution and the reference FEM solution.

7.6.1.1 High voltage cable cross section

For the circular cross-section geometry, consider

$$f(t,x,y) = \sin\left(\frac{(x+1)\pi}{2}\right)\sin\left(\frac{(y+9)\pi}{1}\right)\sin(t), \tag{7.18}$$

for $(x,y) \in [-1,1] \times [-9,-8]$. In the modelled geometry, the outer and the inner circles form the boundary Γ where the solution vanishes. The radii of the outer and the inner circles are 12 and 4 units respectively. The centre of the outer circle corresponds to the origin. The centres of the inner circles are equidistant from the origin, located at the points (0,6), (-5.19,-3), and (5.19,-3) that form an equilateral triangle. The considered computational domain is shown in Figure 7.11. The problem is solved for the total time period $T = 70$. The step-size in time is $\Delta t =$

Figure 7.10: Computational mesh (far left), and the snapshots of the numerical solutions obtained with the PUFEM-BD method for the example of rectangular waveguide. Solutions are for (top) the unstructured grid with 655 nodes and $Q = 9$, (middle) the structured mesh m3 with 741 nodes and $Q = 9$. Reference solution (bottom) is obtained with linear FEM on the structured very fine mesh with 12561 nodes. These snapshots correspond to the time instants t =0.4, 1.1, 1.5, 2, 3, 4, 5, 6, 7, 8, 9 and 10 (left to right).The range on the colour legend is (-0.02,0.02).

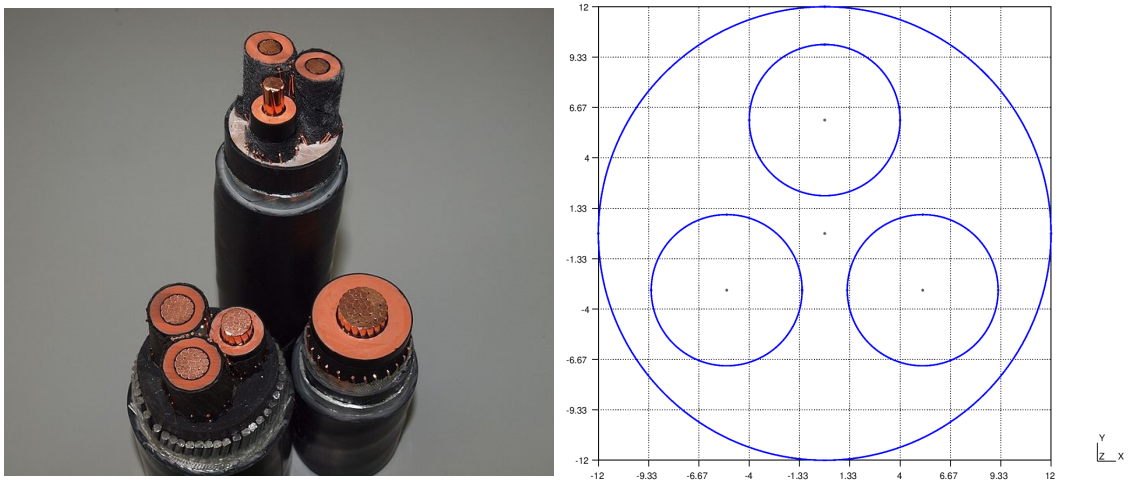

Figure 7.11: High voltage electrical cables (left) and modelled geometry for the circular cross-section of an electrical cable (right).

0.001 and the simulation is run for a total of 70000 time steps. The wave speed $c = \frac{1}{\pi}$. The angular frequency $\omega = 1$ for the source term as seen in equation (7.18), which provides the wavenumber $k = \pi$ to be used for the enrichment functions. To arrive at a converged solution, again employ the aforementioned strategy of q-convergence and mesh refinement. To this end consider six different meshes with a total of 364, 588, 962, 1336, 1842, and 2342 nodes respectively, termed here as meshes m1, m2, m3, m4, m5, and m6. Subsequently for each mesh, consider three different number of enrichment functions $Q = \{5, 7, 9\}$ and solve the wave problem of equation (7.14) using the PUFEM-BD method. This gives us 18 different numerical solutions, termed here as BD-miQj using the same convention as for the numerical solutions for the waveguide geometry. Here, the total number of degrees of freedom ranges from 1820 (for BD-m1Q5) to 21078 (for BD-m6Q9). The time evolution for the numerical solutions BD-m4Q9, BD-m5Q9 and BD-m6Q9 are shown in Figure 7.12, depicting mesh refinement for $Q = 9$ to obtain a converged solution.

From the test cases studied in this section, it can be clearly seen that the numerical solutions converge for the PUFEM-BD method with increasing degrees of freedom as expected. The method is also seen to be applicable with unstructured meshes, and produces similar results when compared with solutions obtained using structured meshes. The PUFEM-BD method could also prove very useful to reduce the time complexities associated with solving the numerical problem, by using parallel computing to distribute the inversion of non-overlapping blocks of the system

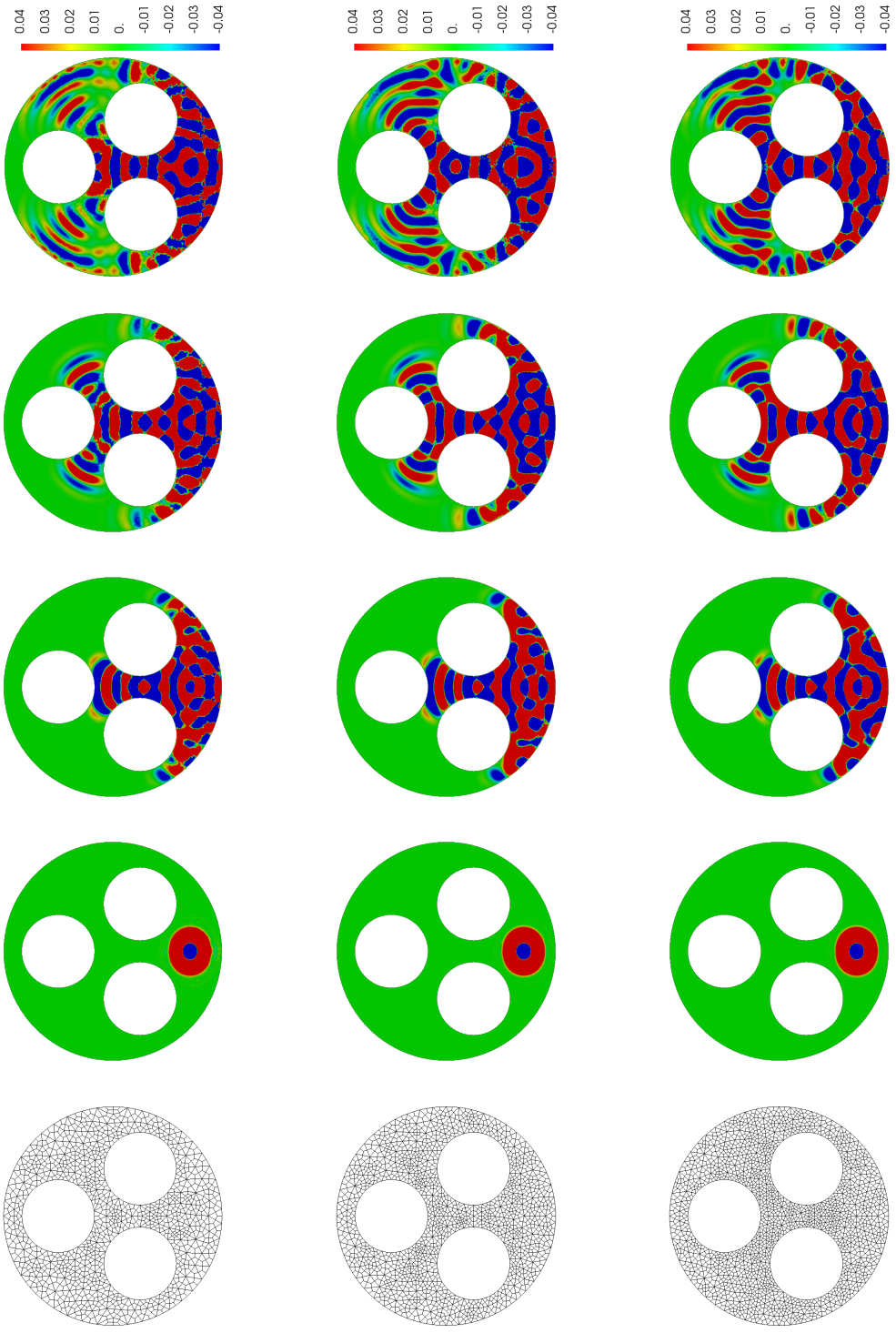

Figure 7.12: Computational mesh (far left), and the snapshots of the numerical solutions obtained with the PUFEM-BD method for the example of high voltage cable cross section. Solutions shown are for (top) the unstructured mesh m4 with 1336 nodes using $Q = 9$, (middle) mesh m5 with 1842 nodes using $Q = 9$, and (bottom) mesh m6 with 2342 nodes using $Q = 9$. These snapshots correspond to the time instants $t = 6.8$, 37.2, 53.2, and 70 (left to right). The range on the colour legend is (-0.04,0.04).

matrix using concurrent computational tools such as OpenMP. This feature could be very useful especially when solving real world problems with massive geometries.

7.7 Conclusions

The various aspects of the numerical code developed in this research are discussed. The chapter outlines the strategy employed to import meshes generated from the open-source package GMSH, detailing the type of meshes and elements considered, as well as the algorithm to automate the calculation of outward normal vectors on element edges. The flowchart for the numerical program is discussed. Challenges incurred when implementing non-homogeneous initial/boundary conditions in conjunction with the PUFEM are addressed, along with the strategy adopted in this research to deal with them. Numerical examples are considered to establish the pertinence of the developed models to real-world applications.

Chapter 8

Conclusions and motivation for future work

8.1 Thesis conclusions

The solution of partial differential equations forms a key aspect of the research community, centred around a wide area of topics such as computational physics and financial mathematics. Of central importance to this thesis, is the domain of numerical solution of the time dependent wave equation, which falls under the hyperbolic family of PDEs.

In Chapter 2, a brief review of various methodologies developed using the finite element technique, to solve a variety of wave problems, is presented. The discussion therein, outlines the work of various groups with promising enrichment techniques developed to improve the performance of the finite element strategies, in the context of solving wave problems. In particular, the theme of incorporating *a priori* knowledge of physical features of the governing partial differential equation into the solution space of finite element approaches is reviewed. The discussion also provides motivation to use plane wave functions as enrichment basis to add to the finite element solution space.

Chapter 3, investigates a class of enriched methodologies, termed as the PUFEM, and proposes an implicit time integration procedure to advance the numerical solution of the time dependent wave equation. The performance of the proposed enriched finite element method is assessed for several test examples. A comparison to the

standard FEM is also undertaken. The numerical results presented therein, show clear advantage of the enriched method over the non-enriched counterpart. The enriched technique significantly reduces the number of degrees of freedom required for a fixed numerical accuracy as compared to the standard FEM, for the solution of transient wave problems. This reduction in degrees of freedom also leads to lower computational costs such as reduced total simulation time at lower run-time memory requirements. This is due to the reduced size of the system matrix obtained with the enriched method, as compared to the standard FEM when solving highly oscillatory wave problems. Similar benefits of the PUFEM are reported in Chapter 4, wherein a comparison between the performances of the enriched method and the non-enriched high order polynomial based FEM is presented.

Further, in Chapter 5 the explicit Euler scheme is proposed for the plane wave based PUFEM, as opposed to the implicit procedure as discussed in previous chapters. The possibility of lumping the system matrix in the case of the explicit formulation is also presented. The performance of both the lumped mass as well as the consistent mass explicit approaches are studied, using various numerical examples. These results are compared against the implicit procedure. The comparison presented therein shows major advantages for the explicit approach with the lumped mass matrix, related to better conditioning of the system matrix and significant reduction in the overall simulation time. The work also consists of a parametric study that shows the utility of plane wave enrichment functions in the context of solving transient wave problems without a dominant frequency, through the aid of a transient Gaussian pulse test example. The lumped mass approach is also shown to be more resilient to the poor quality of elements used for meshing, as opposed to the consistent mass approach. Moreover, the explicit procedures, even though conditionally stable depending on the CFL number for the problem, are shown to perform equally well for the same mesh parameters and step-size in time as compared to the unconditionally stable implicit counterpart, using plane wave enrichment functions.

In Chapter 6, higher order integration schemes for discretization in time are considered. The performance of various explicit as well as implicit schemes amongst the high order RKM family is studied through numerical examples. It is observed that the numerical accuracy associated with the low order integration schemes is very

similar to that of the higher order counterparts for fine step-size in time. Whereas, for coarse step-size in time, the higher order schemes show significant advantage in terms of numerical accuracy as compared to the low order schemes. This is observed for both explicit as well as implicit procedures.

The flowchart for the numerical program developed to implement the finite element procedures investigated in this research is provided in Chapter 7. The chapter also consists of some discussion on the algorithmic aspects of the FEM such as meshing and computing outward normal vectors on the element edges. There is also a section discussing the challenges incurred and strategies adopted when decomposing initial/boundary values for the coefficients of the plane wave functions used as basis in the enriched method. Finally, some numerical problems are solved to motivate the relevance of this research in the context of real-world problems in engineering.

8.2 Recommendations

From the numerical examples considered in this thesis, we have seen a reduction of around 70% - 90% in the TOTDOF for the PUFEM as compared to the higher order p-FEM (up to 4^{th} order). It can be seen that the total degrees of freedom per wavelength *i.e.*, τ of around 5 is sufficient for low wavenumbers in the solution to the wave equation. For shorter wavelengths, the requirement on τ becomes less stringent as we have seen $\tau \approx 2.5$ to be sufficient for high wavenumbers in Chapter 3. Thus, $\tau = 5$ could be taken as a starting value for determining the number of nodal enrichment functions Q to be used for the numerical approximation using the PUFEM. It would be beneficial to develop adaptive measures to adjust τ that could be used for determining the value of Q. However, it should be noted that increasing Q tends to push the system matrix towards poor conditioning, owing to the closely packed spatial directions of the plane wave enrichment functions. One way to avoid this could be to use coarser mesh. Although this may not be ideal, since coarser mesh may give more stable systems matrices but it would lead to less accurate solutions. An alternative could be to use the lumped mass approach. It should be noted that the PUFEM system matrices with condition number as high as 10^7 could be trusted to produce relevant numerical solutions as seen in the previous chapters. An impor-

tant limitation to the research presented in this thesis is that the wavenumber of the problem must be provided as an *a priori* knowledge for choosing the enrichment functions. Perhaps one could develop methods to identify the range of dominant frequencies in the problem and adjust the enrichment functions adaptively. Some of the relevant literature has been discussed in Chapter 2. Another limitation comes from the time independence of the enrichment functions considered in this research. The spatial plane waves only provide ways to deal with rapid spatial variations in the solution, with the help of short wavelength of the enrichment functions. This approach, as seen through previous chapters, works well for problems with single dominant spatial frequency. However, for real world applications, where the phase velocity and the angular frequency may be significantly high, the PUFEM would surely require adjustments to attack the fast variations in time. One such approach could be to introduce time dependent enrichment functions in the finite element solution space, along with using high order integration schemes for temporal discretization. The following section provides basis and motivation for future work to develop the research outlined in this thesis.

8.3 Motivation for future work

The features of the enriched method investigated through this research, make it an attractive alternative for solvers based on standard finite element techniques, especially for various wave applications, such as the electromagnetic and the acoustic wave problems in engineering. The enriched method presented in this work, relies on fixed wavenumber of the plane wave basis functions used for enrichment. However, the real-world applications may have multiple discrete frequencies or a continuous band of frequencies dominant in the wave problem. Thus, the enrichment methodology proposed in this research could benefit by modifying the enrichment strategy. Potential modifications could be to include plane wave functions that differ not only in the wave direction, but also in their wavenumber. Thus, the finite element approximations could be parameterized as

$$E_h(t,\mathbf{x},k) = \sum_{j=1}^{N_d}\sum_{q=1}^{Q}\sum_{z=1}^{Z} \hat{E}_j^{q,z}(t)\mathcal{E}_q(k,\mathbf{x})\mathcal{N}_j(\mathbf{x})\mathcal{N}_z(k), \tag{8.1}$$

where the bump functions $\mathcal{N}_z(k)$ provide discretization in the frequency domain represented by the frequency variable k. The enrichment function $\mathcal{E}_q(k, \mathbf{x})$ depends on the index q of the angle of the plane wave as well as on the discretized frequency k. The scaling coefficient $\hat{E}_j^{q,z}(t)$ now has an extra index of z to denote the discretization in frequency. Notice that such a parameterization in the frequency domain is conformal, as well as variable separable. Thus, such a modification could be easily integrated into the existing enrichment procedure.

The improved accuracy for coarser step-size in time, when using high order RKM schemes as discussed in previous chapters, comes at the cost of storing and evaluating extra intermediate slope vectors. Thus, one can investigate the usage of low storage methods for the time discretization. Also, symplectic time integration schemes could be promising when used in the context of the enriched method proposed in this thesis. Developing adaptive techniques for time discretization depending on the conditioning of the system matrix could also be worth a while. Moreover, parameterization techniques such as in equation 8.1 could also be proposed for the angular frequency in time using space-time finite element methodologies.

Due to highly oscillatory nature of the enrichment functions, the number of integration points required for the quadrature scheme when computing elementary matrices is high. Thus it would be beneficial to develop exact integration schemes for the wave based enrichment method. This could lead to reduction in the assembly time as well as improvement in the numerical accuracy of the enriched procedure. Furthermore, the problems considered in this research are two-dimensional. A similar approach could be developed for three-dimensional wave problems.

Appendix A

Function definitions

This appendix contains the definitions for the propagator functions used in chapter 3 to model the test problems considered in section 3.7. The purpose of these propagators is to facilitate a pre-modelled analytic solution for a transient wave problem with vanishing initial conditions, that is then recovered with the proposed numerical method for a case study.

A.1 Definition of the propagator $\mathbf{F_1}$

We consider a piecewise linear function given as

$$f_L(p) = \frac{p + |p|}{2}, \tag{A.1}$$

which is a continuous function but not differentiable at $p = 0$. The derivative of this function is given by

$$f'_L(p) = \frac{d\, f_L(p)}{d\, p} = \frac{f_L(p)}{|p|}, \qquad \text{with} \quad p \neq 0.$$

Thus, the derivative of the function is undefined for $p = 0$. Similarly for higher order derivatives $o \geq 2$ one obtains

$$\frac{d^o\, f_L}{d\, p^o} = 0, \qquad \text{with} \quad p \neq 0.$$

Note that

$$(f_L'(p))^o = f_L'(p) = \frac{f_L(p)}{|p|}, \qquad \text{for} \quad o \geq 1.$$

For the test problem in chapter 3, the independent variable p is chosen to be $t - \frac{r}{c}$ where t is time, r is the magnitude of the radial position vector $r = \sqrt{x^2 + y^2}$ and c is the speed of wave. Thus the propagator function is denoted as follows

$$f_L(t, x, y) = \frac{t - \frac{r}{c} + |t - \frac{r}{c}|}{2}$$

This selection would facilitate to model the problem considered in chapter 3 as a radially expanding wave centred at the origin (*i.e.* at $r = t = 0$).

A.2 Definition of the propagator $\mathbf{F_2}$

The propagator F_1 defined above is not well behaved around the origin. To overcome this drawback we define the propagator F_2 which resolves this problem and retains all the desired properties of the propagator F_1. In addition, the propagator F_2 promotes implementation of a radially evolving wave centred at $r = t = 0$. Hence, the function $f_L(p)$ in (A.1) is replaced by

$$f_L(p) = \frac{1}{1+a}\left(\text{erf}\left(\frac{p-p_0}{b}\right)(p-p_0) + ap + \frac{b}{\sqrt{\pi}}e^{-\frac{(p-p_0)^2}{b^2}}\right), \tag{A.2}$$

where $\text{erf}(\cdot)$ denotes the error function and p_0 is used to shift it towards the left or the right side of the origin. The parameters a and b are fixed to control the smoothness of the slope of the function near the origin. In the simulations reported in chapter 3 we use $a = 1$, $b = 5$ and $p_0 = 10$. The derivative of the function $f_L(p)$ in (A.2) is given by

$$\frac{d\, f_L(p)}{d\, p} = \frac{\text{erf}\left(\frac{p-p_0}{b}\right) + a}{1+a}.$$

Thus, the derivative of the function $f_L(p)$ in (A.2) is a shifted and normalised error function which is well behaved. We used the following notation for the function $f_L(p)$

$$f_L(t, x, y) = \frac{1}{1+a}\left(\text{erf}\left(\frac{t - \frac{r}{c} - p_0}{b}\right)(t - \frac{r}{c} - p_0) + a(t - \frac{r}{c}) + \frac{b}{\sqrt{\pi}}e^{-\frac{(t-\frac{r}{c}-p_0)^2}{b^2}}\right)$$

Appendix B

GMSH data file

This appendix contains an example output file of the open source package GMSH, in the SU2 format, containing the mesh data for the PUFEM mesh as used in Figure 3.1.

B.1 Example "SU2" file

NDIME= 2

NELEM= 16

9 0 4 16 15 0

9 15 16 17 14 1

9 14 17 18 13 2

9 13 18 12 3 3

9 4 5 19 16 4

9 16 19 20 17 5

9 17 20 21 18 6

9 18 21 11 12 7

9 5 6 22 19 8

9 19 22 23 20 9

9 20 23 24 21 10

9 21 24 10 11 11

9 6 1 7 22 12

9 22 7 8 23 13

9 23 8 9 24 14

9 24 9 2 10 15

NPOIN= 25

0.07957747154594243 0.07957747154594243 0

1.079577471545943 0.07957747154594243 1

1.079577471545943 1.079577471545943 2

0.07957747154594243 1.079577471545943 3

0.3295774715453886 0.07957747154594243 4

0.5795774715446784 0.07957747154594243 5

0.829577471545332 0.07957747154594243 6

1.079577471545943 0.3295774715453886 7

1.079577471545943 0.5795774715446784 8

1.079577471545943 0.829577471545332 9

0.8295774715469723 1.079577471545943 10

0.5795774715484572 1.079577471545943 11

0.3295774715472106 1.079577471545943 12

0.07957747154594243 0.8295774715469723 13

0.07957747154594243 0.5795774715484572 14

0.07957747154594243 0.3295774715472106 15

0.3295774715457853 0.3295774715466125 16

0.3295774715461718 0.5795774715468769 17

0.3295774715466109 0.829577471546544 18

0.5795774715456794 0.3295774715461452 19

0.579577471546233 0.5795774715462075 20

0.5795774715468696 0.8295774715461151 21

0.8295774715457523 0.3295774715457588 22

0.8295774715461239 0.5795774715456515 23

0.8295774715465387 0.8295774715457404 24

NMARK= 1

MARKER_TAG= Neumann

MARKER_ELEMS= 16

3 1 7

3 7 8

3 8 9

3 9 2

3 2 10

3 10 11

3 11 12

3 12 3

3 3 13

3 13 14

3 14 15

3 15 0

3 0 4

3 4 5

3 5 6

3 6 1

Bibliography

[1] Amara, M., Djellouli, R., and Farhat, C. (2009). Convergence analysis of a discontinuous Galerkin method with plane waves and lagrange multipliers for the solution of Helmholtz problems. *SIAM Journal on Numerical Analysis*, 47(2):1038–1066.

[2] Ang, W.-T. (2007). *A Beginner's Course in Boundary Element Methods*. Universal Publishers.

[3] Babuška, I., Caloz, G., and Osborn, J. (1994). Special finite element methods for a class of second order elliptic problems with rough coefficients. *SIAM Journal on Numerical Analysis*, 31(4):945–981.

[4] Babuška, I. and Guo, B. (1992). The h, p and h-p version of the finite element method; basis theory and applications. *Advances in Engineering Software*, 15(3):159–174.

[5] Babuška, I. and Melenk, J. M. (1997). The partition of unity method. *International Journal for Numerical Methods in Engineering*, 40(4):727–758.

[6] Bae, S. Y., Kang, G., and Seo, J. K. (2015). Thermal and electromagnetic characteristics for cross-sectional design optimization of the integrated production umbilical. In *2015 IEEE Energy Conversion Congress and Exposition (ECCE)*, pages 3630–3636.

[7] Barros, F. B., Proença, S. P. B., and de Barcellos, C. S. (2004). On error estimator and p-adaptivity in the generalized finite element method. *International Journal for Numerical Methods in Engineering*, 60(14):2373–2398.

[8] Bathe, K.-J. (2006). *Finite Element Procedures*. Prentice Hall.

[9] Bathe, K.-J. (2014). Frontiers in finite element procedures and applications. In Topping, B. H. V. and Ivanyi, P., editors, *Computational Methods for Engineering Technology*. Saxe-Coburg Publications.

[10] Belytschko, T. and Black, T. (1999). Elastic crack growth in finite elements with minimal remeshing. *International Journal for Numerical Methods in Engineering*, 45(5):601–620.

[11] Belytschko, T., Gracie, R., and Ventura, G. (2009). A review of extended/generalized finite element methods for material modeling. *Modelling and Simulation in Materials Science and Engineering*, 17(4):043001.

[12] Bennett, C. L. and Ross, G. F. (1978). Time-domain electromagnetics and its applications. *Proceedings of the IEEE*, 66(3):299–318.

[13] Bériot, H., Gabard, G., and Perrey-Debain, E. (2013). Analysis of high-order finite elements for convected wave propagation. *International Journal for Numerical Methods in Engineering*, 96(11):665–688.

[14] Bériot, H., Perrey-Debain, E., Tahar, M. B., and Vayssade, C. (2010). Plane wave basis in Galerkin bem for bidimensional wave scattering. *Engineering Analysis with Boundary Elements*, 34(2):130–143.

[15] Bériot, H., Prinn, A., and Gabard, G. (2016). Efficient implementation of high-order finite elements for Helmholtz problems. *International Journal for Numerical Methods in Engineering*, 106(3):213–240.

[16] Bernatz, R. A. (2010). *Fourier Series and Numerical Methods for Partial Differential Equations*. John Wiley & Sons, Inc.

[17] Beylkin, G., Coifman, R., and Rokhlin, V. (1991). Fast wavelet transforms and numerical algorithms i. *Communications on Pure and Applied Mathematics*, 44(2):141–183.

[18] Blanes, S. and Moan, P. (2002). Practical symplectic partitioned runge-kutta and runge-kutta-nyström methods. *Journal of Computational and Applied Mathematics*, 142(2):313–330.

[19] Buffa, A., Costabel, M., and Schwab, C. (2002). Boundary element methods for Maxwell's equations on non-smooth domains. *Numerische Mathematik*, 92(4):679–710.

[20] Buffa, A. and Hiptmair, R. (2003). Galerkin boundary element methods for electromagnetic scattering. In *in Topics in Computational Wave Propagation. Direct and inverse Problems*, pages 83–124. Springer.

[21] Buffa, A., Hiptmair, R., Petersdorff, T. v., and Schwab, C. (2003). Boundary element methods for Maxwell transmission problems in lipschitz domains. *Numerische Mathematik*, 95(3):459–485.

[22] Buffa, A. and Monk, P. (2008). Error estimates for the ultra weak variational formulation of the Helmholtz equation. *ESAIM: Mathematical Modelling and Numerical Analysis*, 42(6):925–940.

[23] Canning, F. (1992). Sparse approximation for solving integral equations with oscillatory kernels. *SIAM Journal on Scientific and Statistical Computing*, 13(1):71–87.

[24] Cessenat, O. and Després, B. (1998). Application of an ultra weak variational formulation of elliptic pdes to the two-dimensional Helmholtz problem. *SIAM Journal on Numerical Analysis*, 35(1):255–299.

[25] Cessenat, O. and Després, B. (2003). Using plane waves as base functions for solving time harmonic equations with the ultra weak variational formulation. *Journal of Computational Acoustics*, 11(02):227–238.

[26] Cessenat, O. and Joly, P. (1996). *Application d'une nouvelle formulation variationnelle aux équations d'ondes harmoniques problémes de Helmholtz 2D et de Maxwell 3D*. PhD thesis.

[27] Chan, J. and Evans, J. A. (2018). Multi-patch discontinuous Galerkin isogeometric analysis for wave propagation: Explicit time-stepping and efficient mass matrix inversion. *Computer Methods in Applied Mechanics and Engineering*, 333:22–54.

[28] Chandler-Wilde, S. and Langdon, S. (2007). A Galerkin boundary element method for high frequency scattering by convex polygons. *SIAM Journal on Numerical Analysis*, 45(2):610–640.

[29] Christodoulou, K., Laghrouche, O., Mohamed, M., and Trevelyan, J. (2017). High-order finite elements for the solution of Helmholtz problems. *Computers and Structures*, 191:129–139.

[30] Ciskowski, R. D. and Brebbia, C. A. (1991). *Boundary Element Methods in Acoustics*. Springer Netherlands.

[31] Cohen, G. (2002). *Higher-Order Numerical Methods for Transient Wave Equations*. Springer.

[32] Congreve, S., Houston, P., and Perugia, I. (2019). Adaptive refinement for hp–version trefftz discontinuous Galerkin methods for the homogeneous Helmholtz problem. *Advances in Computational Mathematics*, 45(1):361–393.

[33] Conti, S., Dilettoso, E., and Rizzo, S. A. (2018). Electromagnetic and thermal analysis of high voltage three-phase underground cables using finite element method. In *2018 IEEE International Conference on Environment and Electrical Engineering and 2018 IEEE Industrial and Commercial Power Systems Europe (EEEIC / I CPS Europe)*, pages 1–6.

[34] Cottrell, J. A., Hughes, T. J. R., and Bazilevs, Y. (2009). *Isogeometric Analysis: Toward Integration of CAD and FEA*. John Wiley & Sons, Ltd.

[35] Davidson, D. B. (2005). *Computational Electromagnetics for RF and Microwave Engineering*. Cambridge University Press.

[36] de La Bourdonnaye, A. (1994). High frequency approximation of integral equations modeling scattering phenomena. *ESAIM: Mathematical Modelling and Numerical Analysis - Modélisation Mathématique et Analyse Numérique*, 28(2):223–241.

[37] Deraemaeker, A., Babuška, I., and Bouillard, P. (1999). Dispersion and pollution of the fem solution for the Helmholtz equation in one, two and three dimen-

sions. *International Journal for Numerical Methods in Engineering*, 46(4):471–499.

[38] Dinachandra, M. and Raju, S. (2018). Plane wave enriched partition of unity isogeometric analysis (puiga) for 2d-Helmholtz problems. *Computer Methods in Applied Mechanics and Engineering*, 335:380–402.

[39] Diwan, G. C. (2014). *Partition of unity boundary element and finite element method: Overcoming non-uniqueness and coupling for acoustic scattering in heterogeneous media.* PhD thesis, Durham University, UK.

[40] Diwan, G. C., Mohamed, M. S., Seaid, M., Trevelyan, J., and Laghrouche, O. (2015). Mixed enrichment for the finite element method in heterogeneousâĂĽmedia. *International Journal for Numerical Methods in Engineering*, 101(1):54–78.

[41] Dlugach, J., I. Mishchenko, M., Liu, L., and W. Mackowski, D. (2011). Numerically exact computer simulations of light scattering by densely packed, random particulate media. *Journal of Quantitative Spectroscopy and Radiative Transfer*, 112:2068–2078.

[42] Drolia, M., Mohamed, M., Laghrouche, O., Seaid, M., and Kacimi, A. E. (2019). Explicit time integration with lumped mass matrix for enriched finite elements solution of time domain wave problems. *Applied Mathematical Modelling.*

[43] Drolia, M., Mohamed, M., Laghrouche, O., Seaid, M., and Trevelyan, J. (2017). Enriched finite elements for initial-value problem of transverse electromagnetic waves in time domain. *Computers and Structures*, 182:354–367.

[44] Duarte, C. A. (1996). *The hp cloud method.* PhD thesis, The University of Texas at Austin, Austin, TX, USA.

[45] Duarte, C. A. and Oden, J. T. (1996a). An *h-p* adaptive method using clouds. *Computer Methods in Applied Mechanics and Engineering*, 139(1):237–262.

[46] Duarte, C. A. and Oden, J. T. (1996b). *h-p* clouds - an *h-p* meshless method. *Numerical Methods for Partial Differential Equations*, 12(6):673–706.

[47] Farhat, C., Harari, I., and Franca, L. P. (2001). The discontinuous enrichment method. *Computer Methods in Applied Mechanics and Engineering*, 190(48):6455–6479.

[48] Farhat, C., Harari, I., and Hetmaniuk, U. (2003a). The discontinuous enrichment method for multiscale analysis. *Computer Methods in Applied Mechanics and Engineering*, 192(28):3195–3209.

[49] Farhat, C., Harari, I., and Hetmaniuk, U. (2003b). A discontinuous Galerkin method with lagrange multipliers for the solution of Helmholtz problems in the mid-frequency regime. *Computer Methods in Applied Mechanics and Engineering*, 192(11):1389–1419.

[50] Farhat, C., Macedo, A., and Lesoinne, M. (2000). A two-level domain decomposition method for the iterative solution of high frequency exterior Helmholtz problems. *Numerische Mathematik*, 85(2):283–308.

[51] Farhat, C., Tezaur, R., and Weidemann-Goiran, P. (2004a). Higher-order extensions of a discontinuous Galerkin method for mid-frequency Helmholtz problems. *International Journal for Numerical Methods in Engineering*, 61(11):1938–1956.

[52] Farhat, C., Wiedemann-Goiran, P., and Tezaur, R. (2004b). A discontinuous Galerkin method with plane waves and lagrange multipliers for the solution of short wave exterior Helmholtz problems on unstructured meshes. *Wave Motion*, 39(4):307–317.

[53] Fish, J. and Belytschko, T. (2007). *A First Course in Finite Elements*. John Wiley & Sons, Inc.

[54] Gamallo, P. and Astley, R. J. (2007). A comparison of two trefftz-type methods: the ultraweak variational formulation and the least-squares method, for solving shortwave 2-D Helmholtz problems. *International Journal for Numerical Methods in Engineering*, 71(4):406–432.

[55] Gibson, W. C. (2014). *The Method of Moments in Electromagnetics; 2nd ed.* Chapman and Hall/CRC.

[56] Gillman, A., Barnett, A. H., and Martinsson, P.-G. (2015). A spectrally accurate direct solution technique for frequency-domain scattering problems with variable media. *BIT Numerical Mathematics*, 55(1):141–170.

[57] Gillman, A., Djellouli, R., and Amara, M. (2007). A mixed hybrid formulation based on oscillated finite element polynomials for solving Helmholtz problems. *Journal of Computational and Applied Mathematics*, 204(2):515–525.

[58] Gillman, A. and Martinsson, P.-G. (2014). An o(n) algorithm for constructing the solution operator to 2d elliptic boundary value problems in the absence of body loads. *Advances in Computational Mathematics*, 40(4):773–796.

[59] Gimperlein, H. and Stark, D. (2018). On a preconditioner for time domain boundary element methods. *Engineering Analysis with Boundary Elements*, 96:109–114.

[60] Gimperlein, H. and Stark, D. (2019). Algorithmic aspects of enriched time domain boundary element methods. *Engineering Analysis with Boundary Elements*, 100:118–124. Improved Localized and Hybrid Meshless Methods - Part 1.

[61] Grosu, E. and Harari, I. (2008). Studies of the discontinuous enrichment method for two-dimensional acoustics. *Finite Elements in Analysis and Design*, 44(5):272–287.

[62] Grosu, E. and Harari, I. (2009). Three-dimensional element configurations for the discontinuous enrichment method for acoustics. *International Journal for Numerical Methods in Engineering*, 78(11):1261–1291.

[63] Ham, S. and Bathe, K.-J. (2012). A finite element method enriched for wave propagation problems. *Computers and Structures*, 94-95:1–12.

[64] Ham, S., Lai, B., and Bathe, K.-J. (2014). The method of finite spheres for wave propagation problems. *Computers and Structures*, 142:1–14.

[65] He, Y., Qin, H., Sun, Y., Xiao, J., Zhang, R., and Liu, J. (2015). Hamiltonian time integrators for vlasov-Maxwell equations. *Physics of Plasmas*, 22(12):124503.

[66] Herrera, I. (1995). Trefftz-herrera domain decomposition. *Advances in Engineering Software*, 24(1):43–56.

[67] Hiptmair, R., Moiola, A., and Perugia, I. (2016). *A Survey of Trefftz Methods for the Helmholtz Equation*, pages 237–279. Springer.

[68] Honnor, M., Trevelyan, J., Bettess, P., El-hachemi, M., Hassan, O., Morgan, K., and Shirron, J. (2009). An integration scheme for electromagnetic scattering using plane wave edge elements. *Advances in Engineering Software*, 40(1):58–65.

[69] Honnor, M., Trevelyan, J., and Huybrechs, D. (2010). Numerical evaluation of the two-dimensional partition of unity boundary integrals for Helmholtz problems. *Journal of Computational and Applied Mathematics*, 234(6):1656–1662.

[70] Hu, Q. and Yuan, L. (2014). A plane-wave least-squares method for time-harmonic Maxwell's equations in absorbing media. *SIAM Journal on Scientific Computing*, 36(4):A1937–A1959.

[71] Hughes, T. (2012). *The Finite Element Method: Linear Static and Dynamic Finite Element Analysis*. Dover Civil and Mechanical Engineering. Dover.

[72] Hughes, T., Cottrell, J., and Bazilevs, Y. (2005). Isogeometric analysis: Cad, finite elements, nurbs, exact geometry and mesh refinement. *Computer Methods in Applied Mechanics and Engineering*, 194(39):4135–4195.

[73] Huttunen, T., Gamallo, P., and Astley, R. J. (2009). Comparison of two wave element methods for the Helmholtz problem. *Communications in Numerical Methods in Engineering*, 25(1):35–52.

[74] Huttunen, T., Kaipio, J., and Monk, P. (2008). An ultra-weak method for acoustic fluid-solid interaction. *Journal of Computational and Applied Mathematics*, 213(1):166–185.

[75] Huttunen, T., Kaipio, J. P., and Monk, P. (2004a). The perfectly matched layer for the ultra weak variational formulation of the 3d Helmholtz equation. *International Journal for Numerical Methods in Engineering*, 61(7):1072–1092.

[76] Huttunen, T., Monk, P., Collino, F., and Kaipio, J. (2004b). The ultra-weak variational formulation for elastic wave problems. *Siam Journal on Scientific Computing*, 25:1717–1742.

[77] Ihlenburg, F. and Babuška, I. (1995). Finite element solution of the Helmholtz equation with high wave number part i: The h-version of the fem. *Computers and Mathematics with Applications*, 30(9):9–37.

[78] Iserles, A. (2008). *A First Course in the Numerical Analysis of Differential Equations*. Cambridge University Press.

[79] Jiang, J., Mohamed, M. S., Seaid, M., and Li, H. (2018). Identifying the wavenumber for the inverse Helmholtz problem using an enriched finite element formulation. *Computer Methods in Applied Mechanics and Engineering*, 340:615–629.

[80] Jin, J. (2002). *The Finite Element Method in Electromagnetics*. Wiley.

[81] Kacimi, A. and Laghrouche, O. (2010). Improvement of pufem for the numerical solution of high-frequency elastic wave scattering on unstructured triangular mesh grids. *International Journal for Numerical Methods in Engineering*, 84:330–350.

[82] Kalashnikova, I., Tezaur, R., and Farhat, C. (2011). A discontinuous enrichment method for variable-coefficient advection-diffusion at high péclet number. *International Journal for Numerical Methods in Engineering*, 87(1-5):309–335.

[83] Kapita, S. and Monk, P. (2018). A plane wave discontinuous Galerkin method with a dirichlet-to-neumann boundary condition for the scattering problem in acoustics. *Journal of Computational and Applied Mathematics*, 327:208–225.

[84] Kergrene, K., Babuška, I., and Banerjee, U. (2016). Stable generalized finite element method and associated iterative schemes; application to interface problems. *Computer Methods in Applied Mechanics and Engineering*, 305:1–36.

[85] Khajah, T., Antoine, X., and Bordas, S. P. (2016). Isogeometric finite element analysis of time-harmonic exterior acoustic scattering problems. *ArXiv*, abs/1610.01694.

[86] Kita, E. and Kamiya, N. (1995). Trefftz method: an overview. *Advances in Engineering Software*, 24(1):3–12.

[87] Kohno, H., Bathe, K.-J., and Wright, J. C. (2010). A finite element procedure for multiscale wave equations with application to plasma waves. *Computers and Structures*, 88(1):87–94.

[88] Kovalevsky, L., Ladevèze, P., Riou, H., and Bonnet, M. (2012). The variational theory of complex rays for three-dimensional Helmholtz problems. *Journal of Computational Acoustics*, 20(04):1250021.

[89] Kovalevsky, L., Riou, H., and Ladevèze, P. (2013). On the use of the variational theory of complex rays for the analysis of 2-D exterior Helmholtz problem in an unbounded domain. *Wave Motion*, 50(3):428–436.

[90] Ladevèze, P., Arnaud, L., Rouch, P., and Blanzé, C. (2001). The variational theory of complex rays for the calculation of medium-frequency vibrations. *Engineering Computations*, 18:193–214.

[91] Laghrouche, O. and Bettess, P. (2000a). Short wave modelling using special finite elements. *Journal of Computational Acoustics*, 08(01):189–210.

[92] Laghrouche, O. and Bettess, P. (2000b). Solving short wave problems using special finite elements - towards an adaptive approach. *The Mathematics of Finite Elements and Applications*, 10.

[93] Laghrouche, O., Bettess, P., and Astley, R. J. (2002). Modelling of short wave diffraction problems using approximating systems of plane waves. *International Journal for Numerical Methods in Engineering*, 54(10):1501–1533.

[94] Laghrouche, O., Bettess, P., Perrey-Debain, E., and Trevelyan, J. (2005). Wave interpolation finite elements for Helmholtz problems with jumps in the wave speed. *Computer Methods in Applied Mechanics and Engineering*, 194(2):367–381.

[95] Laghrouche, O. and Mohamed, M. (2010). Locally enriched finite elements for the Helmholtz equation in two dimensions. *Computers and Structures*, 88(23):1469–1473.

[96] Langdon, S. and Chandler-Wilde, S. (2006). A wavenumber independent boundary element method for an acoustic scattering problem. *SIAM Journal on Numerical Analysis*, 43(6):2450–2477.

[97] Lee, J.-F. (2004). *Finite Element Methods for Microwave Engineering*, pages 285–301. Springer.

[98] Li, S. and Liu, W. K. (1999). Reproducing kernel hierarchical partition of unity, part iiâĂŤapplications. *International Journal for Numerical Methods in Engineering*, 45(3):289–317.

[99] Liszka, T. J., Duarte, C. A., and Tworzydlo, W. W. (1996). hp-meshless cloud method. *Computer Methods in Applied Mechanics and Engineering*, 139(1):263–288.

[100] Luostari, T., Huttunen, T., and Monk, P. (2011). The ultra weak variational formulation using bessel basis functions. *Communications in Computational Physics*, 11:400–414.

[101] Luostari, T., Huttunen, T., and Monk, P. (2013). Improvements for the ultra weak variational formulation. *International Journal for Numerical Methods in Engineering*, 94(6):598–624.

[102] Maaskant, R., Ivashina, M. V., Wijnholds, S. J., and Warnick, K. F. (2012). Efficient prediction of array element patterns using physics-based expansions and a single far-field measurement. *IEEE Transactions on Antennas and Propagation*, 60(8):3614–3621.

[103] Mahmood, M., Laghrouche, O., Trevelyan, J., and Kacimi, A. (2017). Implementation and computational aspects of a 3d elastic wave modelling by pufem. *Applied Mathematical Modelling*, 49:568–586.

[104] Massimi, P., Tezaur, R., and Farhat, C. (2008). A discontinuous enrichment method for three-dimensional multiscale harmonic wave propagation problems in multi-fluid and fluid-solid media. *International Journal for Numerical Methods in Engineering*, 76(3):400–425.

[105] Massimi, P., Tezaur, R., and Farhat, C. (2010). A discontinuous enrichment method for the efficient solution of plate vibration problems in the medium-frequency regime. *International Journal for Numerical Methods in Engineering*, 84(2):127–148.

[106] Mayer, P. and Mandel, J. (1997). The finite ray element method for the Helmholtz equation of scattering: first numerical experiments. *University of Colorado at Denver, Center for Computational Mathematics*.

[107] Melenk, J. and Babuška, I. (1996). The partition of unity finite element method: Basic theory and applications. *Computer Methods in Applied Mechanics and Engineering*, 139(1):289–314.

[108] Melenk, J. M. (1995). *On Generalised Finite Element Methods*. PhD thesis, The University of Maryland, USA.

[109] Moës, N., Dolbow, J., and Belytschko, T. (1999). A finite element method for crack growth without remeshing. *International Journal for Numerical Methods in Engineering*, 46(1):131–150.

[110] Mohamed, M. S., Laghrouche, O., and El-Kacimi, A. (2010). Some numerical aspects of the pufem for efficient solution of 2d Helmholtz problems. *Computers and Structures*, 88(23):1484–1491.

[111] Mohamed, M. S., Seaid, M., Trevelyan, J., and Laghrouche, O. (2013a). A partition of unity fem for time-dependent diffusion problems using multiple enrichment functions. *International Journal for Numerical Methods in Engineering*, 93(3):245–265.

[112] Mohamed, M. S., Seaid, M., Trevelyan, J., and Laghrouche, O. (2013b). Time-independent hybrid enrichment for finite element solution of transient conduction-radiation in diffusive grey media. *Journal of Computational Physics*, 251:81–101.

[113] Mohamed, M. S., Seaid, M., Trevelyan, J., and Laghrouche, O. (2014). An enriched finite element model with q-refinement for radiative boundary layers in glass cooling. *Journal of Computational Physics*, 258:718–737.

[114] Monk, P. and Wang, D.-Q. (1999). A least-squares method for the Helmholtz equation. *Computer Methods in Applied Mechanics and Engineering*, 175(1):121–136.

[115] Mutonkole, N. and de Villiers, D. I. L. (2015). Characteristic basis function patterns method for reflector antenna calibration: An extension to multiple frequencies. In *2015 9th European Conference on Antennas and Propagation (EuCAP)*, pages 1–5.

[116] Mutonkole, N., Samuel, E. R., de Villiers, D. I. L., and Dhaene, T. (2016). Parametric modeling of radiation patterns and scattering parameters of antennas. *IEEE Transactions on Antennas and Propagation*, 64(3):1023–1031.

[117] Nguyen, V. P., Anitescu, C., Bordas, S. P., and Rabczuk, T. (2015). Isogeometric analysis: An overview and computer implementation aspects. *Mathematics and Computers in Simulation*, 117:89–116.

[118] Oden, J., Duarte, C., and Zienkiewicz, O. (1998). A new cloud-based hp finite element method. *Computer Methods in Applied Mechanics and Engineering*, 153(1):117–126.

[119] Peake, M., Trevelyan, J., and Coates, G. (2013). Extended isogeometric boundary element method (xibem) for two-dimensional Helmholtz problems. *Computer Methods in Applied Mechanics and Engineering*, 259:93–102.

[120] Perrey-Debain, E. (2006). Plane wave decomposition in the unit disc: Convergence estimates and computational aspects. *Journal of Computational and Applied Mathematics*, 193(1):140–156.

[121] Perrey-Debain, E., Laghrouche, O., Bettess, P., and Trevelyan, J. (2004a). Plane-wave basis finite elements and boundary elements for three-dimensional wave scattering. *Philosophical Transactions: Mathematical, Physical and Engineering Sciences*, 362(1816):561–577.

[122] Perrey-Debain, E., Trevelyan, J., and Bettess, P. (2002). New special wave boundary elements for short wave problems. *Communications in Numerical Methods in Engineering*, 18(4):259–268.

[123] Perrey-Debain, E., Trevelyan, J., and Bettess, P. (2003a). P-wave and s-wave decomposition in boundary integral equation for plane elastodynamic problems. *Communications in Numerical Methods in Engineering*, 19(12):945–958.

[124] Perrey-Debain, E., Trevelyan, J., and Bettess, P. (2003b). Plane wave interpolation in direct collocation boundary element method for radiation and wave scattering: numerical aspects and applications. *Journal of Sound and Vibration*, 261(5):839–858.

[125] Perrey-Debain, E., Trevelyan, J., and Bettess, P. (2003c). Use of wave boundary elements for acoustic computations. *Journal of Computational Acoustics*, 11(02):305–321.

[126] Perrey-Debain, E., Trevelyan, J., and Bettess, P. (2004b). Wave boundary elements: a theoretical overview presenting applications in scattering of short waves. *Engineering Analysis with Boundary Elements*, 28(2):131–141.

[127] Petersen, S., Farhat, C., and Tezaur, R. (2009). A space-time discontinuous Galerkin method for the solution of the wave equation in the time domain. *International Journal for Numerical Methods in Engineering*, 78(3):275–295.

[128] Pitchai, K., Birla, S., Subbiah, J., Jones, D., and Thippareddi, H. (2012). Coupled electromagnetic and heat transfer model for microwave heating in domestic ovens. *Journal of Food Engineering*, 112(1):100–111.

[129] Pozar, D. M. (2005). *Microwave engineering; 3rd ed.* Wiley.

[130] Pozrikidis, C. (2014). *Introduction to Finite and Spectral Element Methods Using MATLAB*. Chapman and Hall/CRC.

[131] Prakash, V. V. S. and Mittra, R. (2003). Characteristic basis function method: A new technique for efficient solution of method of moments matrix equations. *Microwave and Optical Technology Letters*, 36(2):95–100.

[132] Qin, H., Liu, J., Xiao, J., Zhang, R., He, Y., Wang, Y., Sun, Y., Burby, J. W., Ellison, L., and Zhou, Y. (2015). Canonical symplectic particle-in-cell method for long-term large-scale simulations of the vlasov–Maxwell equations. *Nuclear Fusion*, 56(1):014001.

[133] Rasoulpoor, M., Mirzaie, M., and Mirimani, S. (2018). Electromagnetic and thermal analysis of underground power solid-conductor cables under harmonic and unbalancing currents based on fem. *International Journal of Numerical Modelling: Electronic Networks, Devices and Fields*, 31(1):e2278. e2278 JNM-16-0233.R2.

[134] Rokhlin, V. (1990). Rapid solution of integral equations of scattering theory in two dimensions. *Journal of Computational Physics*, 86(2):414–439.

[135] Sanz-Serna, J. (1992). Symplectic runge-kutta and related methods: recent results. *Physica D: Nonlinear Phenomena*, 60(1):293–302.

[136] Sauter, S. and Schwab, C. (2011). *Boundary Element Methods*. Springer.

[137] Schweitzer, M. A. (2011). Stable enrichment and local preconditioning in the particle-partition of unity method. *Numerische Mathematik*, 118(1):137–170.

[138] Strouboulis, T., Babuška, I., and Copps, K. (2000a). The design and analysis of the generalized finite element method. *Computer Methods in Applied Mechanics and Engineering*, 181(1):43–69.

[139] Strouboulis, T., Babuška, I., and Hidajat, R. (2006). The generalized finite element method for Helmholtz equation: Theory, computation, and open problems. *Computer Methods in Applied Mechanics and Engineering*, 195(37):4711–4731.

[140] Strouboulis, T., Copps, K., and Babuška, I. (2000b). The generalized finite element method: an example of its implementation and illustration of its performance. *International Journal for Numerical Methods in Engineering*, 47(8):1401–1417.

[141] Strouboulis, T., Hidajat, R., and Babuška, I. (2008). The generalized finite element method for Helmholtz equation. part ii: Effect of choice of handbook functions, error due to absorbing boundary conditions and its assessment. *Computer Methods in Applied Mechanics and Engineering*, 197(5):364–380.

[142] Taflove, A. and Brodwin, M. E. (1975). Numerical solution of steady-state electromagnetic scattering problems using the time-dependent Maxwell's equations. *IEEE Transactions on Microwave Theory and Techniques*, 23(8):623–630.

[143] Taflove, A. and Hagness, S. (2005). *Computational Electrodynamics: The Finite-difference Time-domain Method*. Artech House Antennas and Prop. Artech House.

[144] Terras, A. (1999). *Fourier Analysis on Finite Groups and Applications*. Cambridge University Press.

[145] Tezaur, R. and Farhat, C. (2006). Three-dimensional discontinuous Galerkin elements with plane waves and lagrange multipliers for the solution of mid-frequency Helmholtz problems. *International Journal for Numerical Methods in Engineering*, 66(5):796–815.

[146] Tezaur, R., Kalashnikova, I., and Farhat, C. (2014). The discontinuous enrichment method for medium-frequency Helmholtz problems with a spatially variable wavenumber. *Computer Methods in Applied Mechanics and Engineering*, 268:126–140.

[147] Tezaur, R., Zhang, L., and Farhat, C. (2008). A discontinuous enrichment method for capturing evanescent waves in multiscale fluid and fluid/solid problems. *Computer Methods in Applied Mechanics and Engineering*, 197(19):1680–1698.

[148] Theodor, T., Griffel, G., and Bertoni, H. L. (1995). *Guided-Wave Optoelectronics*. Springer.

[149] Wang, D., Tezaur, R., Toivanen, J., and Farhat, C. (2012). Overview of the discontinuous enrichment method, the ultra-weak variational formulation, and the partition of unity method for acoustic scattering in the medium frequency regime and performance comparisons. *International Journal for Numerical Methods in Engineering*, 89(4):403–417.

[150] Wu, H. and Li, Z. L. (2009). Scale issues in remote sensing: A review on analysis, processing and modeling. *Sensors*, 9(3):1768–1793.

[151] XING, Y., LIU, B., and LIU, G. (2010). A differential quadrature finite element method. *International Journal of Applied Mechanics*, 02(01):207–227.

[152] Yang, J., Hu, H., and Potier-Ferry, M. (2019). Least-square collocation and lagrange multipliers fortaylor meshless method. *Numerical Methods for Partial Differential Equations*, 35(1):84–113.

[153] Yang, Y., Xu, D., and Zheng, H. (2018). Explicit discontinuous deformation analysis method with lumped mass matrix for highly discrete block system. *International Journal of Geomechanics*, 18(9):04018098.

[154] Yang, Y., Zheng, H., and Sivaselvan, M. (2017). A rigorous and unified mass lumping scheme for higher-order elements. *Computer Methods in Applied Mechanics and Engineering*, 319:491–514.

[155] Yee, K. S. (1966). Numerical solution of initial boundary value problems involving Maxwell's equations in isotropic media. *IEEE Trans. Antennas and Propagation*, pages 302–307.

[156] Yuan, L. (2018). The plane wave discontinuous Galerkin method combined with local spectral finite elements for the wave propagation in anisotropic media. *Numerical Mathematics: Theory, Methods and Applications*, 12(2):517–546.

[157] Yuan, L. and Hu, Q. (2019a). Error analysis of the plane wave discontinuous Galerkin method for Maxwell's equations in anisotropic media. *Communications in Computational Physics*, 25(5):1496–1522.

[158] Yuan, L. and Hu, Q. (2019b). Generalized plane wave discontinuous Galerkin methods for nonhomogeneous Helmholtz equations with variable wave numbers. *International Journal of Computer Mathematics*, pages 1–22.

[159] Zhang, L., Tezaur, R., and Farhat, C. (2006). The discontinuous enrichment method for elastic wave propagation in the medium-frequency regime. *International Journal for Numerical Methods in Engineering*, 66(13):2086–2114.

[160] Zienkiewicz, O., Taylor, R., and Zhu, J. Z. (2013). *The Finite Element Method: Its Basis and Fundamentals*. The Finite Element Method. Butterworth-Heinemann.

[161] Zienkiewicz, O. C. (2000). Achievements and some unsolved problems of the finite element method. *International Journal for Numerical Methods in Engineering*, 47(1-3):9–28.